UNIVERSITY OF OKLAHOMA

GRADUATE COLLEGE

MELT BLOWING WITH LOUVERS AND THEIR EFFECTS ON FIBER ATTENUATION AND MOTION

A THESIS

SUBMITTED TO THE GRADUATE FACULTY

in partial fulfillment of the requirements for the

Degree of

MASTER OF SCIENCE

By

KAYLA ANN FOLEY
Norman, Oklahoma
2017

MELT BLOWING WITH LOUVERS AND THEIR EFFECTS ON
FIBER ATTENUATION AND MOTION

A THESIS APPROVED FOR THE
SCHOOL OF CHEMICAL, BIOLOGICAL AND MATERIALS ENGINEERING

BY

_____
Dr. Robert L. Shambaugh, Chair

_____
Dr. Edgar A. O' Rear III

_____
Dr. Dimitrios V. Papavassiliou

ACKNOWLEDGEMENTS

I would like to offer my thanks to the people below for their support during my work in this thesis and as a student in past years:

The physics machine shop for developing such beautiful louvers. Without these, there would be no point to this thesis.

Dr. R. L. Shambaugh, for serving as my advisor, for his guidance, encouragement, and many discussions over the years, and for sparking an interest in research and a love for polymers.

Dr. O' Rear for serving on my committee and for teaching MoHeat I. While Fundamentals and Computing do introduce us to chemical engineering knowledge, the "what did I get myself into" feeling doesn't really hit until MoHeat I. Thank you for being an excellent teacher in this early chemical engineering class and encouraging us to stick to it even when it seemed hard.

Dr. Papavassiliou for serving on my committee.

Dr. Harwell for teaching Computing and Visual Basic. I would not have been able to write the Frequency and Amplitude code with out the knowledge I learned from your class.

Dr. Shambaugh, Dr. Resasco, Dr. Walters, and Dr. Papavassiliou for letting me TA for you and sparking the desire to teach.

Dr. Grady for allowing me to continue to TA and thus continue to learn the ways of teaching.

Dr. Huang and Dr. Wang for our random moments of saying "hi" in the hall.

Dr. Nollert for always being willing to listen and for believing in me, especially when I didn't believe in myself. I can't begin to express what this has meant to me.

Terri, Donna, Madena, and Gretchen for helping with all my CBME questions, numerous AirGas orders, and for our conversations over the years.

Alan and Dennis for fixing "the Beast", making louver tabs, and more importantly, keeping research going.

My minions over the years for helping me run the Beast and collect data.

Matt for being my friend, being my research-partner-in-crime, and for the numerous DQ trips

My CHE friends, both old and new, for their friendship as we endeavored to become chemical engineers over the years.

Monique for being my friend and partner during our first teaching experience.

My roommates, friends and family for listening, supporting me, and laughing with me over the years.

My brother for his occasionally reluctant but always loving support and friendship for the past 21 years.

Finally, to Mom and Dad for being the best loving parents I could ever ask for. Everything I am and do, I owe to you.

TABLE OF CONTENTS

LIST OF TABLES

LIST OF ILLUSTRATIONS

CHAPTER 1

CHAPTER 2

CHAPTER 3

APPENDIX II

ABSTRACT

A physical plateau in the air field below a melt blowing die was imposed by airfoil shaped louvers. These louvers prevented air jet spreading and imposed a constant average air velocity on the polymer filament, resulting in greater attenuation. Fibers were collected and measured offline using optical microscopy. Fiber diameters were found to be significantly reduced when louvers are in the air field compared to normal melt blowing conditions. Longer chords expose longer lengths of the fiber threadline to the nondecaying air velocity, causing a greater forwarding force on the fiber and thus greater attenuation and finer diameters. Angled chords act as a nozzle and expose the fiber to an increasing air velocity. This was found to be more beneficial for shorter chords that expose less of the threadline to the nondecaying air velocity. Louvers placed closer to the die resulted in finer diameters and less fiber sticking.

High Speed Photography was employed to observe the motion of a melt blown polymer filament when louvers were in the air field. Videos of the fiber were taken with a Redlake HS-4 camera capable of high frame rates. The position of the fiber over time was tracked at different distances below the die, and a code was implemented to calculate the frequency and amplitude of the fiber for various positions, configuration, and louver sizes.

A methodology for online fiber temperature measurements with the louvers in the air field is presented.

CHAPTER 1

INTRODUCTION, LITERATURE REVIEW, AND SCOPE OF WORK

1.1 Introduction to Melt Blowing

Melt blowing is an industrial process that produces fibers in a nonwoven sheet. These nonwoven materials are often used in applications such as filtration and adsorbent materials. Molten polymer is extruded through a small orifice in a die into jets of heated air. Typically, this die is of the "Exxon" type with dual slots that produce two converging jets of air. The high air velocity from the jets compared to the lower polymer velocity provides a drag force that rapidly attenuates the polymer into a fine fiber soon after leaving the die. These fibers are then collected on a screen or collector belt below the die head. Typical fiber diameters produced in melt blowing can range from 0.1 to 10 microns or larger, but fibers in the nanometer range can also be produced (Hassan, 2016). Usually, fine diameters are desired because fine fibers enhance filtrations. Furthermore, because fine fibers have large fiber surface area per unit volume of polymer, fine fibers have better sorptive capability versus fibers of larger diameters. Applications for melt blown fibers include medical gowns, filters, baby diapers, and numerous other uses.

1.2 Literature Review

1.2.1 Modeling and Fiber Motion

Most previous work has been done in studying and modeling the fiber formation and the air field in melt blowing as well as investigations into improving the process. Early modeling of the melt blowing process evolved from modeling of the polymer spin-line in the melt spinning process. Compared to melt blowing, the melt spinning process uses a mechanical take-up roll to attenuate the fiber. Air is involved in this process, but

the air serves to quench the hot filaments. The air does not provide a forwarding force to the fibers. Uyttendaele and Shambaugh (1990) applied one-dimensional continuity, momentum, and energy equations similar to those developed for melt spinning with an adjustment in end boundary conditions to account for the lack of a take-up roll in melt blowing. They applied an iterative solution by estimating an initial fiber stress and performing calculations until reaching a "freeze point" where the air drag and gravitational forces were balanced, and fiber attenuation was assumed to stop. Later work by Rao and Shambaugh (1993) and Marla and Shambaugh (2003) updated this bottom boundary condition to a "stop point" where the fiber and air velocities become equal and the stress on the fiber becomes zero.

Non-axial fiber motion during melt blowing is of particular interest because this motion both affects the fiber laydown pattern. This laydown pattern determines the quality of the sheet goods made during melt blowing. A wide, even laydown (i.e., uniform laydown) gives a good product.

As the fiber whips back and forth in the air jet, the fiber experiences a drag force not only due to the air velocity in the axial direction, but also due to the air velocity normal to the fiber and at oblique angles to the fiber (Ju and Shambaugh, 1994), (Ellison, 2007). The whipping motion can be quantified with variables such as fiber frequency and amplitude. These variables can affect fiber attenuation, the uniformity of fiber laydown, and defect formation. Uyttendaele and Shambaugh's one-dimensional model considered only axial motion. Rao and Shambaugh (1993) extended Uyttendaele's model to two dimensions, and Marla and Shambaugh (2003) extended the model in two and three dimensions. Both fiber frequency and amplitude were included in this 2D and 3D work.

Chhabra (1996) studied fiber cone amplitude and frequency with high-speed photography and laser doppler velocimetry. Beard (2007), used high-speed photography to observe the frequency and amplitude of the melt blown filament. The findings of (Rao and Shambaugh, 1993), (Marla and Shambaugh, 2003), and (Beard et al. 2007) agree that both fiber amplitude and frequency increase with increasing air flow rate and decreasing polymer flow rate. Frequency also decreases with increasing polymer temperature. Fiber amplitude increases with increasing distance below the die. These studies were done with fiber diameters in the micron range. Xie (2013) studied fiber motion with high speed photography and attempted to measure fiber attenuation by measuring fiber perimeter for a tracked loop as it traveled further beneath the die. Their amplitude and frequency trends were similar to those seen above. Fiber diameters were about 20 microns in this study, but they project these trends to extend to the nanometer fiber diameter range.

Significant fiber whipping can also have a detrimental effect on the polymer fiber and the resulting nonwoven sheet. Too violent vibrations, can cause fiber breakage, shots, and sticking (Ellison, 2007; Chung and Kumar, 2013; Hassan, 2016). Chung and Kumar (2013) studied the causes of whipping using a quasi-one-dimensional model for liquid jets developed and implemented by Yarin (2010) (1984) for melt blowing. They found that high inertia of the polymer and air jets (increasing Reynold's number) and varying drag force on the filament could lead to the spin-line "back-folding" on itself, leading to violent whipping motions. Initial vibration in the filament immediately exiting the die was also required for whipping to occur, with increasing effect as this initial frequency increased. The variation in the drag force most-likely comes from the vibrating fiber filament leaving the centerline region with higher air velocities and entering the regions

of lower air velocity before returning to the centerline. When the air jet undergoes entrainment with ambient air, the air jet spreads and there is greater variation in air velocity in the transverse direction moving away from the centerline. A way to prevent air jet spreading and form a more uniform velocity profile could lessen this variation and possibly lessen whipping.

1.2.2 Modifications and Optimizations

Other work has been done in studying the main process variables and making modifications for optimal conditions. As the main fiber attenuation occurs due to the air drag force, the air velocity and temperature are important process variables in addition to polymer temperature and flow rate. In general (Shambaugh, 1988) (Bresse, 2003), it has been found that higher air velocities at the centerline induces greater stress on the fiber filament resulting in greater fiber attenuation. High air temperatures help maintain higher polymer temperatures, which keeps the polymer molten for longer, allowing for more attenuation. Low mass flow rates also produce finer diameters. Entrainment with ambient air causes air velocity and temperature to decrease and for spreading in the air jet. As a high air velocity is needed to obtain the fine diameters desired, modifications have been studied to attempt to maintain or increase air velocity and temperature as well as to prevent jet spreading. Most of these modifications have been either alterations to die geometry or to add-ons to the process. Motivation for these modifications have consisted of both economic and technical goals such as reducing air consumption, improving fiber laydown, and producing nanofibers.

Tate and Shambaugh (1998) (2004) and Krutka et al. (2003) (2004) have studied different die geometries both experimentally and computationally. Tate studied the

effects of 60 and 70 degree sharp and blunt die nose pieces on the air jet velocity profile and spreading (Fig 1.1). They have found that dual air jets merge sooner with sharp die nose pieces compared to blunt ones, producing higher centerline velocities and narrower jets. As the polymer fiber is mainly affected by the air at the centerline, having a narrow jet with higher air velocities is ideal. It was also found that the 60 degree die air jets merged slightly sooner than that of the 70 degree dies. The temperature profiles were similar to these results, with the 60 degree sharp die having the narrowest profile with higher centerline temperatures. Krutka et. al. (2003) extended the study through computational fluid dynamics to include inset and outset dies. They found that inset dies (where the nose tip is recessed into the die) produce higher centerline velocities near the die, but it also was more prone to turbulence. Outset dies had less of an effect on the centerline velocity, but it has had less turbulent fluctuations. Krutka also studied non-isothermal melt blowing with sharp dies of varying angles of 45, 50, 60, and 70 degrees. The dies with smaller slot angles showed higher average air velocities and turbulence intensity. Overall, they showed that sharp die geometry with moderately smaller angles and some inset can improve melt blowing air field conditions.

Hassan (2016) studied the effect of modifying a die with attached "air constrictors" to the die through computational fluid dynamics using a K-ε Turbulence model. These "constrictors" resemble dual rectangular plates attached perpendicularly to the die face, such that the plate is parallel to the fiber spin-line. In their study, they tested different constrictor widths, lengths, and angles (Fig 1.2). Overall, they found that the constrictors did increase centerline air velocity and maintained air temperature for a longer distance below the die compared to the case without constrictors as they prevented

entrainment of ambient air. They also performed a brief experimental study using an industrial die and conditions. Greater fiber attenuation was found, particularly for smaller constrictor distances; however, these fabrics showed more “shots” (globs of polymer) and “roping” when the constrictor width was small. Overall, their best constrictor conditions were for constrictor widths between 14 and 20 mm.

Chelikani (2013) added a plane wall as an extension of the die face at one slot end and studied the resulting “Coanda” effect of the wall on the air field with the goal of creating a more uniform laydown pattern at the outer edges. Essentially, they were able to increase the centerline air velocity at the edges of the slot lengths and for some distance beyond. Tan et al. (2012) studied the effect of increasing inlet air pressure in the melt blowing die and the effect of an added Laval nozzle attached to the die face. Increasing inlet air pressure lead to a transition from subsonic to supersonic flow with compression waves occurring at inlet pressures greater than 15 psig. The corresponding centerline air velocity increased with increasing air pressure until reaching supersonic flow where it begins to oscillate. This can lead to defects and probably significant whipping. The addition of a Laval nozzle suppressed these compression waves up to a certain air pressure.

1.2.3 Fiber Temperature Studies

There are several works that study the online measurement of fiber diameter. Breese and Ko (2003) made online fiber temperature measurements using an infrared thermometer with an adjustable emissivity. Gozhar (2004) used infrared photograph to take online measurements of temperature, and developed a method of measuring fiber diameter in the melt spinning process with temperature data. Marla and Beard (Marla,

2007) (Marla, 2009) (Beard, 2006) also used infrared photography to study online fiber temperature. Marla developed a procedure for determining fiber emissivity and the camera spatial resolution effect on fiber temperature with infrared photography. In a later work, Marla studied the online temperature of the fiber in both melt spinning and melt blowing. Beard studied the effect of varying melt blowing process variables on the fiber temperature with infrared photography.

1.2.4 A Plateau in the Air Field

Our current work is a continuation of the work done by B. Shambaugh (2011) (2012) and Shambaugh (2015). In (Shambaugh, 2011), they suggested that a "plateau" could be used to optimize the air field below a die. This "plateau" would be a section where the air velocity and temperature fields would be kept constant between positions z_1 and z_2 below the die head (Fig. 1.3). Before and after this "plateau" the air temperature and velocity would still decrease as it normally would without the "plateau." As these profiles would be kept constant for a certain distance, the fiber would be exposed to higher temperatures and air velocities for a longer time, thus allowing for lower polymer viscosities, greater drag force, and ultimately greater fiber attenuation. Also, potentially less air would be needed to attain the same fiber diameters, so the economic costs of the gas stream is reduced.

In a following work, B. Shambaugh (2012) used a comprehensive melt blowing model they developed to test the effect on the polymer fiber of various "plateau" widths and positions in the air field. They found that a 2 cm "plateau," when placed near the die, resulted in higher fiber velocity and temperature profiles and higher fiber stress with the maximum located nearer to the die. Simulated fiber diameters also showed a reduction

compared to the case without a "plateau." This effect was greatest when the "plateau" was placed within 2 cm below the die. This is expected as most fiber attenuation due to air drag occurs within the first few centimeters below the die (Shambaugh, 1988) (Bresse and Ko, 2003). Wider "plateaus" also showed better performance than smaller plateaus. For instance, their results showed that a 4 cm plateau located at the die face reduced the fiber diameter from 53.8 microns to 20 microns while the 2 cm plateau at the same location reduced the diameter to only 30 microns. However, their computer simulations began to show instability when the plateau width became too long and placed at distances farther beneath the die.

Experimentally, Shambaugh (2015) extended this study using louvers below a melt blowing die to create the "plateau" in the air velocity profile. They would keep this profile constant by preventing ambient air form entraining with the air jets and decaying the air velocity. Two louvers (air foils) were placed in the air field below the die parallel to the spin-line (Fig.1.4). The width of the "plateau" they create is the chord length of the louvers between positions z_1 and z_2. This chord length was 2cm for this study and the leading-edges were placed at z_1= 2 cm. The louvers were made of basswood, were rounded at the leading-edge, and tapered at the trailing edge (Fig. 1.4). Using a melt blowing die on a test stand, air velocity profiles were measured at room temperature using a pitot tube for different louver separations and angles. Louver separations of 12, 10, 8, and 6 mm were tested. They found that each case showed an increased centerline velocity at the trailing-edge of the louvers, and this effect increases as the louver separation decreased. The velocity profiles also become flatter and more uniform between the louvers as the separation decreases. Angled positions, where the separation between the

trailing-edges is smaller than that of the leading-edges, were also tested. For example, for a leading-edge separation of 8 mm, the trailing-edge separations were 8, 6, and 4 mm, with the greatest louver angle for the 4 mm separation. It was found that the centerline velocities were higher for increased angle (Fig. 1.5).

1.3 Motivation and Scope of Work

The louvers have been shown to be successful in preventing air entrainment and maintaining higher centerline velocities with flatter velocity profiles around the die, which would ideally lead to greater fiber attenuation and finer fiber diameters. Louvers would provide an inexpensive add on that does not require modifying die assemblies, while also achieving the goal of increasing centerline velocities. They could potentially reduce air costs as fiber diameters typically achieved at higher air flowrates might be achievable at lower air flowrates.

The Laval nozzle (Tan, 2012) and the air constrictors (Hassan, 2016) do require attachment to the die face while the louvers may easily and quickly be moved to different locations below the die face, making them more customizable. The use of the "Coanda" plane wall (Chelikani, 2013) was used with the goal of reducing end effects and creating a more uniform fiber mat, while the louvers are intended to maintain or even increase centerline velocity for longer distances below the die.

However, these louvers have not yet been evaluated for their effectiveness in reducing fiber diameter, and indeed, this is a goal in our work, which will be discussed in Chapter 2. As the air field is being modified, it would be of interest to evaluate the effect of the air field on fiber motion. Chapter 3 will discuss our study of the effect of louvers on fiber frequency and amplitude. It is expected that the air temperature profile will be

maintained at higher temperature for longer below the die due to the louvers in the field, so it would also be of interest to study the effect of the louvers on the fiber temperature. A methodology for this study is discussed in chapter4. Finally, Chapter 5 will conclude the work and discuss future possibilities. Several appendixes are included describing additional data as well as further details on procedures, software, code, and cameras.

A Note on Formatting

Throughout this work references and figures are located at the end of each chapter and appendix. Chapter 2 has been written with the intention of publication. The references for Chapter 2 are listed in order of appearance in the text, while other chapters are listed alphabetically by author name.

REFERENCES

Beard, J. H.; Shambaugh, R. L.; Shambaugh, B. R.; Schmidtke, D.W. On-line Measurement of Fiber Motion During the Melt Blowing. *Ind. Eng. Chem. Res.*, 2007, *46* (22), 7340-7352.

Beard. J. H. Analysis of fiber temperature and motion in the melt blowing process. Thesis (M.S.) University of Oklahoma, 2006.

Bresse, R. R.; Ko, W. C. Fiber Formation During Melt Blowing. *Int. Nonwovens J.* 2003, 12, 21.

Chelikani, S.; Sparrow, E. M. Numerical Simulations of Plane-Wall Coanda Effects for Control of Fiber Trajectories in the Melt-Blown Process. Ind. Eng. Chem. Res. 2013, 52, 11639−11645.

Chhabra, R. C.; Shambaugh, R. L. Experimental Measurements of Fiber Threadline Vibrations in the Melt-Blowing Process. Ind. Eng. Chem. Res. 1996, 35, 4366.

Chung, C.; Kumar, S. Onset of Whipping in the melt blowing process. *Journal of Non-Newtonain Fluid Mechanics.* 2013, *192*, 37-47

Ellison, C. J.; Phatak, A.; Giles, D. W.; Macosko, C. W.; Bates, F. S. Melt blown nanofibers: Fiber diameter distributions and onset of fiber breakup. Polymer 2007, 48, 3306.

Golzar, M.; Beyreuther, R.; Brunig, H.; Tandler, B.; Vogel, R. Online Temperature Measurement and Simultaneous Diameter Estimation of Fibers by Thermography of the Spinline in the Melt Spinning Process. *Adv. Polym. Technol*. 2004, *23* (3), 176-185.

Hassan, M. A.; Anantharamaiah, N.; Khan, S. A.; Pourdeyhimi, B. Computational Fluid Dynamics Simulations and Experiments of Meltblown Fibrous Media: New Die Designs to Enhance Fiber Attenuation and Filtration Quality. *Ind. Eng. Chem. Res.*, 2016, *55* (7), 2049-2058.

Y.D. Ju, R.L. Shambaugh, Air drag on fine filaments at oblique and normal angles to the air stream, Polym. Eng. Sci. 34 (1994) 958–964.

Krutka, H. M.; Shambaugh, R. L.; Papavassiliou, D. V. Effects of Die Geometry on the Flow Field of the Melt Blowing Process. *Ind. Eng. Chem. Res.* 2003, *42* (22), 5541

Krutka, H. M.; Shambaugh, R. L.; Papavassiliou, D. V. Effects of Temperature and Geometry on the Flow Field of the Melt Blowing Process. *Ind. Eng. Chem. Res.* 2004, *43* (15), 4199

Marla, V. R.; Shambaugh, R. L. Three-Dimensional Model of the Melt Blowing Process. *Ind. Eng. Chem. Res.* 2003, *42* (26), 6993-7005.

Marla, V. T.; Shambaugh, R. L.; Papavassiliou, D. V. Use of an Infrared Camera for Accurate Determination of the Temperature of Polymer Filaments. *Ind. Eng. Chem. Res.* 2007, *46* (1), 336–334.

Marla, Vishnu T., Shambaugh, Robert L., and Papavassiliou, Dimitrios, Online Measurement of Fiber Diameter and Temperature in the Melt Spinning and Melt Blowing Process. Ind. Eng. Chem. Res., 48 (2009), p 8736

Rao, R.; Shambaugh, R. L. Vibration and Stability in the Melt Blowing Process. *Ind. Eng. Chem. Res.* 1993, *32* (12), 3100-3111.

Shambaugh, B. R.; Papavassiliou, D. V.; Shambaugh, R. L. Next Generation Modeling of Melt Blowing. *Ind. Eng. Chem. Res.* 2011, 50 (21), 12233-12245.

Shambaugh, B. R.; Papavassiliou, D. V.; Shambaugh, R. L. Modifying Air Fields to Improve Melt Blowing. *Ind. Eng. Chem. Res.* 2012, 51, 3472-3483.

Shambaugh, R. L. A Macroscopic View of the Melt Blowing Process for Producing Microfibers. *Ind. Eng. Chem. Res*. 1988, 27, 2363

Shambaugh, R. L.; Krutty, J. D.; Singleton, S. M. Melt Blowing Dies with Louvers. *Ind. Eng. Chem. Res.*, 2015, *54* (51), 12999-13004.

Tan, D. H.; Herman, P. K.; Janakiraman, A.; Bates, F. S.; Kumar, S.; Macosko, C. W. Influence of Laval Nozzles on the Air Flow Field in Melt Blowing Apparatus. Chem. Eng. Sci. 2012, 80, 342−348.

Tate, B. D.; Shambaugh, R. L. Modified Dual Rectangular Jets for Fiber Production. *Ind. Eng. Chem. Res.* 1998, 37 (9), 3772-3779.

Tate, B. D.; Shambaugh, R. L. Temperature Fields below Melt Blowing Dies of Various Geometries. *Ind. Eng. Chem. Res.* 2004, 43 (17), 5405-5410.

Uyttendaele, M. A. J.; Shambaugh, R. L. Melt Blowing: General Equation Development and Experimental Verification. *AIChE J.* 1990, *36* (2), 175-186.

Rao, R.; Shambaugh, R. L. Vibration and Stability in the Melt Blowing Process. *Ind. Eng. Chem. Res.* 1993, *32* (12), 3100-3111

Xie, S.; Zeng, Y. Online Measurement of Fiber Whipping in the Melt-Blowing Process. Ind. Eng. Chem. Res. 2013, 52, 2116.

A. L. Yarin, S. Sinha-Ray, B. Pourdeyhimi, Meltblowing: ii-linear and nonlinear waves on viscoelastic polymer jets, J. Appl. Phys. 108 (2010) 034913

A.L. Yarin; V. M Entov, The dynamics of thin liquid jets in air, J. Fluid Mech. 140 (1984). 91-111

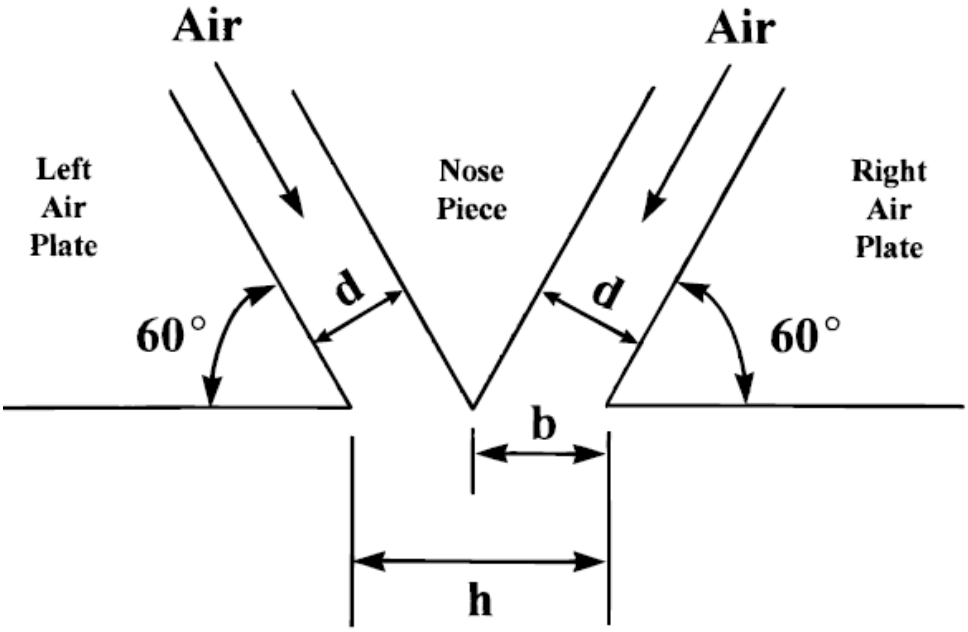

Fig. 1.1. Schematic depicting a sharp 60 degree melt blowing slot die. A blunt die would not have a sharp tip, but rather a flat one separating the two slots. This illustration was taken from Tate and Shambaugh (1998).

Effect of air constrictor length	0	Ref. Config.	1	L = 10 mm W= 20 mm	2	L = 20 mm W= 20 mm	3	L = 30 mm W= 20 mm
				1 cm, 1 cm		1 cm, 2 cm		1 cm, 3 cm
Effect of air constrictor width	4	W= 6 mm L = 10 mm	5	W= 10 mm L = 10 mm	6	W= 30 mm L = 10 mm	7	W= 40 mm L = 10 mm
		0.3 cm, 1 cm		0.5 cm, 1 cm		1.5 cm, 1 cm		2 cm, 1 cm
Effect of air constrictor angle	8	Φ = 45° L=30 mm	9	Φ = 60° L=30 mm	10	Φ = 72° L=30 mm	11	Φ = 90° L=30 mm
		45°		60°		72°		90°

Fig. 1.2. Tabulation of the different air constrictor positions. Figure taken from Hassan et al (2016).

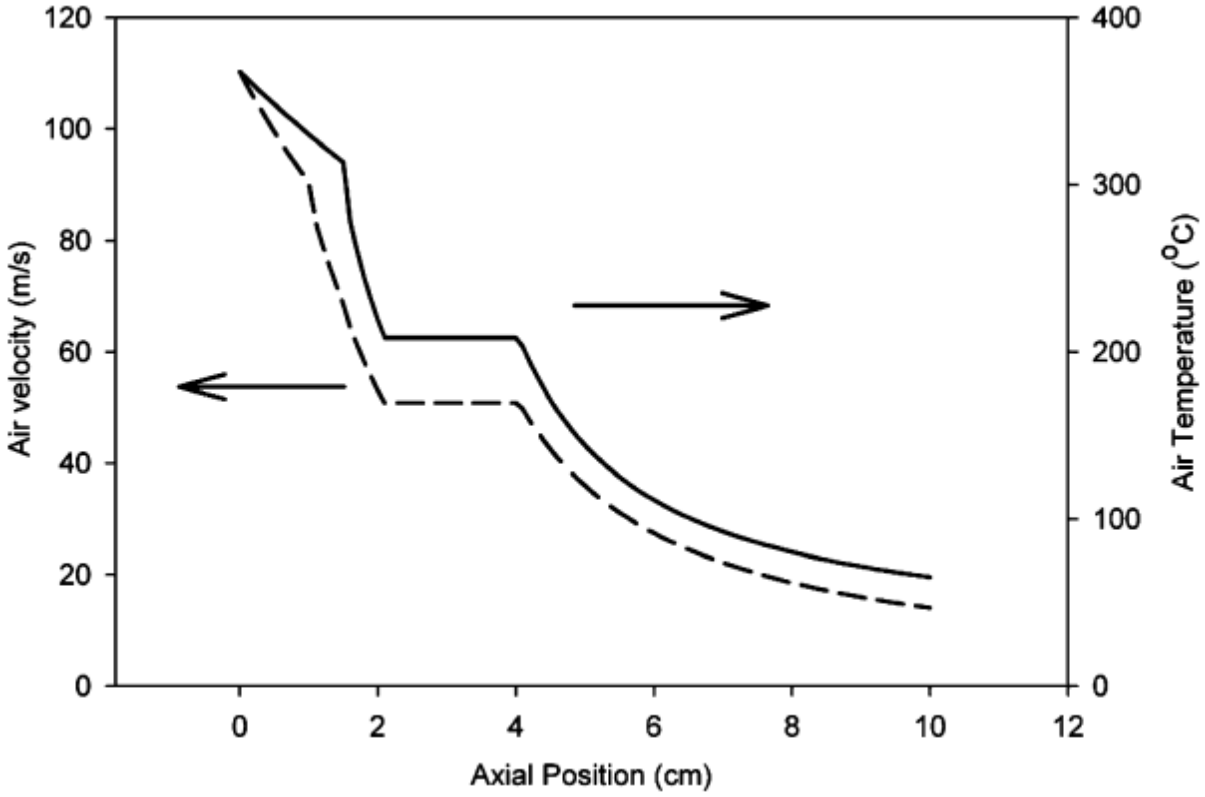

Fig. 1.3: The graph shows centerline air velocity and temperature correlations below the die with a "plateau" in the air field between 2 and 4 cm below the die face. This graph is taken from B. Shambaugh et al (2012).

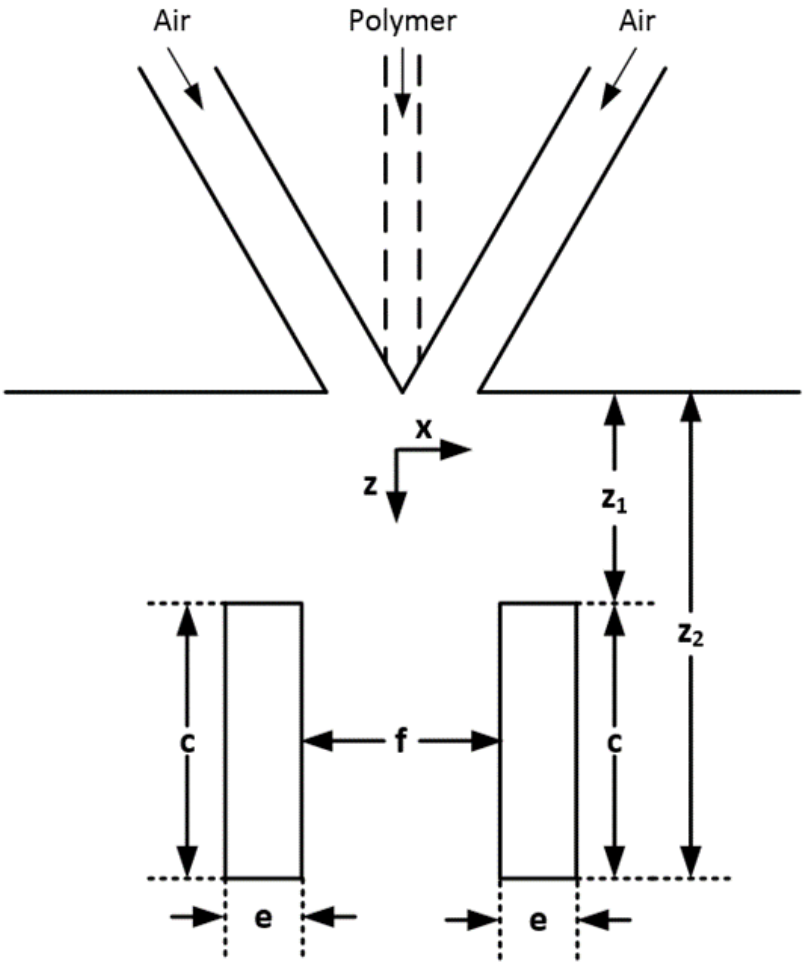

Fig. 1.4. Schematic of louvers in the air field below a melt blowing die.

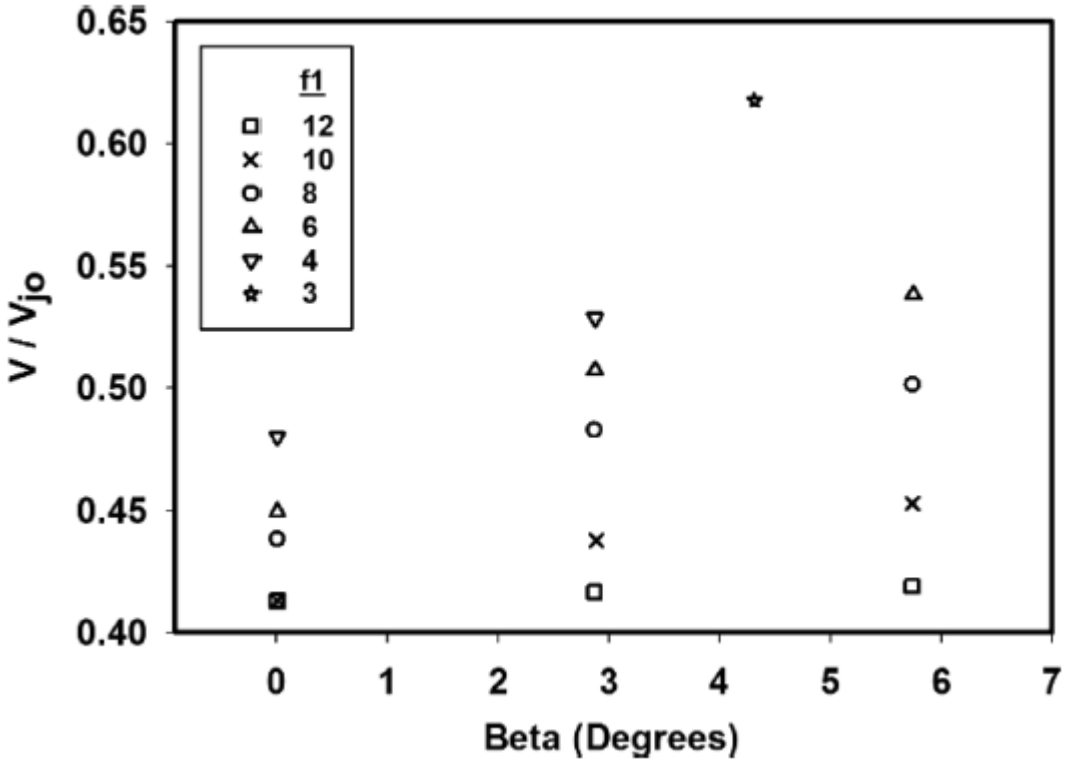

Fig. 1.5. This graph shows the effect of louver angle on the centerline air velocity. f_1 is the leading-edge separation. v/v_{jo} is the nondimensionalized air velocity where v_{jo} is the air velocity exiting the die. Beta is the angle of the louvers with respect to the plane parallel to the fiber filament. This graph is taken from Shambaugh et al. (2015).

CHAPTER 2

FIBER SPINNING WITH AIRFIELDS ENHANCED BY AIRFOIL LOUVERS

Abstract

Airfields are used in common polymer fiber spinning processes such as melt blowing and spunbonding. A pair of louvers was installed in the air flow field of a melt blowing slot die. Melt blowing runs were made with variable louver size (chord), louver separation, louver distance from the die face, the angle of the louvers relative to the die face, and air flowrate. Fibers were collected and fiber diameters were measured.

2.1 Introduction

In some fiber spinning processes, mechanical rolls provide the forwarding force that draws the polymer from the die orifice and attenuates the fiber to a fine diameter. In other spinning processes, such as melt blowing and spunbonding, airfields provide the forwarding force. Melt blowing and spunbonding are common processes used in industry to produce nonwoven fibers. In melt blowing, heated gas streams impinge upon molten filaments as the filaments emerge from a heated die. The force of the gas upon the filaments causes rapid attenuation of the filaments to fine diameters. The attenuated fibers are cooled and captured upon a mesh screen placed some distance away from the die. The resulting nonwoven mass of fibers can be used as a filter, an absorbent medium, as reinforcement, or numerous other uses. See Shambaugh[1], Buntin et al.[2], and Bresee and Ko[3].

The most common type of melt blowing die is the slot, or "Exxon" die; see Tate and Shambaugh[4]. The upper half of Fig. 2.1 is a cross-sectional view of such a die. The center piece is called the nosepiece. Two other pieces (the air plates or knives) are located to the left and right of the nosepiece. The spaces between the nosepiece and the air plates are the

air slots. Hot air flows through the two slots and impinges on polymer filaments as they emerge from the bottom of the nosepiece. The die width (in the direction perpendicular to the plane of Fig. 2.1) can range from centimeters to a meter or more. Fig. 2.1 shows a vertical orientation of the die wherein the air and polymer filaments move downward. Horizontal melt blowing is also common. The bottom half of Fig.2.1 shows louvers that are parallel. Fig. 2.2 shows louvers that are slanted inward toward the major axis of the die assembly. In Figures 2.1 and 2.2, the view of the two louvers is "end on", or cross-sectional.

The high velocity airfield is what drives the melt blowing process. As shown in Tate and Shambaugh[4], there is a rapid decay of the air velocity field below a melt blowing die. The temperature field decays similarly; see Tate and Shambaugh[5]. If this decay could be reduced, less air would be needed to fabricate the fibers. Using less air would improve the economics of melt blowing, since the cost of compressing, heating, and recycling the air is significant.

Shambaugh et al.[6,7] used an advanced model for melt blowing to predict the effects of velocity and temperature plateaus in the airfield below a melt blowing die. A plateau was (mathematically defined as) a vertical range over which the air velocity and temperature were constant. For wide plateaus placed near the die face, the effect of the plateau was substantial. Final (product) fiber diameters were reduced (by up to 50%) versus diameters for when there was no plateau. Typical model input conditions involved a 2 cm plateau placed between z = 2 and z = 4 cm (see the coordinate system shown on Fig. 2.1). More recently[8] these model predictions were tested by taking experimental air velocity measurements below a melt blowing die with louvers. The goal of the louvers

was to physically impose a plateau on the air field. These experiments only involved die operation with air on a die test stand – air, but no polymer, was run through the die. The results of Shambaugh et al.[8] showed that the air velocities below the louvers were as much as 60% higher than for when no louvers were present. Our goal in the present research is to show experimentally whether these higher air velocities do indeed produce significant reduction in fiber diameter.

This paper discusses the use of baffles, or louvers, placed below the melt blowing die; see the lower half of Fig. 2.1. As shown by the previous modeling work[7] and air velocity measurements[8], the louvers physically delay spreading of air in the space between the louvers. This delay should cause improved melt blowing. Other researchers have suggested equipment modifications to improve the air field below the melt blowing die. Shambaugh et al.[8] summarize some of these suggestions (see also Chelikani and Sparrow[9], Meyer et al.[10], Arseneau and Johnston[11], Gerking [12], Abbot and von Doenhoff [13], and Tan et al.[14]).

2.2 Experimental Equipment and Procedures

Except for the addition of the louvers, the experimental setup was very similar to that used by Marla et al.[15]. A Brabender extruder of 19.1 mm (0.75 in.) diameter and 381 mm length was used to melt and pressurize the polymer. The barrel had a 20:1 L/D ratio and a 3:1 compression ratio. The polymer exiting from the extruder was then fed to a modified Zenith pump that accurately metered molten polymer through a melt blowing slot die with a single polymer capillary. The polymer capillary had a diameter of 0.420 mm. The two air slots were set flush with the nosepiece, and the slot widths were 0.65 mm. Each slot had a length of 74.6 mm (2.94 in.). The die assembly was heated with two

250 W cartridge heaters. The louvers were held in place by an adjustable metal framework that allowed the louvers to be moved to a wide range of positions below the melt blowing die. A rotameter was used to measure the air feed rate. The polypropylene (PP) used in the experiments was 88 MFR Fina Dypro® isotactic polypropylene. This polymer had an M_w of 165 000 g/mol and an M_n of 41 500 g/mol. The base conditions for the experiments, unless otherwise specified, were m_p = 0.50 g/min, $T_{f,die}$ = 230 °C, and $T_{a,die}$ = 300 °C. Air flow rates of 80, 100, and 110 slpm (1.34×10^{-3}, 1.67×10^{-3}, and 1.84×10^{-3} m^3/s) were used in the experiments. Fiber samples were collected on a metal screen placed 0.45 meters below the melt blowing die. Fiber diameters were measured off-line with a Nikon Labaphot II optical microscope equipped with a micrometer eyepiece. For each fiber sample collected, 10 to 15 fiber diameters were measured.

The coordinate system for the experiments is shown in Fig. 2.1. The origin is at the center of the face of the die. The z direction is vertical, and the x direction is parallel to the face of the die. Perpendicular to the plane of Fig. 2.1 is the y direction (not shown).

Two louvers are shown in the bottom half of Fig. 2.1. These louvers are in the flow field below the melt blowing die. In Fig. 2.1 the view of the two louvers is “end on”, or cross-sectional. For our experimental work, the length of the louvers (in the direction perpendicular to the plane of the figure) was 256 mm (10 inches), and this length was centered such that the louvers completely covered the length of the die slots (the slots had a length of 74.6 mm in the y direction). For a commercial melt blowing die, where the slot length might be on the order of 1 meter, the louver length would be somewhat larger than 1 meter. In other words, for the louvers to completely control the flow field over the

entire length of a slot die, the louver lengths must always be longer than the slot length. The louvers were fabricated from aluminum.

Because of the turbulence and high drag coefficient of bluff bodies, it is advantageous to replace the rectangular louvers with aerodynamically smooth louvers. So, for our experimental work we did not use blunt louvers of the type shown in Figures 2.1 and 2.2. Instead, airfoil-shaped louvers were used. Specifically, the shape shown in Fig. 3 was used. In the parlance of airfoil design[13], the airfoil in Fig. 3 has an overall thickness "e" of 1.588 mm (1/16 of an inch) and a chord width "c" of 20 mm. This airfoil is symmetric (the top and bottom are mirror images of each other), has a half-circle leading edge, and has a trailing edge that is a simple wedge. For clarity, Fig. 2.3 has an exaggerated vertical scale. Fig. 2.4 shows four airfoils with the correct e/c ratio (i.e., the figure is true scale). Fig. 2.4 shows airfoils with chords of 12.5, 20, 30 and 40 mm (the 20 mm airfoil is the true scale version of the airfoil in Fig. 2.3). All four of these airfoils have the same half-circle leading edge and the same 10 mm long trailing edge that is dimensioned in Fig. 2.3. Of course, much more complicated airfoil designs could have been used[13], but the shapes shown in Figures 2.3 and 2.4 are simple to fabricate and proved to be effective in melt blowing. The four airfoils shown in Fig. 2.4 were airfoils used in our experiments.

2.3 Results and Discussion

As mentioned in the introduction, air flow rates of 80, 100, and 110 slpm (1.34×10^{-3}, 1.67×10^{-3}, and 1.84×10^{-3} m^3/s) were used in the experiments. Also mentioned earlier is that the chord widths tested were 12.5, 20, 30 and 40 mm; see Fig. 2.4.

Another important variable is z_1, the distance between the die face and the leading edge of the louvers (see Figures 2.1 and 2.2). For our experiments, z_1 values of 5, 10, 15 and 20 mm were used. The separation between the louvers is f_1 at the top of the louvers and f_2 at the bottom of the louvers (see Figures 2.1 and 2.2). Parallel louvers are when $f_1 = f_2 = f$. For our experiments, f_1 = 10, 8, and 6 mm were used. Similarly, for the bottom spacing, f_2 = 10, 8, and 6 mm were used. Table 2.1 is a summary of louver configurations and experimental conditions used.

For the positioning of the airfoils (Figures 2.1 and 2.2), values of f_1 and f_2 were based on measurements for a rectangular approximation of the airfoil shape. Specifically, the f_1 and f_2 values were set based on a rectangular louver with a thickness of 1.588 mm. Because of the rounding of the leading edges of the airfoils (see Figures 2.3 and 2.4), the actual distance between the tops of the airfoil pair is slightly greater than f_1. Likewise, because of the tapering of the trailing edges of the airfoils, the actual spacing between the trailing edges is slightly greater than f_2.

For Fig. 2.5 and elsewhere, the values of f_1 and f_2 are indicated by nomenclature of the form "f_1,f_2". Thus, "10,8" is shorthand for f_1 = 10 mm and f_2 = 8 mm. For our melt blowing runs, Fig. 2.5 shows how the distance between the die face and the louvers affects the fiber diameter. When no louvers are present, the fiber diameter was approximate 40 microns. However, there is a significant fiber diameter reduction when louvers are present. At minimum, the fiber diameter was reduced by 5 microns (to a final diameter of 35 microns) when the louvers were in the configuration f_1,f_2 = 8,8 . The largest fiber reduction was by 14 microns (to a final diameter of 26 microns) for a f_1,f_2 = 10,6 configuration. With louvers in the configuration f_1,f_2. = 10,10, the fiber diameters

steadily decreased as z_1 was decreased from 15 to 5 mm. The fiber diameters for z_1 values of 15 and 20 were similar at approximately 34 microns. Use of angled louvers with $f_1,f_2.$= 10,8, $f_1,f_2.$=10,6, and $f_1,f_2.$=6,6 also resulted in a general reduction in fiber diameters as z_1 was decreased from 20 to 5 mm. Furthermore, over the entire range of z_1 that was tested, $f_1,f_2.$= 10,8 and $f_1,f_2.$= 10,6 also gave lower fiber diameters than $f_1,f_2.$= 10,10. At the larger z_1 values of 15 and 20 mm, some of the angled configurations (with f2 < f1) precluded fiber collection because the fiber impacted and stuck to the louver walls. These configurations are summarized in Table 2.2.

Fig. 2.6 is similar to Fig. 2.5, except that the chord is 30 mm instead of 20 mm. There is a significant fiber diameter reduction when louvers are present. The minimum fiber reduction shown in Fig. 2.6 is 2.8 microns for f_1,f_2 = 8,8 at a z_1 value of 15 mm. The maximum fiber diameter reduction was 15.1 microns for the f_1,f_2 = 8,8 at a z_1 value of 5 mm. The three cases with f_1 = 10 mm show that the parallel louver case (($f_1,f_2.$= 10,10) gives finer diameters than the angled louver cases ($f_1,f_2.$= 10,8 and $f_1,f_2.$= 10,6). As described for Fig. 2.5, this is reverse of what happens when the chord is 20 mm (in Fig. 2.5, the angled cases produced finer diameters). Similarly, the two cases with f_1 = 8 mm show that the parallel louver case (($f_1,f_2.$= 8,8) gives finer diameters than the angled louver case ($f_1,f_2.$= 8,6). Parallel (($f_1,f_2.$= 6,6) louvers were also tested. This configuration gives slightly less diameter reduction than the $f_1,f_2.$= 10,10 configuration.

Of course, Fig. 2.6 only shows results for when fibers could be successfully collected. Table 2.2 is a summary of the conditions for which fibers could not be collected. Like the 20 mm chord, the 30 mm chord had fiber sticking difficulties for angled louvers at larger values of z_1 (see Table 2.2).

In addition to the runs shown in Figures 2.5 and 2.6, many additional runs were made wherein z_1 was varied. These additional runs indicated that (as shown in Figs 2.5 and 2.6) z_1 of 5 or10 mm gives excellent louver performance.

Fig. 2.7 shows the effect of f_1 on fiber diameter. In this graph the term $\Delta f = f_1 - f_2$ is used. Parallel louvers are when $\Delta f = 0$, and angled louvers are when $\Delta f > 0$. Data are shown for $\Delta f = 0$, 2 and 4 mm. The data indicate that $f_1 = 6$ and $f_1 = 10$ mm give superior performance, particularly for angled cases. For $f_1 = 10$ and 8 mm, the angled positions produced finer diameters than the parallel case.

Fig. 2.8 is similar to Fig .2.7, except the chord width is 30 mm instead of 20 mm. Unlike what happens for when c = 20 mm, the results show that the $f_1 = 8$ mm case gives better performance (smaller diameters) than the $f_1 = 6$ or $f_1 = 10$ mm cases. Also, the parallel cases produced finer fiber diameters than the angled cases.

An ANOVA statistical analysis can also be used in the analysis of two or more sets of data (while a t-test analyzes the difference between pairs of data sets). If we use ANOVA to examine the data sets for Figures 2.7 and 2.8, it is found that the fiber diameter results are closer together for different f_1 when the 30 mm chords are used (versus using the 20 mm chords).

Louver separations with $f_1 = 10$, 8, and 6 mm are included in Figures 2.7 and 2.8. The louver configuration of $f_1, f_2 = 6,4$ was attempted, but this configuration is not shown in these figures because of fiber sticking. Runs (data not shown) were also considered with $f_1 = 12$ and 4 mm. A louver spacing of 12 mm (or greater) is so wide that the airflow controlling effects of the louvers are minimal. Ergo, we did not run any tests with f_1 or f_2

> 10 mm. A louver spacing of 4 mm is inoperable because, with this narrow separation, the fibers entangle and stick to the louvers

Fig. 2.9 shows the effect of air flowrate on fiber diameter for 20 mm chords. Melt blowing is driven by the high velocity airfield, and the effect of this dominant force is shown in the figure. For all the configurations considered in Fig. 2.9, a roughly 40 percent increase in airflow resulted in a halving of the fiber diameter. Fig 2.9 also shows the air saving benefits that the louvers provide. For instance, without the louvers, fibers with a 46 micron diameter were produced at an air flowrate of 100 slpm. However, with a louver configuration of f_1,f_2 = 6,6, an air rate of 80 slpm produced close to the same fiber diameter (49 microns). Fig. 2.10 is similar to Fig. 2.9, except the chord width c = 30 mm. Fig. 10 also shows the dominant effect of air flowrate on fiber diameter.

For the base case (no louvers) in Figures 2.9 and 2.10, the fiber diameters were 72, 46, and 42 microns, respectively, for air flowrates of 80, 100, and 110 slpm. At these same flowrates the minimum fiber reductions for the 20 mm chord louvers were 10, 6, and 5 microns, respectively. For the 30 mm chord, the minimum fiber reductions were 21, 11, and 10 microns, respectively. The minimum reductions for the 30 mm chords are nearly double that for the 20 mm chords. (The minimum fiber reduction is the difference, at a set value of air flowrate, between the no louver diameter and the highest diameter value in the cluster of data points representing the louver configurations that were tested.)

Fig.2.11 shows the effect of chord length c on fiber diameter. In terms of diameter reduction, c = 30 mm is best. The c = 20 mm size also works well. For c = 12.5 mm, there were many runs with various values of z_1, f_1, and f_2. But diameter reductions were poor with this louver chord size, so these data were not included in this paper. For c = 40

mm, fibers were only collectable at a z_1 value of 5 mm, and, even then, there were some defects that were apparent in the collected web for angled configurations ($f_2 < f_1$) and closer separations (f_2=6 mm, f_1 =8 or 6). The defects in the web were the result of the polymer filament briefly sticking to the louver walls, detaching on the air flow, and entangling with more incoming polymer. This resulted in small woven fiber strands in the produced web. Larger z_1 values resulted in significant fiber sticking for this chord size.

Interestingly, the louver configuration (f_1,f_2) appears to have less effect for longer chords compared to configuration effects on shorter chords. This can be seen in Figs. 2.9 and 10 where the fiber diameters produced with 30 mm louvers were closer together than the fiber diameters produced with 20 mm chords. This is also seen in Fig. 2.11. For the 20 mm chords, Fig. 2.11 shows fiber diameters ranging from 36 to 28 microns, an 8 micron difference. For the 30 and 40 mm chords. the fiber diameters ranged, respectively, from 31 to 26 microns (a 5 micron difference) and 33 to 31 microns (a 2 micron difference).

Longer chords expose a greater length of fiber to a (relatively) constant air velocity compared to shorter chords. In the no louvers case, the air velocity steadily decays due to entrainment with ambient air. Shorter chords (c = 10 and 20 mm) perform better with increased angle as discussed above for Fig 2.7 and as can be seen in Fig. 2.11.

Figures 2.5-2.11 are representative of runs that were “operable” with no fiber entangling or sticking to the louvers. Also, these runs demonstrated the successful (in terms of less air required) use of louvers. Many other experimental runs were made, but data from these are not included in this paper. In general, these data were not included

because (a) the run conditions were not operable, or (b) the results were not as good in terms of fiber size reduction. In addition, some data were not included if there were any redundancy in results compared to the data in Figures 2.5-2.11

2.4 Conclusions

(1) When louver airfoils are placed below a melt blowing die, fiber diameter reductions of 30 percent or more are possible.

(2) Louvers work well if z_1, the distance between the louvers and the die face, is about 5 or 10 mm.

(3) The louvers' leading edges should have a separation (f_1) of about 6 to 10 mm.

(4) Parallel louvers ($f_1 = f_2$) work well, particularly for longer chords. Sometimes (depending on the chord width) angled louvers – with $f_2 < f_1$ – work even better, particularly for shorter chords.

(5) For the type of louver shown in Fig. 4, the louver chord should be about 20 or 30 mm.

Nomenclature

c = louver chord width as defined in Figures 1 and 2, mm

e = louver thickness as defined in Figures 1 and 2, mm

f = louver spacing for parallel louvers (see Fig. 1), mm

f_1 = louver spacing at top of louvers (see Fig. 2), mm

f_2 = louver spacing at bottom of louvers (see Fig. 2), mm

M_n = number average molecular weight of polymer, g/mol

M_p = polymer mass flowrate, g/min

M_w = weight average molecular weight of polymer, g/mol

$T_{a,die}$ = temperature of the air at the die face, °C

$T_{f,die}$ = temperature of polymer fiber at the die face, °C

v = velocity, m/s

v_{jo} = discharge velocity, m/s

x = Cartesian coordinate defined on Figures 1 and 2, mm

y = Cartesian coordinate direction perpendicular to the planes of Figures 1 and 2, mm

z = distance below the die as defined on Figures 1 and 2, mm

z_1 = distance from the die face to the leading edge of the louvers, mm

z_2 = distance from the die face to the trailing edge of the louvers, mm

Greek Symbols

α = angle as defined in Fig. 2, deg

Δf = f_1, f_2, mm

REFERENCES

(1) Shambaugh, R.L. A Macroscopic View of the Melt Blowing Process for Producing Microfibers. *Ind. Eng. Chem. Res*. 1988, *27*, 2363.

(2) Buntin, R. R.; Keller, J. P.; Harding, J. W. Nonwoven Mats by Melt Blowing. U.S. Patent 3,849,241, Nov 19, 1974.

(3) Bresee, R.R.; Ko, W.C. Fiber Formation During Melt Blowing. *International Nonwovens Journal*, Summer 2003, p. 21.

(4) Tate, B.D.; Shambaugh, R.L. Modified Dual Rectangular Jets for Fiber Production. *Ind. Eng. Chem. Res.* 1998, *37*(9), 3772-3779.

(5) Tate, B.D.; Shambaugh, R.L. Temperature Fields below Melt Blowing Dies of Various Geometries. *Ind. Eng. Chem. Res.* 2004, *43*(17), 5405-5410.

(6) Shambaugh, B. R.; Papavassiliou, D.V.; Shambaugh, R. L. Next-Generation Modeling of Melt Blowing. *Ind. Eng. Chem. Res*. 2011, *50*(21), 12233–12245.

(7) Shambaugh, B. R.; Papavassiliou, D.V.; Shambaugh, R. L. Modifying Air Fields to Improve Melt Blowing. *Ind. Eng. Chem. Res*. 2012, *51*, 3472-3483.

(8) Shambaugh, Robert L., Krutty, John D., and Singleton, Shawn M., "Melt Blowing Dies with Louvers", *Ind. Eng. Chem. Res*., 2015, 54 (51), pp 12999–13004.

(9) Chelikani, S.; Sparrow, E.M. Numerical Simulations of Plane-Wall Coanda Effects for Control of Fiber Trajectories in the Melt-Blown Process. *Ind. Eng. Chem. Res*, 2013, *52*, 11639-11645.

(10) Meyer, Daniel E.; Krueger, Dennis L; Bodaghi, Hassan "Oriented Melt-Blown Fibers, Processes for Making Such Fibers, and Webs Made from Such Fibers" U.S. Patent 4,988,560, Jan. 29, 1991

(11) Arseneau, Warren; Johnston, Gord W. "Method of Melt Blowing Polymer Filaments through Alternating Slots" U.S. patent 6,562,282, May 13, 2003

(12) Gerking, Luder "Method and device for the production of an essentially continuous fine fiber" U.S. patent 6,800,226, October 5, 2004

(13) Abbott, I.H.; von Doenhoff, A. E. *Theory of Wing Sections*; Dover Publications, 1959.

(14) Tan, D. H; Herman, P. K.; Janakiraman, A.; Bates, F. S.; Kumar S.; Macosko, C.W. Influence of Laval Nozzles on the Air Flow Field in Melt Blowing Apparatus, *Chem. Eng. Sci*. 2012, *80*, 342–348.

(15) Marla, V.T., Shambaugh, R.L., and Papavassiliou, D.V., Online Measurement of Fiber Diameter and Temperature in the Melt-Spinning and Melt-Blowing Processes, *Ind. Eng. Chem. Res*., 2009, *48*(18), 8736-8744.

Table 2.1. The experimental conditions used in our study. The experimental conditions with the louvers included louver chord length c, leading-edge distance z_1 below the die, air flowrate Q_a, and configurations f_1,f_2 (which are the leading-edge/ trailing-edge separations of the louvers). As indicated in the table, 198 runs were made with 198 different arrangements of c, z_1, Q_a, and f_1,f_2.

Experimental Conditions Used in Our Study	
c(mm)	12.5 20 30 40
z_1 (mm)	5 10 15 20
Q_a (liters/ min)	80 100 110
f_1, f_2	10,10 10,8 10,6 8,8 8,6 6,6
Number of Combinations	198
Notes	All runs were done at a polymer flowrate of 0.50 g/min, polymer temperature of 230 C, and air temperature of 300 C The 4 cm chords were only evaluated at z_1 =5 mm. The z_1=20 mm distance below the die was used for 2 cm chords.

Table 2.2. The louver positions and configurations where fibers could not be collected due to the fiber sticking to the louver walls.

Louver Configurations where fibers were not collectable		
c (mm)	**z_1 (mm)**	**f_1,f_2**
20	20	10,6 8,6 6,6
	15	10,6 8,6 6,6
30	15	10,8 10,6 8,6 6,6
	10	8,6
40	5	10,6
	10	All configurations
	15	All configurations

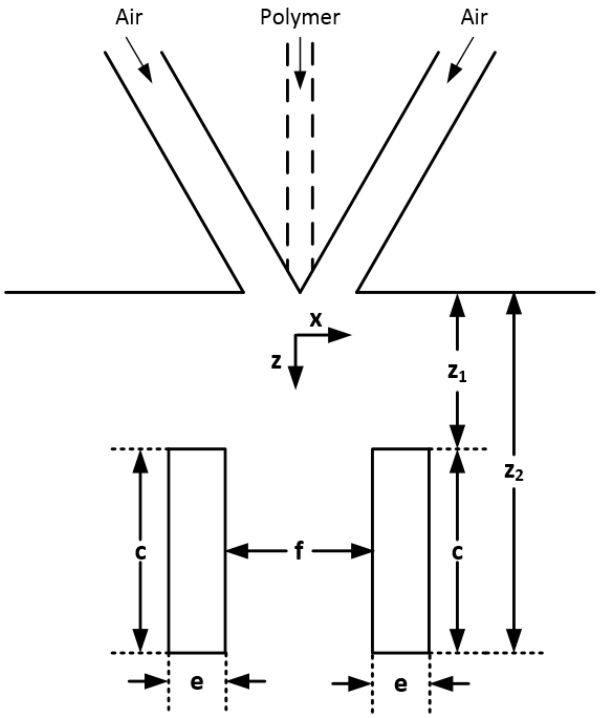

Fig. 2.1. Melt blowing die with louvers added.

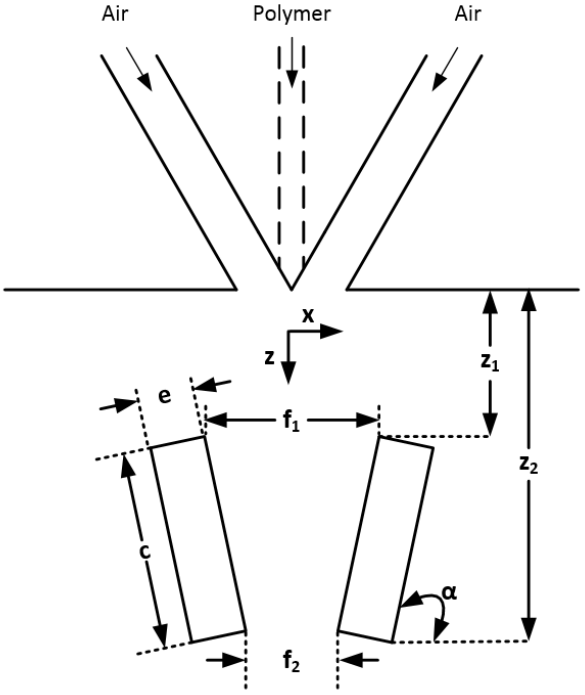

Fig. 2.2 Melt blowing die with angled louvers.

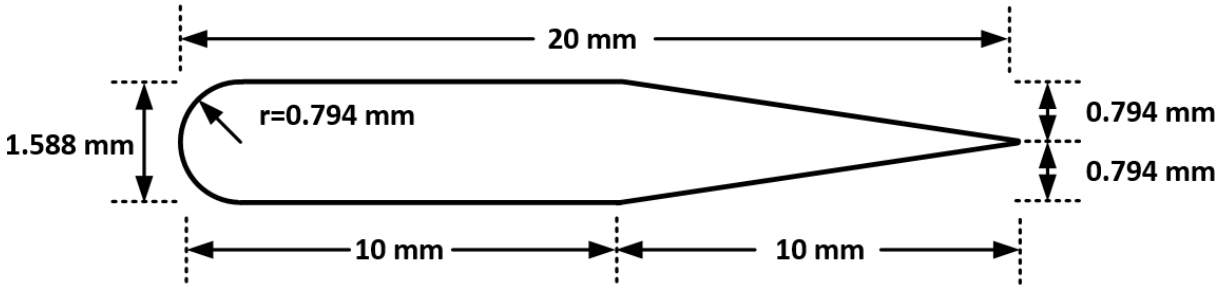

Fig 2.3. Airfoil louver. In this cross-sectional view, the vertical scale is exaggerated (the vertical scale is twice as large as the horizontal scale). For this airfoil, e = 1.588 mm and c = 20.0 mm (see Fig. 2.1 and 2.2).

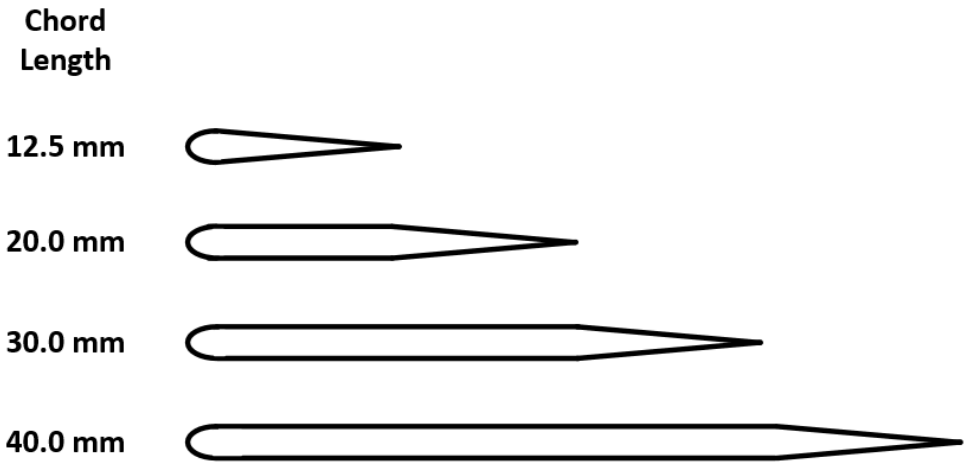

Fig. 2.4. Cross-sectional view of louvers with chords of 1.25, 2, 3, and 4 cm. These drawings show the true aspect ratio (the ratio of airfoil thickness e to airfoil chord c).

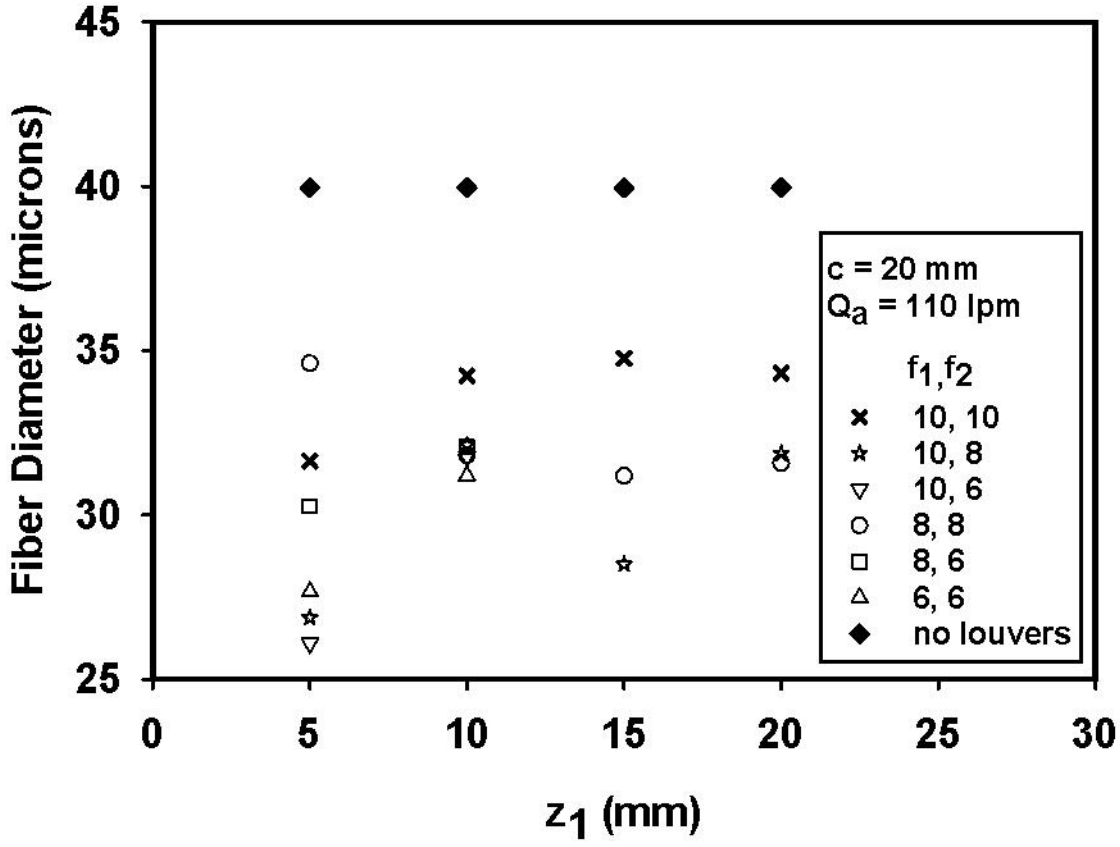

Fig. 2.5. The effect of z_1 on fiber diameter. For this graph, c = 20 mm and air flowrate = 110 L/min. Curves are shown for each f_1, f_2 configuration. The polymer temperature was 230 °C, the air temperature was 300 °C, and the polymer flowrate was 0.5 g/min.

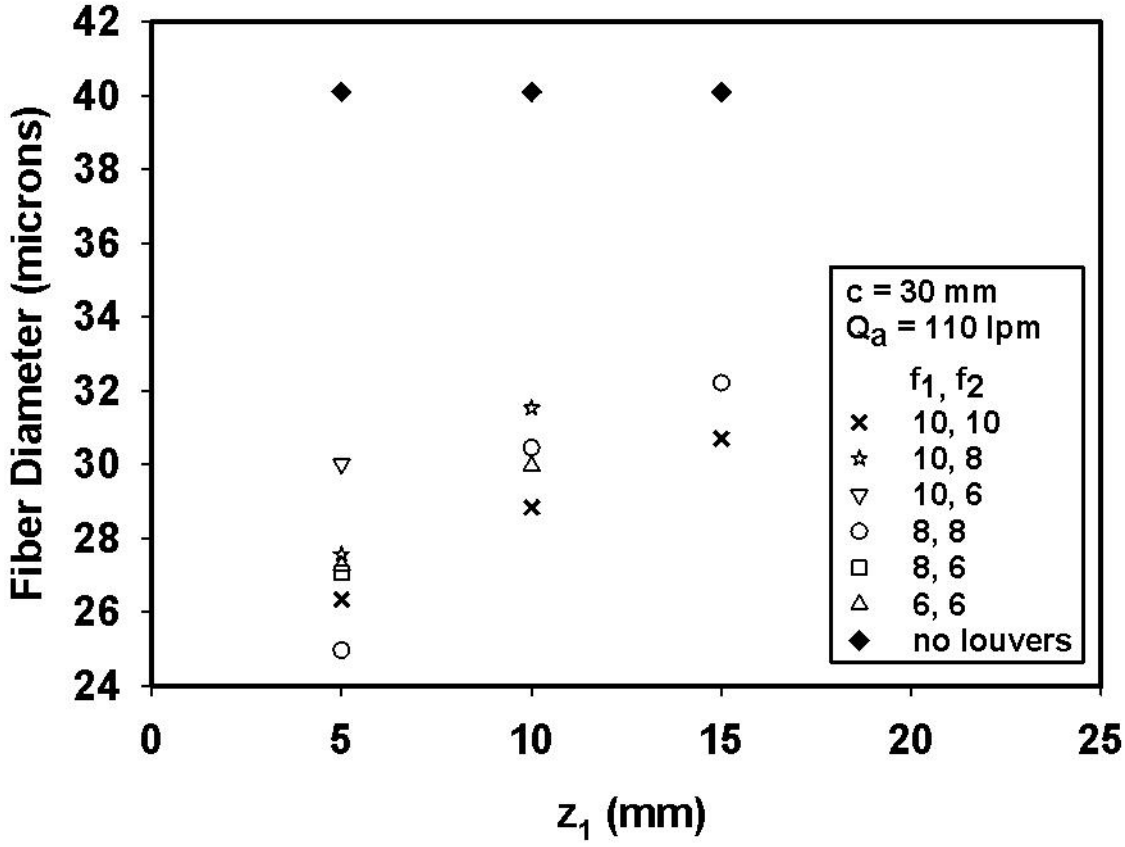

Fig. 2.6. The same as Fig. 2.5, except the chord width is c = 30 mm.

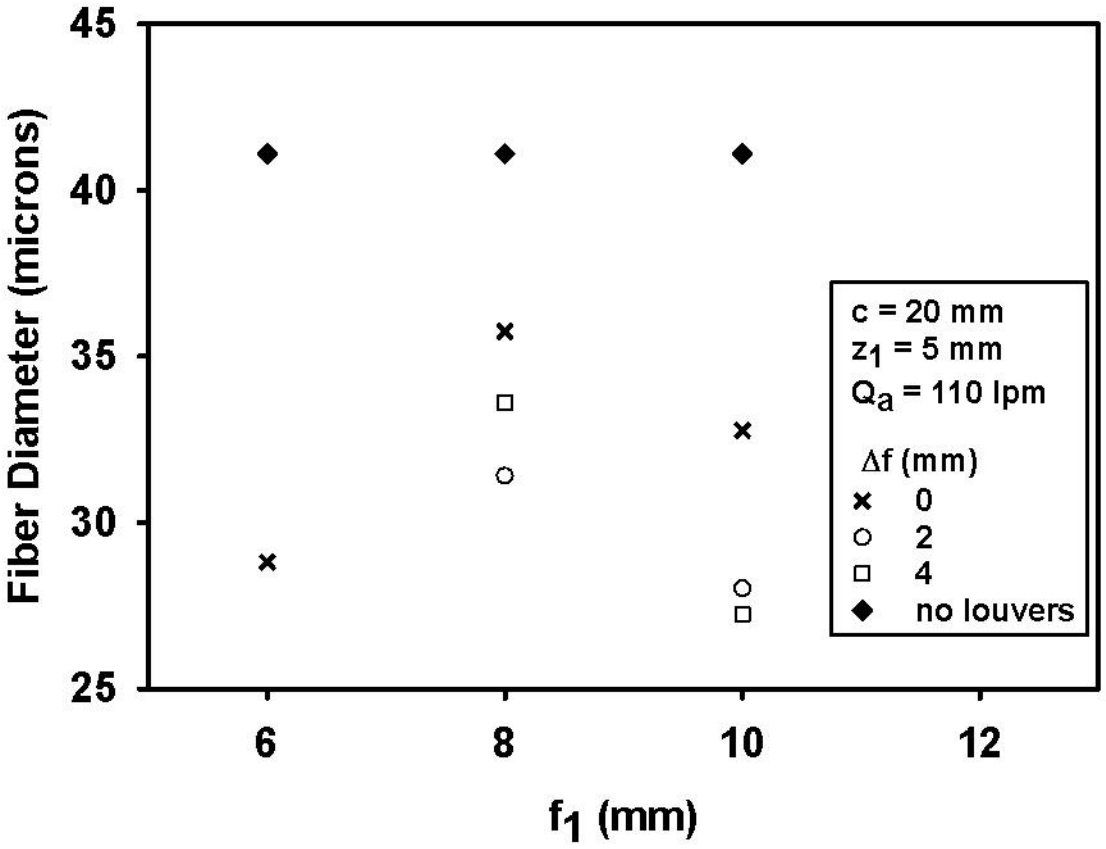

Fig. 2.7. The effect of f_1 on fiber diameter. For this graph, c = 20 mm, z_1 = 5 mm, and air flowrate = 110 L/min. Curves are shown for $\Delta f = f_1 - f_2 = 0$, 2 and 4 mm. The polymer temperature was 230 °C, the air temperature was 300 °C, and the polymer flowrate was 0.5 g/min.

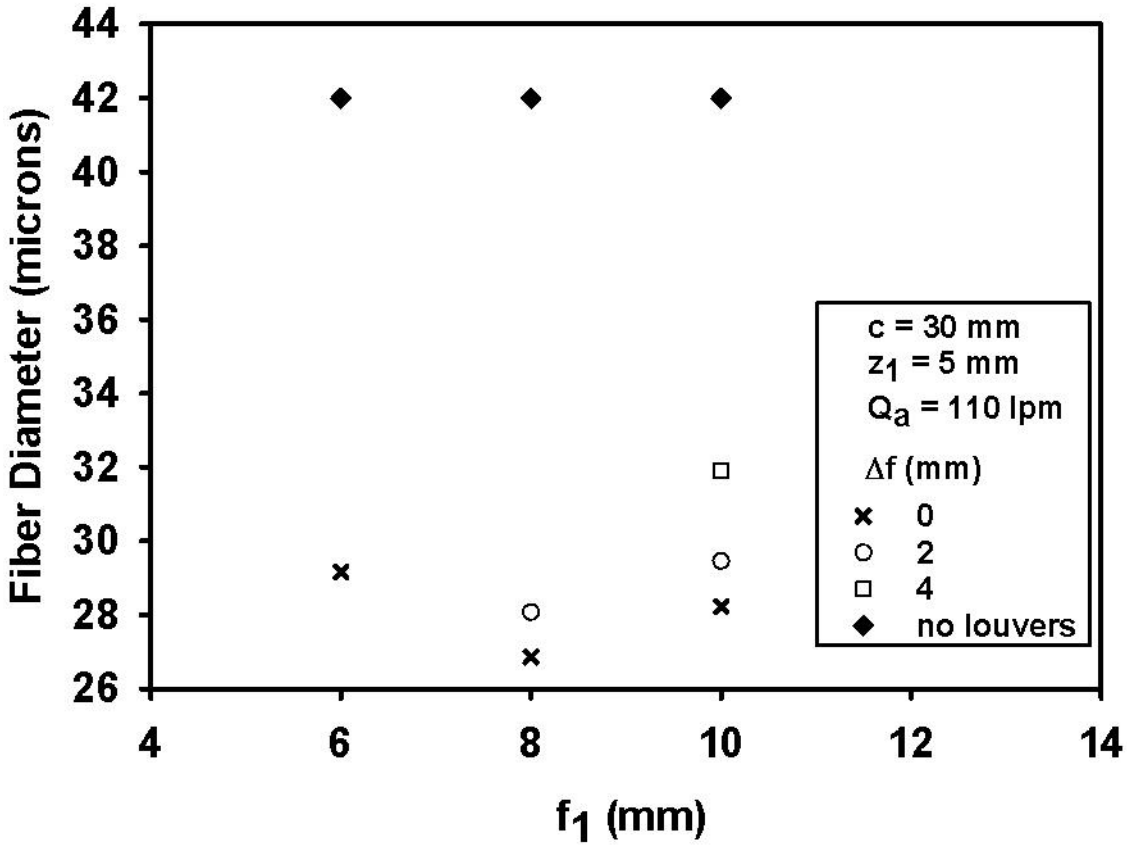

Fig. 2.8. The same as Fig. 2.7, except the chord width is c = 30 mm.

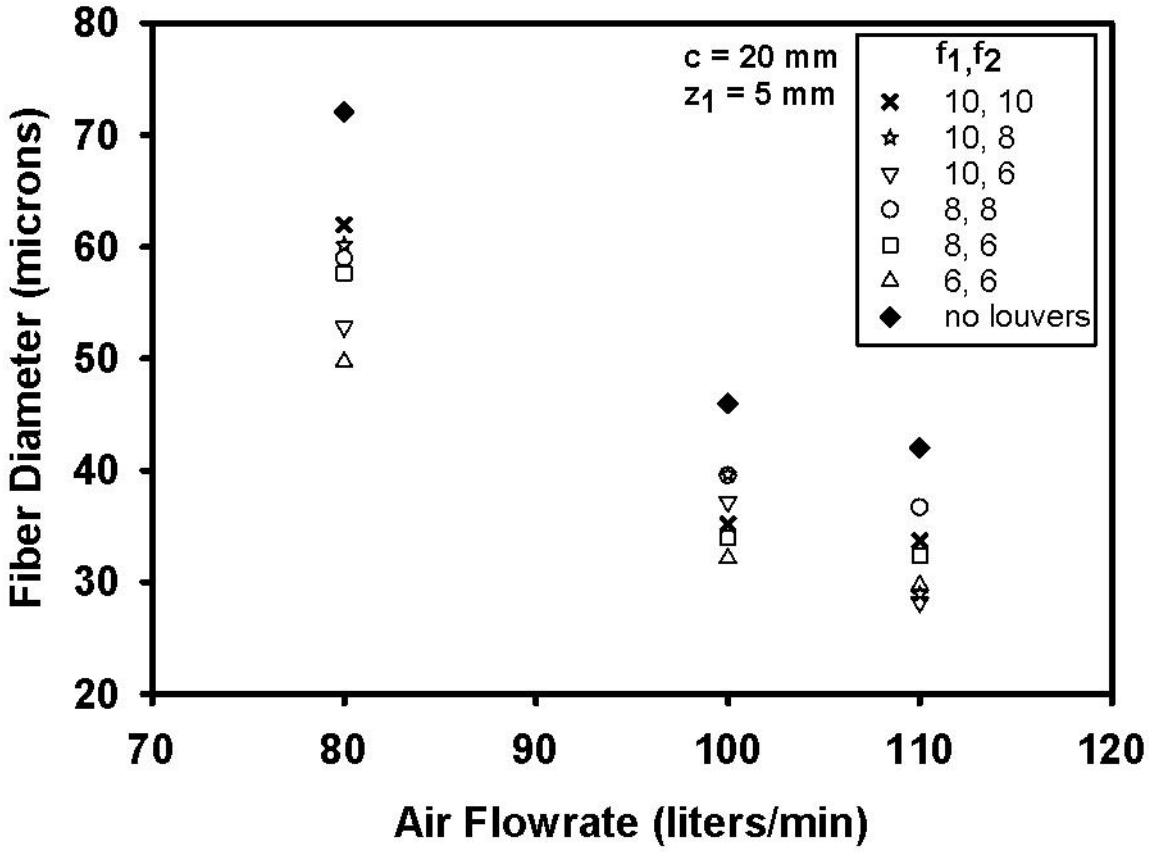

Fig. 2.9. The effect of air flowrate on fiber diameter. For this graph, c = 20 mm and z_1 = 5 mm. Curves are shown for each f_1, f_2 configuration. The polymer temperature was 230 °C, the air temperature was 300 °C, and the polymer flowrate was 0.5 g/min.

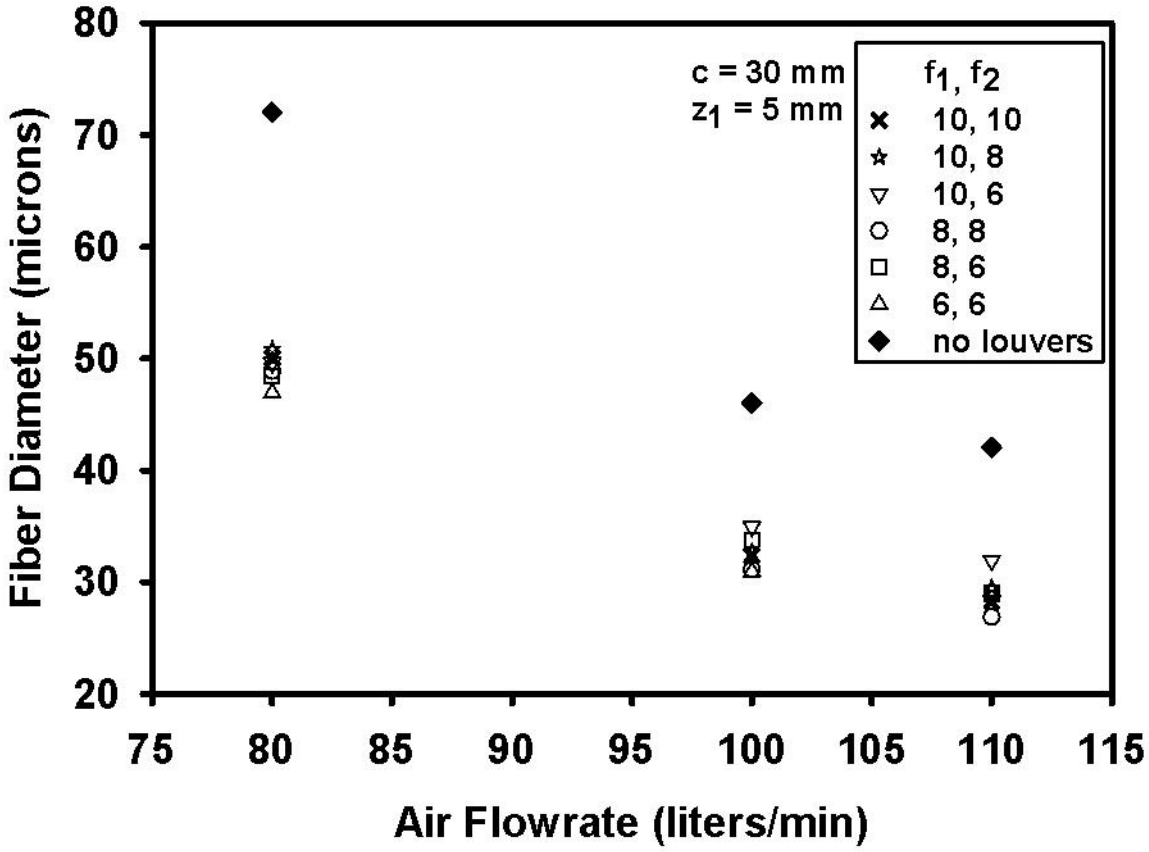

Fig. 2.10. The same as Fig. 2.9, except the chord width is c = 30 mm.

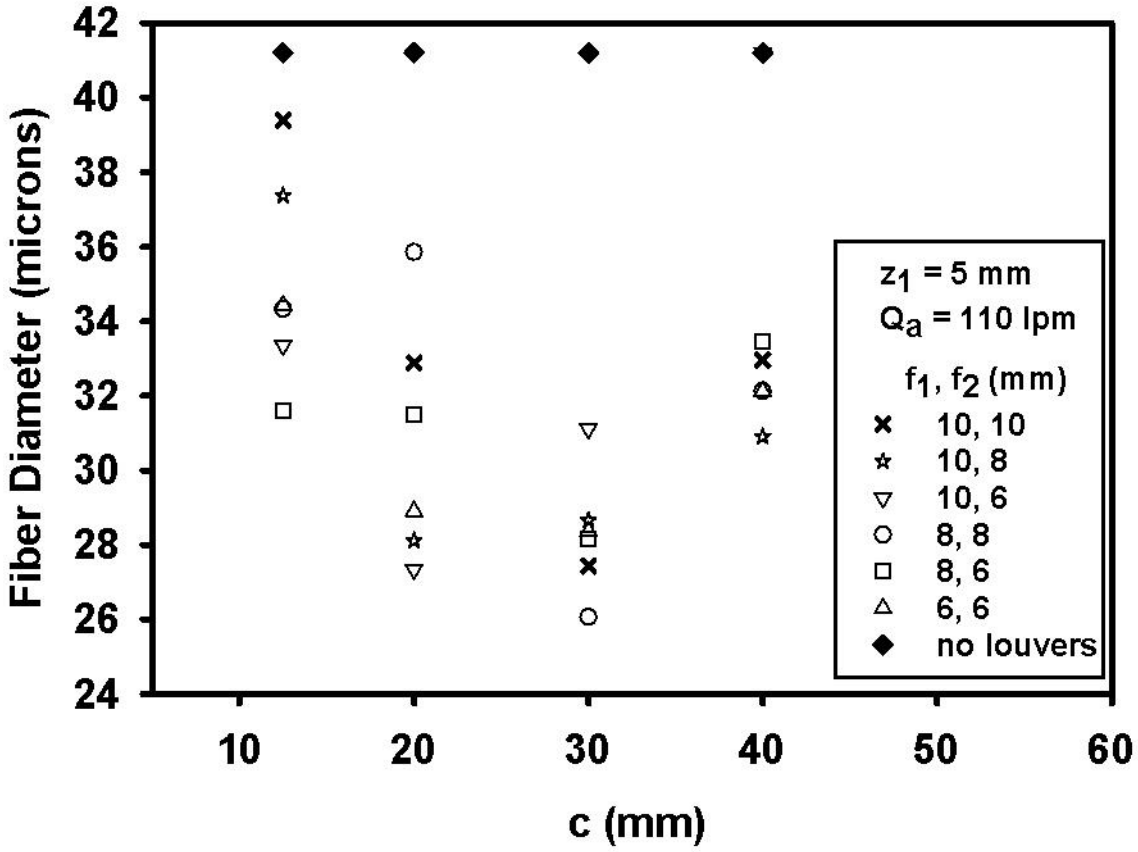

Fig. 2.11. The effect of chord length c on fiber diameter. For this graph z_1 = 5 mm and air flowrate = 110 L/min. Curves are shown for each f_1, f_2 configuration. The polymer temperature was 230 °C, the air temperature was 300 °C, and the polymer flowrate was 0.5 g/min.

CHAPTER 3

FIBER MOTION WITH LOUVERS IN THE AIR FIELD

Abstract

Fiber frequency and amplitude are important parameters in studying the fiber motion in the melt blowing process. These parameters were studied for when airfoil louvers are placed below the die. High speed photography was used to collect fiber positional data over time. These data were used to calculate fiber frequency and amplitude.

3.1 Introduction

Melt blowing is a single-step process that produces a nonwoven sheet of fine fibers. The melt blowing process with a slot die of the "Exxon" type has dual converging air jets that impinge upon the fiber, resulting in significant attenuation. Fibers produced from this process typically have diameters ranging from 0.1 to 10 microns, but fibers in the nanometer range can also be produced (Shambaugh, 1988; Hassan, 2016). Applications for melt blown mats include filtration and sorbent materials.

In order to control and optimize the melt blowing process, an understanding of fiber motion is important. The whipping or vibrations of the fiber filament in the air field affects the quality of the nonwoven product that is collected below the die. Furthermore, wild whipping or vibrations can jam the melt blowing equipment or cause defects in the produced web. As the fiber whips back and forth in the air jet, the fiber is also experiencing a drag force not only due to the air velocity in the axial direction, but also due to the air velocity normal to the fiber and at oblique angles to the fiber (Ju and Shambaugh, 1994; Ellison et al., 2007). This brings into importance variables such as

fiber vibrational frequency and amplitude. These variables can affect fiber attenuation, uniformity of fiber laydown, and defect formation.

Previous works in studying fiber motion have involved both modeling and experimentally studying the frequency and amplitude of the vibrating fiber. Rao and Shambaugh (1993) and Marla and Shambaugh (2003) developed two- and three-dimensional models for the motion of the threadline. Their work was later experimentally confirmed by Beard et al. (2007), and more recently by Xie and Zeng (2013). Both Beard et al. (2007) and Xie and Zeng (2013) used high speed photography to study the amplitude and frequency of the threadline. In general, it has been found that fiber frequency:

- Increases with increasing air flowrate
- Increases with decreasing polymer flowrate
- Decreases with increasing polymer temperature

Fiber amplitude has been found to:

- Increase with increasing air flow rate
- Increase with decreasing polymer flow rate
- Increase with increasing distance below the die.

Chung and Kumar (2013) studied the onset of fiber breakage due to violent fiber whipping. They used a quasi-one-dimensional model to study initial whipping characteristics.

In the work described in Chapter 2, louvers were placed in the melt blowing air field to approximate a "plateau" of constant air velocity and temperature that would expose the threadline to higher air velocities and temperatures for longer distances below the die and thereby elicit greater attenuation (Fig 2.1 and Fig 2.2). Finer diameters were

achieved with louvers in the air field (see Chapter 2). With a modification to the air field, several questions are raised. In particular, with louvers present, does the fiber amplitude and frequency change? If amplitude and frequency change, are these changes related to the decrease in fiber diameter caused by the louvers? Also, since some louver arrangements resulted in fiber sticking, can we relate this sticking to amplitude and frequency? This chapter describes the use of high speed photography to study the frequency and amplitude of the threadline with louvers in the air field.

3.2 The High-Speed Camera and Analysis Procedure

A Redlake Motion Pro HS-4 high speed video camera was used to capture video of the fiber vibrating in the air field above, between, and below the louvers. A full frame had a resolution of 512 x 512 pixels. It is possible to obtain this resolution at frame rates up to 5130 frames per second. Beyond 5130 frames per second, the cameras resolution steadily decreases. At the camera's highest frame rate of 150,000 frames per second, the resolution is 16 x 512 pixels (Beard, 2007). For our work, a frame rate of 2000 frames per second was found adequate for recording the frequency and amplitude of the melt blown fiber. This rate also allowed for a full resolution frame.

A Nikon 105 mm macro lens was attached to the camera and was used in 1:2 reproduction ratio mode. This lens had a field of view angle of 6° in the vertical and horizontal directions. The lens face was kept at a working distance of 48 cm from the fiber. This provided sufficient room to move the louver device in and out of the camera's field and to safely clean the louvers of sticking fibers when the louvers were moved into position below the die. A 4 x 4 cm image size was used during the photography. Additional lighting was needed for an adequate image of the fiber, so four Bayco 8.5 inch

clamp-on flood lamps were used to light up the fiber. The bulbs in the lamps were 100 watt (equivalent) LED bulbs. For the lens aperture size, a f-stop of 4.8 was used. This allowed for enough light to enter the camera while also allowing large enough depth of field to view the fiber vibrating back and forth in the y direction. Offline tests with the lens showed that, with a lens working distance of 48 cm, the depth of field for the lens ranged from 46.5 to 49.5 cm. The camera was paced on a tripod that could be adjusted vertically. The "above" videos imaged the z = 0 to 4 cm region, however, due to the louver device blocking the camera line of sight, only the z= 0.5 to 1.5 cm region was analyzed in the video. The "below" videos imaged the z = 8 to 12 cm region.

The camera did not have any external controls, but rather was controlled through communication with a laptop computer via a USB connection. The software used to record videos and control the camera settings was *IDT Motion Studio* from Integrated Design Tools, Inc. Within this software, the frame rate, exposure time, and recording time could be specified. A 2000 frames per second frame rate, 150 second exposure time, and a 3 second recording time were used for these experiments. These settings produced videos with 6000 frames. After a video was recorded, the software would save the video as an *.avi* file. Typical saving times were about 4 to 5 minutes per video. See Appendix III for more information on the usage of *Motion Studio*.

The videos were uploaded to *ProAnalyst*, a motion analysis software by Xcitex. The 1D tracking feature was used to track the motion of the fiber along a horizontal line at a distance *z* below the die head. These tracking lines were placed in the image at each z distance of 0.5, 1, 1.5, 9, 10, and 11 cm below the die. Intermediate values were not used since the bracket holding the louvers blocked the camera line of sight. The initial

positional data were in pixels, and these data were converted to millimeters through a user-specified calibration. The fiber position over time data were then exported from the software to an Excel spreadsheet to calculate the frequency and amplitude of the fiber vibrations in a procedure similar to that described by Beard et al.(2007). The 6000 frames were divided into sets of 600 frames for a total of 10 frequency and amplitude calculations per video. A student's t-test with a criterion t-value of 0.05 was then applied to verify the significant difference in the average frequency and amplitude with and without the louvers. A *Visual Basic* code was developed to automate these calculations (for more details see Appendix III for *ProAnalyst* and Appendix IV for calculation code).

3.3 Experimental Details

A Brabender extruder with a diameter of 19.1 mm and a length of 381 mm was used to melt and pressurize polymer for melt blowing. The extruder had a barrel L/D ratio of 20:1 and a compression ratio of 3:1. A modified Zenith pump was attached to the extruder and used to accurately regulate the polymer mass flowrate. A single-hole slot die was used for all experiments. The die had a polymer capillary diameter of 0.420 mm. The two air slots were 74.6 mm in length with a slot width of 0.65 mm. The slot die had a flush sharp nose configuration with a slot to die face angle of 60°. The polymer used was 88 MFR fina Dypro isotatic polypropylene with a M_w of 165,000 g/mol and a M_n of 41, 500 g/mol. Fibers were collected on a metal screen located 0.45 m below the die head. Compressed air was fed through a heater such that the air exiting the die was maintained at 300 °C. Air flowrates were measured using Dwyer Digital Pressure Gauges and a set of correlations developed to determine the volumetric flowrate of the air in liters per minute when the heaters were set to a temperature of 300 °C. All experiments were done

at a mass flowrate of 0.5 grams/min and air flowrates of 80, 100, and 110 slpm (1.34 x 10^{-3}, 1.67 x 10^{-3}, and 1.84 x 10^{-3} m^3/s). The temperature of the air and the polymer at the die face were maintained at 300 °C and 230 °C, respectively.

For each of the videos collected with the Redlake camera, the louvers were placed in the air field below the die. Each louver had a thickness of 1.588 mm (1/16 in) and a chord length *c* of either 12.5, 20, 30, or 40mm. The trailing-edge portion of the chord lengths ended in a 10 mm taper length; see Figure 2.4. The leading-edges were also rounded to reduce the air drag on the louvers in the turbulent air field. The length of the louvers (in the plane parallel to the die face) is 256 mm. More details on the louvers and their nomenclature can be found in the preceding chapter. The louvers were placed at different distances below the die head such that the leading edges were at z_1 = 5, 10, and 15 mm below the die head. The leading-edge separations were at f_1 = 10, 8, and 6 mm. Similarly, trailing-edge separations were f_2 = 10, 8, and 6 mm. Several parallel experiments were done such that the leading and trailing-edges separations were equal (f_1 = f_2). Several angled cases were also done where $f_1 > f_2$.

For each experiment set, four videos were taken. Two videos were taken at the "above" position (z= 0.5 to 1.5 cm), one video with and one video without the use of louvers. Two videos were similarly taken at the "below" position (z = 9 to 11 cm). Intermediate z values (z = 2 to 8.5 cm) could not be obtained as the current louver bracket and device block the camera line of sight. Two sets of fiber samples were taken before and after recording the videos for a total of four fiber samples. Two samples were produced when using the louvers, and two were produced without using the louvers. The diameters of the fibers were then measured off-line with a Nikon optical microscope and

micrometer eyepiece. For each diameter determination, at least 10 separate measurements were taken. A student's t-test was then performed on each collection set to verify that the mean diameters were significantly different when using the louvers compared to not using the louvers.

3.4 Results and Discussion

The frequency and amplitude for each video was calculated by first shifting the exported positional data such that the oscillations centered about the x-axis. Fig. 3.1a is a truncated portion of a single video's data, and Fig 3.1b shows this shifting. Fig. 3.1c is a further truncation of Fig. 3.1b, and will be used to demonstrate the calculation of frequency and amplitude. The *Visual Basic* code was used to determine the time points immediately after the fiber crossed the centerline. These points were considered the "zeros" of Fig. 3.1c. The absolute extrema between (and including) each "zero" point was then determined. Points A, E, I, K, and O are considered maxima and points C, G, J, M, and Q are considered minima. The absolute value of the amplitudes at these maxima and minima were averaged to determine the amplitude of the fiber for the video. The frequency was determined by taking the time difference between adjacent extrema points, multiplying this by two to determine the cycle period, and then taking the inverse. For more details see Appendix IV. As mentioned above, chord lengths of 20 and 30 mm in the air field were studied at different leading edge distances below the die of z_1 = 5, 10, and 15 mm.

3.4.1 Fiber Frequency

Fig. 3.2, 3.3, and 3.4 show the frequency of the fiber filament with increasing z distance below the die for different louver configurations (f_1,f_2). Fig. 3.3 and 3.4 divide

Fig. 3.2 into two regions (z = 0.5 to 1.5 cm and z= 9 to 11 cm) for easier viewing. Both the 20 and 30 mm chords are shown for a z_1 value of 5 mm. Base case frequencies were 147 ± 11, 150 ± 10, 152 ± 10, 176 ± 16, 165 ± 17, and 155± 17 Hz, respectively, for z distances of 0.5, 1, 1.5, 9, 10, and 11 cm below the die. The frequency slightly increases with increasing distance below the die, reaches a maximum somewhere between 2 and 8.5 cm, and then begins to decrease. This matches the results of Beard et al. (2007) who found a peak in frequency at approximately 5 cm below the die for an air flowrate of 100 slpm.

As was mentioned above, a t-test was performed to compare the louver frequency to the base case without louvers. Ten frequency calculations were made per video at each z distance below the die. The average of these calculations was then examined. Standard deviations ranged from 5 to 20 Hz for the z = 0.5 to 1.5 cm region below the die and 9 to 20 Hz for the z = 9 to 11 cm region. There were several cases where a t-test signified that the frequencies determined with the louvers were not significantly different than the frequencies determined without the louvers. These cases are summarized in Table 3.1. The t-value criterion was 0.05; therefore, a t-test that resulted in a number greater than 0.05 signified that the average frequency produced with the louvers was not significantly different than that produced without the louvers.

In the region of the louvers for when z = 0.5 to 1.5 (see Fig. 3.3), all cases were found to be significantly different with the t-test. The frequency for each louver configuration was greater than the frequency for the base case (no louvers). The greatest frequencies were found at the closest louver position below the die (z_1 = z = 0.5 cm) with the following conditions:

(1) 328 ± 20 Hz for c=30 mm and f_1,f_2 = 8,8

(2) 301 ± 13 Hz for c = 30 mm and f_1,f_2 = 10,8

(3) 260 ± 13 Hz for c = 20 mm and f_1,f_2 = 13

Excluding these three runs, the next highest frequencies of about 200 Hz were observed for the 30 mm chord configurations and the angled 20 mm chord configurations. The lowest frequencies were observed for the 20 mm chord with f_1,f_2 = 10,10 . The lowest frequencies were 162 ± 10, 170 ± 15, and 170 ± 9 Hz.

In the region below the louvers with z = 9 to 11 cm (see Fig. 3.4), the parallel configurations for the 30 mm chord produced frequencies that were insignificantly different from the no louver case. The f_1,f_2 = 10, 8 configuration for this chord was on the edge of passing the t-test.

The greatest frequencies were seen for the 20 mm chords in the louver configurations f_1,f_2 = 8,6 with frequencies of 224 ± 14 , 213 ± 9, and 200 ± 15 Hz for z= 9, 10, and 11 cm, respectively. Closely following this position were the louver configurations of f_1,f_2 = 10,6 6,6 and 10,8 for the 20 mm chords. The only case where the frequency was lower than the base case frequency was for 20 mm chords in the f_1,f_2 = 10,10 configuration in the region below the louvers. Its frequency was roughly 45 Hz lower than the base case. There was a slight downward trend with increasing z for this position in the z =0.5 to 1.5 cm region, perhaps resulting in the frequency being lower in the z = 9 to 11 cm range.

Figs 3.5, 3.6, and 3.7 are the same as Figures 3.3-3.5, except the louvers are at a leading edge distance of z_1 = 10 mm. In Fig. 3.6, the frequencies were above the base case frequencies in the region near the die, except for one outlier of 66 Hz produced with

20 mm chords at f_1,f_2 =8,8. Another outlier was produced for 20 mm chords at f_1,f_2 =8,6 with a frequency of 268 ± 15 Hz. Both outliers occurred at 0.5 cm below the die. Excluding these two points, the greatest frequencies were observed for the 30 mm configurations f_1,f_2 = 10,10 and 8,8 and the 20 mm configurations of 10,8 and 10,6. The parallel 20 mm configurations, as well as the f_1,f_2 = 8, 6 case, were closer to the base case, but still above the base case. f_1,f_2 = 10,10 and 10,8 for 20 mm chords were found insignificant through a t-test at z=0.5 cm.

In Fig 3.7, the 20 mm chords in the f_1,f_2 = 8,6 configuration produced the highest frequencies followed by f_1,f_2 = 10,6. This is consistent with the result seen for the z_1 = 5 mm leading edge distance. The frequencies for the 20 mm chord configurations of f_1,f_2 = 8,8 and 6,6 were closer to the base case but still considered significantly above the base case through a t-test. f_1,f_2 = 10, 10 for 20 mm chords were found insignificant by a t-test. The only case where the frequency was below the base case was for the 30 mm chord with f_1,f_2 = 10,10.

Figs 3.8, 3.9, and 3.10 show the frequency with increasing distance below the die for a louver leading edge of z_1= 15 mm. In the region near the louvers (Fig. 3.9) the frequencies are still higher than the base case. The greatest frequency was at the leading edge for c = 20 mm and f_1,f_2 =8,8. In this case, the greater frequencies were seen for most of the 20 mm chords except for f_1,f_2 = 6,6 and 10,6. In the region below the louvers, the greatest frequencies were observed again for 20 mm chords in configurations of f_1,f_2 = 8,6 10,6 and 6,6 with frequencies roughly 40 Hz above the base case. The parallel cases with wider separations for the 20 mm chords and all configurations of the 30 mm chords were closer to the base case.

In melt blowing, the majority of the fiber attenuation takes place in the first few centimeters below the die before the fibers cool enough such that the polymer solidifies, and the air drag force is no longer great enough to stress the fibers (Bresse and Ko, 2003; Ellison et al, 2007; Shambaugh, 1988). In Chapter 2 it was seen that all configurations of the 20 and 30 mm chords produced fibers with finer diameters, particularly the 30 mm chords and some of the angled 20 mm chord configurations. This means that more attenuation took place in this region (z=0.5 to 1.5 cm), and the fibers were becoming rapidly smaller. Finer filaments can be moved with less force per unit length, so they vibrate more easily and at higher frequencies.

Fig. 3.11 shows the effect of increasing leading edge separation f_1 on the frequency of the fiber at 0.5 cm below the die. Results are shown for f_1 for different louver angles This figure is for 20 mm louvers at a leading edge of z_1 = 5 mm. The different louver angles are notated as $\Delta f = f_1\text{-}f_2$. For example, $\Delta f = 10 - 8 = 2$ for the louver configuration f_1,f_2 = 10,8.

There is a slight increase in frequency as the parallel louver separation decreases, changing from 162 ± 10 Hz at f_1,f_2 =10,10 to 203 ± 7 Hz at f_1,f_2 = 6,6. As the louver separation decreases, the air velocity profiles become flatter. Wider louver separations have a sharper profile; consequently, the fiber will move into regions of lower air velocity as the fiber moves out from the centerline. This means that the fiber is exposed to lower forces due to exposure to the slower air outside the centerline. The flatter air velocity profile provides a higher and a more consistent force on the fiber as it moves away from the centerline, thus resulting in higher fiber frequencies.

There is also an increase in frequency with increasing Δf seen for both 20 and 30 mm chords. Angled louvers act as a converging nozzle, and, by continuity, the air velocity must increase as the louver separation decreases with increasing distance below the die. As the air velocity increases, the force on the fiber is also increasing, causing the fiber to vibrate at higher frequencies.

3.4.2 Fiber Amplitude

Fig 3.12, 3.13 and 3.14 show the fiber amplitude (in millimeters) for increasing z distance below the die for z_1 = 5 mm. Similar to the frequency figures, Fig 3.12 shows the entire z range, while Figs. 3.13 and 3.14 divide the range in two. A similar t-test was also performed on the amplitude data. Table 3.2 shows the amplitude values that were not considered significantly different to the base case. Standard deviations for the amplitude ranged from 0.005 to 0.06 mm for the z=0.5 to 1.5 cm region and from 0.07 to 0.4 mm for the z = 9 to 11 cm region. In all cases, the amplitude increased with increasing z. This is consistent with the findings of both Beard et al. (2007) and Xie and Zeng (2013). Amplitudes in the louver region (z= 0.5 to 1.5 cm) ranged from 0.09 to 0.56 mm, and amplitudes below the louvers (z=9 to 11 cm) ranged from 1.33 to 2.64 mm. Amplitudes for the base case were 0.18 ± 0.02, 0.29 ± 0.02, 0.43 ± 0.04, 2.08 ± 0.14, 2.15 ± 0.15, and 2.21 ± 0.16mm for z= 0.5, 1, 1.5, 9, 10, and 11 cm, respectively.

In Fig. 3.13, the greatest amplitude is seen for the slightly angled, shorter chord of 20 mm in a louver configuration of f_1,f_2 = 10, 8. The observed amplitudes were 0.19 ± 0.01, 0.38 ± 0.02, and 0.53 ± 0.03 mm. The 30 mm louver configuration f_1,f_2 =10,10 started with a lower amplitude than the base case (at smaller z), but the amplitude increased and crossed the values for the base case. However, the amplitudes are very

close to one another, with the range between the highest and lowest amplitude of 0.12, 0.13, and 0.14 mm at z= 0.5, 1, and 1.5 cm, respectively.

In Fig. 3.14, the 20 mm louver configurations of f_1,f_2 = 10,10 and 6,6 were above the base case while the f_1,f_2 =8,8 was significantly below. The 30 mm louver configurations of f_1,f_2 =10,10 was also above the base case. All angled configurations for both chords did not show significantly different amplitudes compared to that of the fiber filament produced without louvers.

Figs. 3.15 and 3.16 show the amplitude data for louvers at a leading edge of z_1=10 mm. In Fig. 3.15 the data range increased slightly from the z_1=5 mm leading edge with ranges of 0.12, 0.22, and 0.27 mm for z=0.5, 1, and 1.5cm, respectively. The amplitude was greatest for the 30 mm f_1,f_2=10,8 configuration.

In Fig. 3.16, all the amplitude data are below the base case. The lowest amplitudes are found for the 30 mm louver configurations of f_1,f_2 = 10,8 and 10,10. The amplitudes produced with the 20 mm chords are closer to the base case, with the lowest amplitude produced from f_1,f_2 = 10,6.

Fig. 3.17 and 3.18 show the amplitude data for louvers at a leading edge position of z_1=15mm. Only the 20 mm chord amplitude data showed significant differences from the base case in the region near the die (Fig 3.17). The highest amplitude was seen for f_1,f_2 = 10,10 and the lowest amplitude was seen for f_1,f_2 = 10,6 mm. The amplitude ranges for this large leading edge were 0.05, 0.12, and 0.28 mm for z = 0.5, 1, and 1.5 cm, respectively.

In Fig. 3.18, all amplitudes were below the base case as was seen with the z_1=10 mm leading edge distance below the die. The lowest amplitudes were seen for the 20 mm

chords at configurations of f_1,f_2 = 10,8 and 6,6 as well as the 30 mm configuration of f_1,f_2 =10,10.

Overall, the amplitude in the region of the louvers was similar to normal melt blowing, although there was an increase in amplitude ranges with increasing z distance below the die. Amplitudes below the louvers tend to be less than normal (no louvers) melt blowing for greater z_1.

3.4.3 Frequency and Amplitude at the Louver Inlet

Fig 3.19 and 3.20 show the frequency and amplitude of the filament at each of the leading edges of z_1= 5, 10, and 15 mm. The greatest deviations in frequency can be seen when the leading edge is z_1 = 5 mm. The frequencies were closest together for the z_1=10 mm leading edge.

In all cases the amplitudes increase with increasing distance below the die. The standard deviation of all amplitudes also increases with increasing distance below the die. There is little difference between amplitudes of the louver case and the base case at the z_1 = 5 mm leading edge. There are some differences between the louver amplitude and the base case amplitude when the louver leading edges are z_1 = 1 and 1.5 cm. The amplitudes for the 20 mm configurations f_1,f_2 =10,10 and 8,8 are lower than the base case when the leading edge is z_1=1 cm, but greater when the leading edge is z1=1.5 cm.

It is perhaps a favorable result that there is not much difference in the amplitudes at the leading edges, meaning that the fiber will easily enter the louvers without sticking to them. When initially putting the louvers in the air field, the problem was not in removing the sticking fibers from the leading edge, but rather the trailing edge, particularly for louvers located farther from the die (larger z_1), louvers with longer chords

(c = 3 cm or greater), or greater angles (such as f_1,f_2 =10, 6). Due to the louver device and bracket blocking the camera line of sight (as mentioned above), the trailing edge of the louvers could not be imaged. Making modifications to the louver device (the end tabs) and the bracket to allow for imaging in the z= 2 to 8.5 cm range would be advantageous.

3.4.4 Fiber Sticking

To understand the "sticking" issue, videos were taken with 20 mm louvers in the f_1,f_2 = 8,8 configuration at leading edges of z_1 = 5, 10, 15, and 20 mm. The z_1 = 20 mm position resulted in sticking at approximately 1.6 seconds into the 3 second video. Only data during the first 1.6 seconds of this video was used in evaluating the amplitude. Fig 3.21 shows the amplitudes produced from this configuration. Although the amplitude for the z_1 = 20 mm position is similar to the amplitude produced from the z_1 = 15 mm position, the standard deviation for the z_1 = 20 mm position is greater. For these videos, the maximum amplitude produced was determined and is shown in Fig. 3.22. Also shown in the figure is a line to represent the louvers at the location of a 20 mm louver between the z_1 = 20 and z_2 = 40 mm position. If the amplitudes continue to increase linearly, then the amplitude of the fiber is very close to the louver tips where a fluctuation in the air profile can be enough to push the fiber onto the louver walls, as was the case for the z_1 = 20 mm video.

3.5 Conclusions

- When the louvers are near the die (z_1=5 and 10 mm) longer chords and angled shorter chords show greater frequency values near the louvers. The greatest frequencies are seen for 20 mm chord with angled positions ($f_2 < f_1$).

- Close to the die, amplitudes produced with louvers are similar to amplitudes produced in normal (no louvers) melt blowing. Amplitudes produced with louvers at larger leading edge distances are smaller than fibers produced in normal melt blowing in regions far from the die.
- Amplitude standard deviation becomes greater with increasing leading edge distance below the die, potentially leading to fiber sticking issues.

REFERENCES

Beard, J. H.; Shambaugh, R. L.; Shambaugh, B. R.; Schmidtke, D.W. On-line Measurement of Fiber Motion During the Melt Blowing. *Ind. Eng. Chem. Res.*, 2007, *46* (22), 7340-7352.

Bresse, R. R.; Ko, W. C. Fiber Formation During Melt Blowing. *Int. Nonwovens J.* 2003, 12, 21.

Chung, C.; Kumar, S. Onset of Whipping in the melt blowing process. *Journal of Non-Newtonain Fluid Mechanics.* 2013, *192*, 37-47

Ellison, C. J.; Phatak, A.; Giles, D. W.; Macosko, C. W.; Bates, F. S. Melt blown nanofibers: Fiber diameter distributions and onset of fiber breakup. Polymer 2007, 48, 3306.

Hassan, M. A.; Anantharamaiah, N.; Khan, S. A.; Pourdeyhimi, B. Computational Fluid Dynamics Simulations and Experiments of Meltblown Fibrous Media: New Die Designs to Enhance Fiber Attenuation and Filtration Quality. *Ind. Eng. Chem. Res.*, 2016, *55* (7), 2049-2058.

Y.D. Ju, R.L. Shambaugh, Air drag on fine filaments at oblique and normal angles to the air stream, Polym. Eng. Sci. 34 (1994) 958–964.

Marla, V. R.; Shambaugh, R. L. Three-Dimensional Model of the Melt Blowing Process. *Ind. Eng. Chem. Res.* 2003, *42* (26), 6993-7005.

Rao, R.; Shambaugh, R. L. Vibration and Stability in the Melt Blowing Process. *Ind. Eng. Chem. Res.* 1993, *32* (12), 3100-3111.

Shambaugh, B. R.; Papavassiliou, D. V.; Shambaugh, R. L. Modifying Air Fields to Improve Melt Blowing. *Ind. Eng. Chem. Res.* 2012, 51, 3472-3483.

Shambaugh, R. L. A Macroscopic View of the Melt Blowing Process for Producing Microfibers. *Ind. Eng. Chem. Res*. 1988, 27, 2363

Shambaugh, R. L.; Krutty, J. D.; Singleton, S. M. Melt Blowing Dies with Louvers. *Ind. Eng. Chem. Res.*, 2015, *54* (51), 12999-13004.

Xie, S.; Zeng, Y. Online Measurement of Fiber Whipping in the Melt-Blowing Process. Ind. Eng. Chem. Res. 2013, 52, 2116.

Table 3.1. A summarization of louver chord lengths c, leading edge distances z_1, f_1,f_2 configurations, and distances below the die head combinations where the fiber frequency was found insignificant compared to frequencies of normal melt blowing through a T-Test. A t-test resulting in a value greater than 0.05 was considered insignificant.

Insignificant Frequency Results via T-Test Criterion: 0.05			
z1 (mm)	**c(mm)**	**f1,f2**	**z (cm)**
0.5	30	10,10	9, 10, 11
		8,8	9, 10, 11
		10,8	10
1	20	10,10	0.5, 9, 10, 11
		10,8	0.5, 11
		8,8	11
1	30	10,10	11
		8,8	9
		10,8	9, 10, 11
1.5	20	6,6	0.5
		10,6	0.5, 1
		10,10	9, 10, 11
		8,8	9, 10, 11
1.5	30	10,10	0.5, 9
		8,8	9, 10

Table 3.2. A summarization of louver chord lengths c, leading edge distances z_1, f_1,f_2 configurations, and distances below the die head combinations where the fiber amplitude was found insignificant compared to amplitudes of normal melt blowing through a T-Test. A t-test resulting in a value greater than 0.05 was considered insignificant.

Insignificant Amplitude Results via T-Test Criterion: 0.05			
z1 (mm)	**c(mm)**	**f1,f2**	**z (cm)**
0.5	20	10,10	1.5
		10,6	0.5, 1, 9, 10, 11
		6,6	0.5
		8,6	0.5, 1.5, 9, 10, 11
		10,8	9, 10, 11
0.5	30	10,10	1.5
		8,8	0.5, 1.5, 9, 10
		10,8	0.5, 1, 1.5, 9, 10, 11
1	20	10,6	0.5
		8,8	0.5, 11
		8,6	0.5
		10,10	10, 11
		10,8	11
1	30	10,10	0.5, 1
		8,8	0.5, 1, 1.5
1.5	20	8,8	0.5
		10,8	0.5, 1.5
		8,6	1
		10,6	0.5, 1
1.5	30	10,10	0.5, 1, 1.5
		8,8	0.5, 1, 1.5

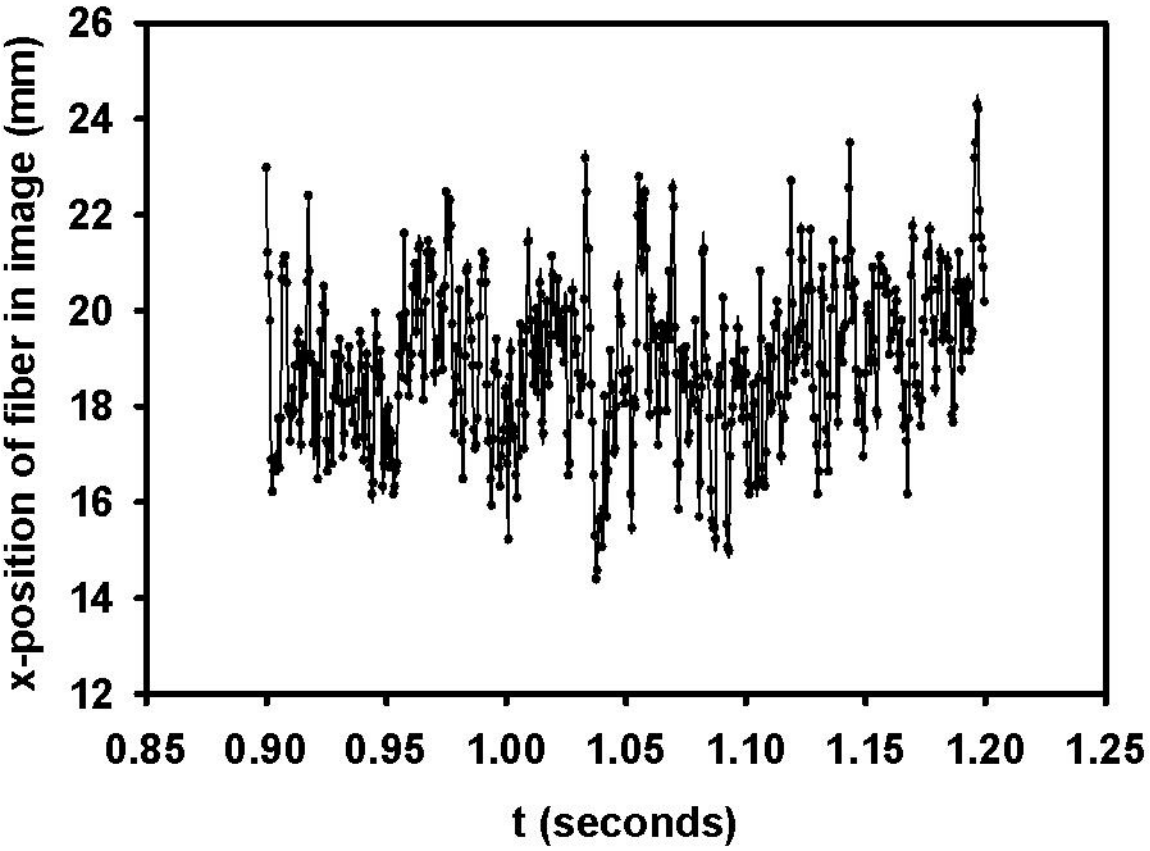

Fig 3.1a Unnormalized x-position versus time data for a time interval 0.90 to 1.20 seconds for the 20 mm chords, with a leading edge distance z_1 of 5 mm and a louver configuration of f_1,f_2= 8,8. The positional data were taken at z = 9 cm below the die head.

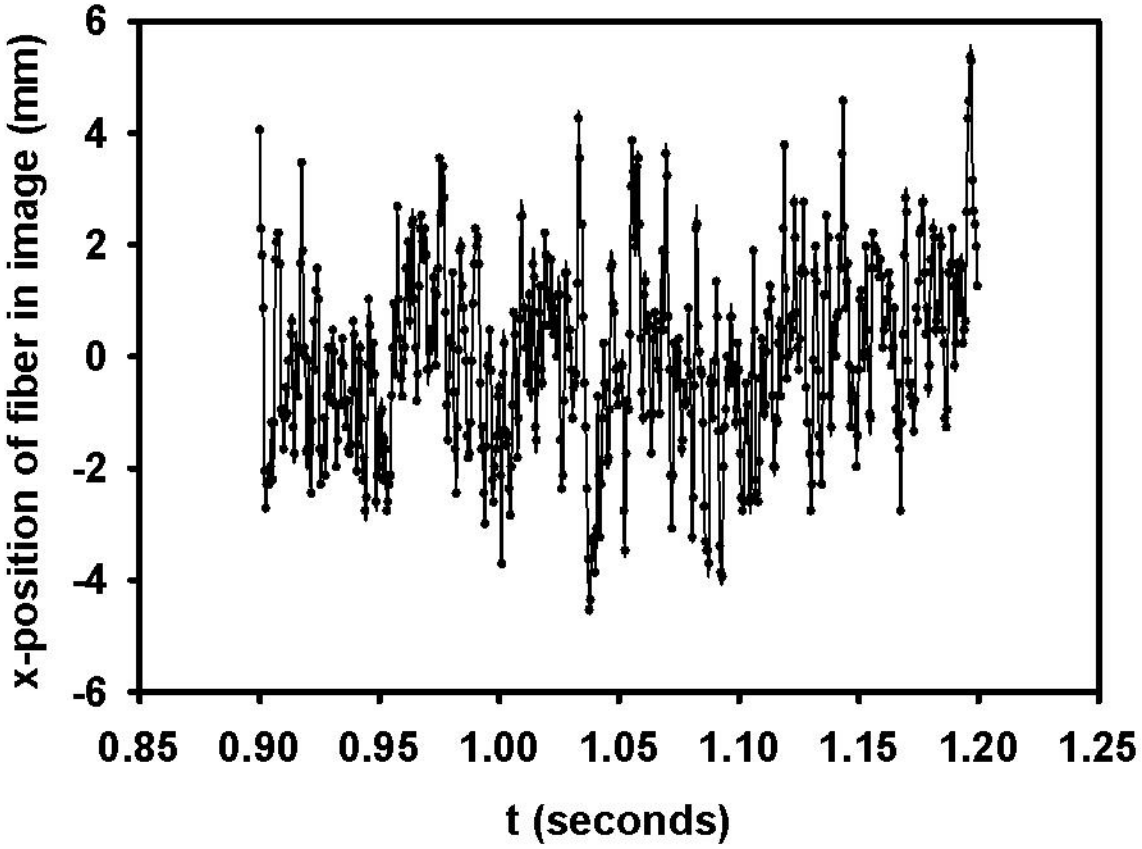

Fig 3.1b. Same as Fig. 3.1a except the data has been normalized to be centered about the x-axis.

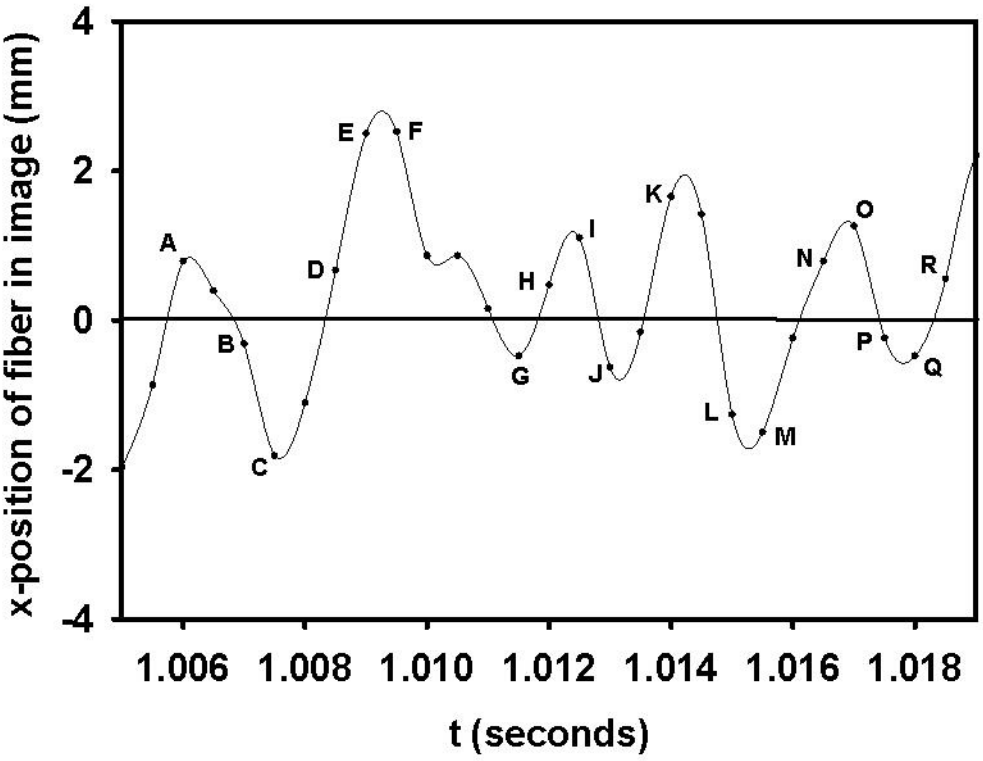

Fig 3.1c Same as the Fig 3.1b except the time interval has been reduced to 1.006 to 1.02 seconds. Letters A through R represent “zero” and extrema points.

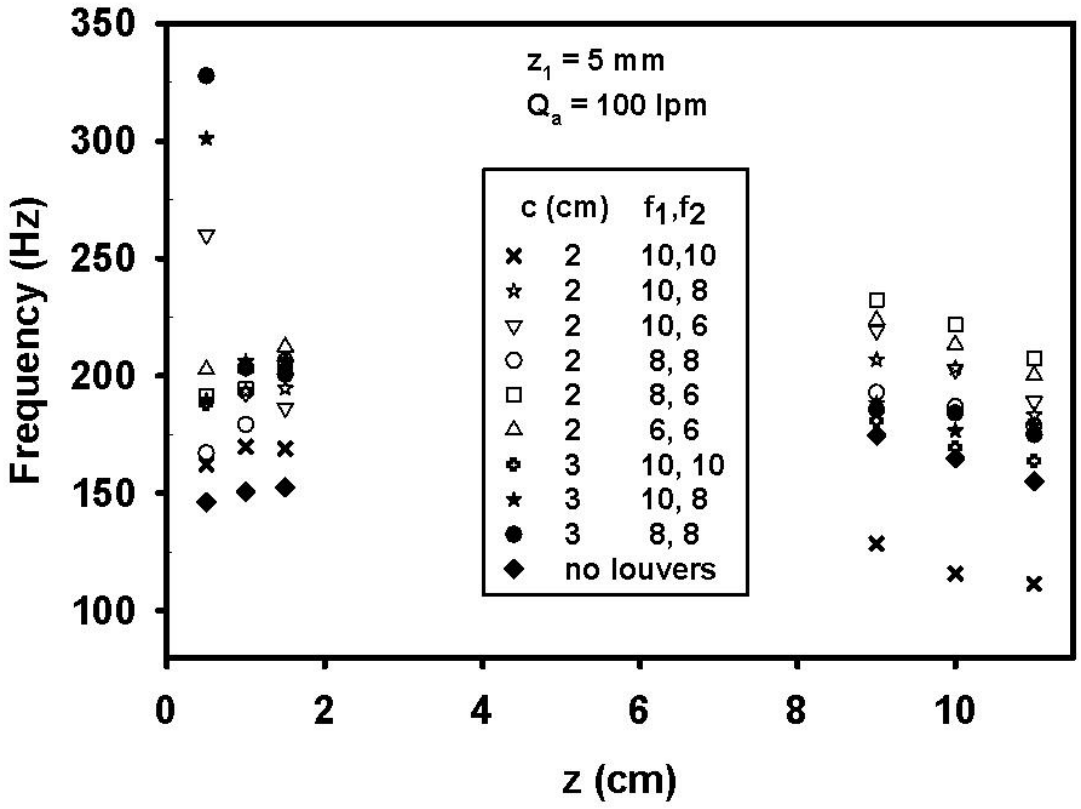

Fig 3.2. Shown is fiber frequency for increasing z distance below the die. Curves are shown for louver configurations f_1,f_2. The leading edge distance was z_1 = 5 mm. The air flowrate was 100 slpm and polymer mass flowrate was 0.5 g/min. Polymer temperature was 230 °C and the air temperature was 300 °C.

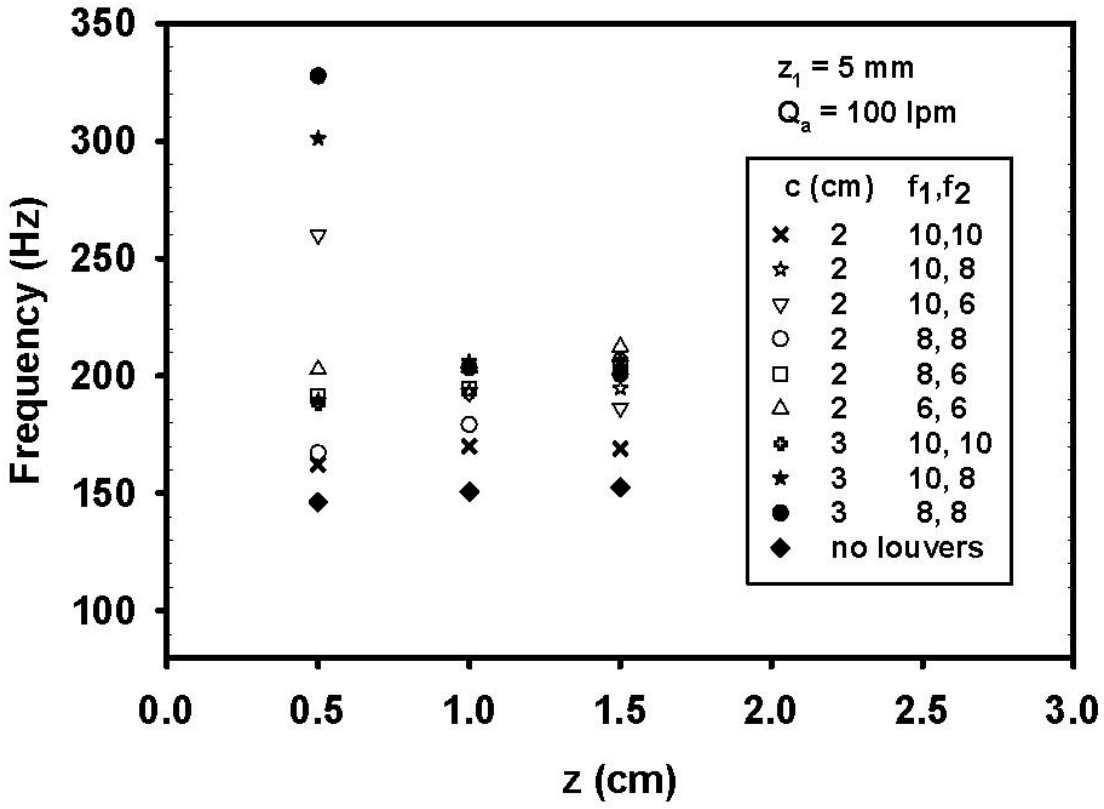

Fig 3.3. Same as Fig 3.2 except only z = 0.5 to 1.5 cm is shown.

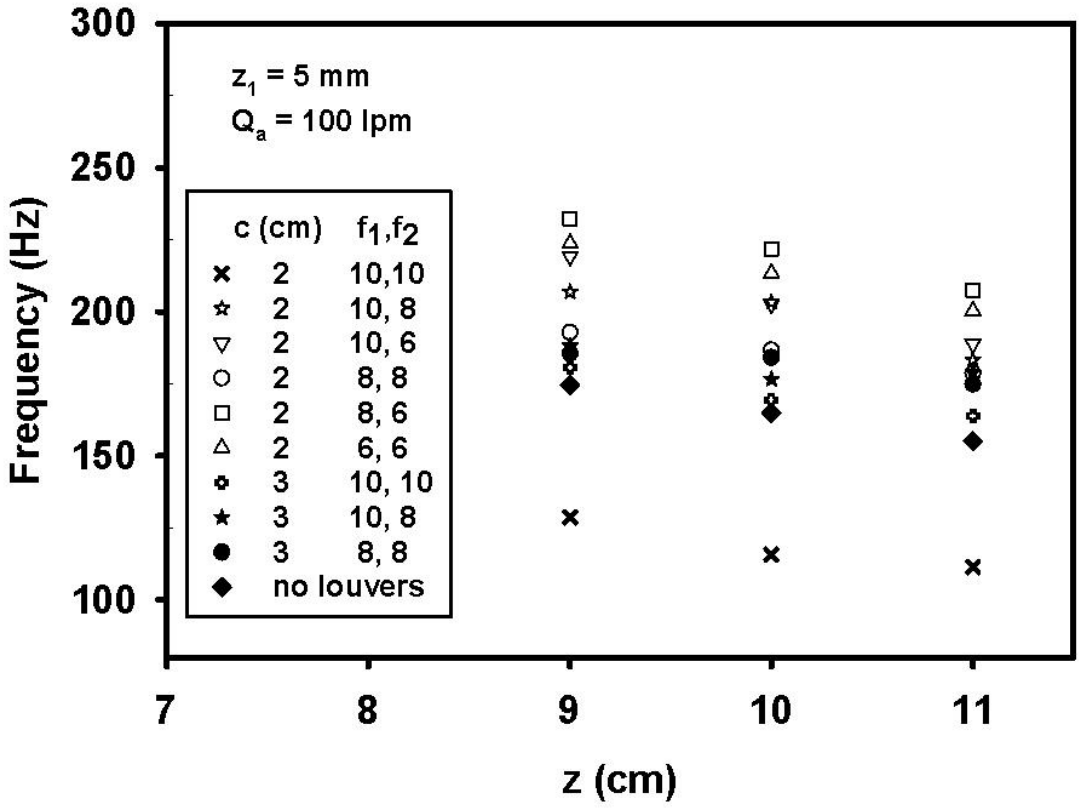

Fig 3.4 Same as Fig 3.2 except only z = 9 to 11 cm is shown.

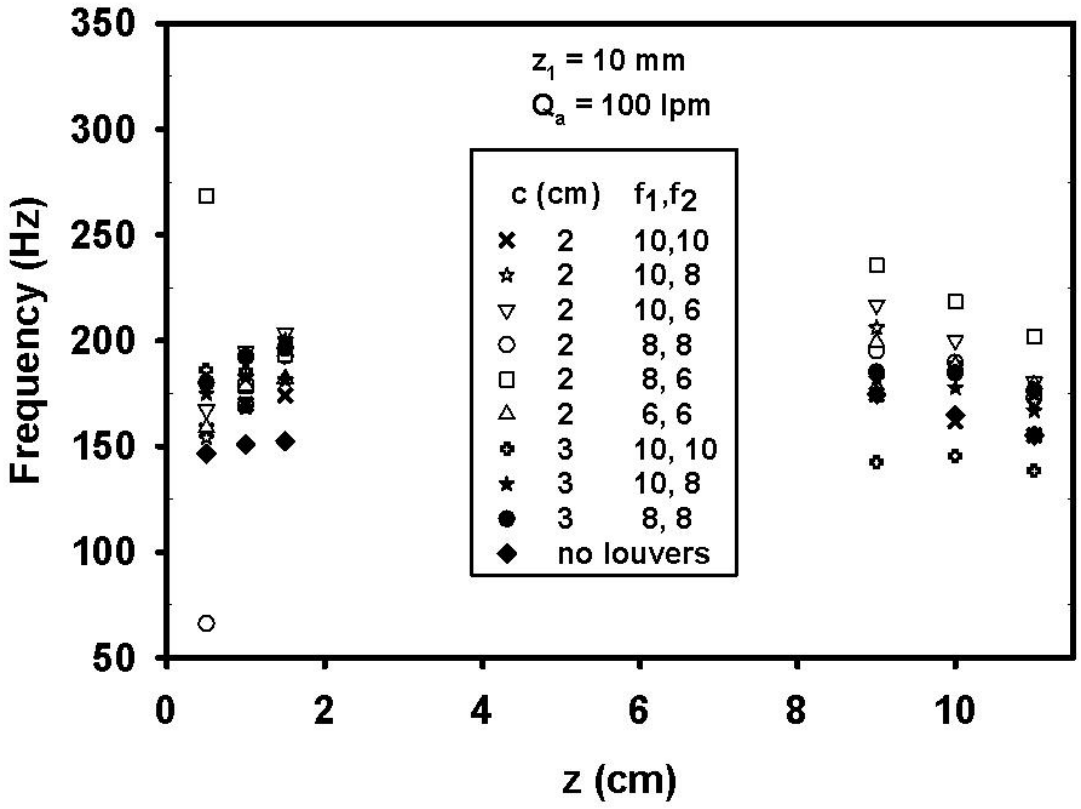

Fig 3.5. Shown is fiber frequency for increasing z distance below the die. Curves are shown for louver configurations f_1,f_2. The leading edge distance was z_1 = 10 mm. The air flowrate was 100 slpm and polymer mass flowrate was 0.5 g/min. Polymer temperature was 230 °C and the air temperature was 300 °C.

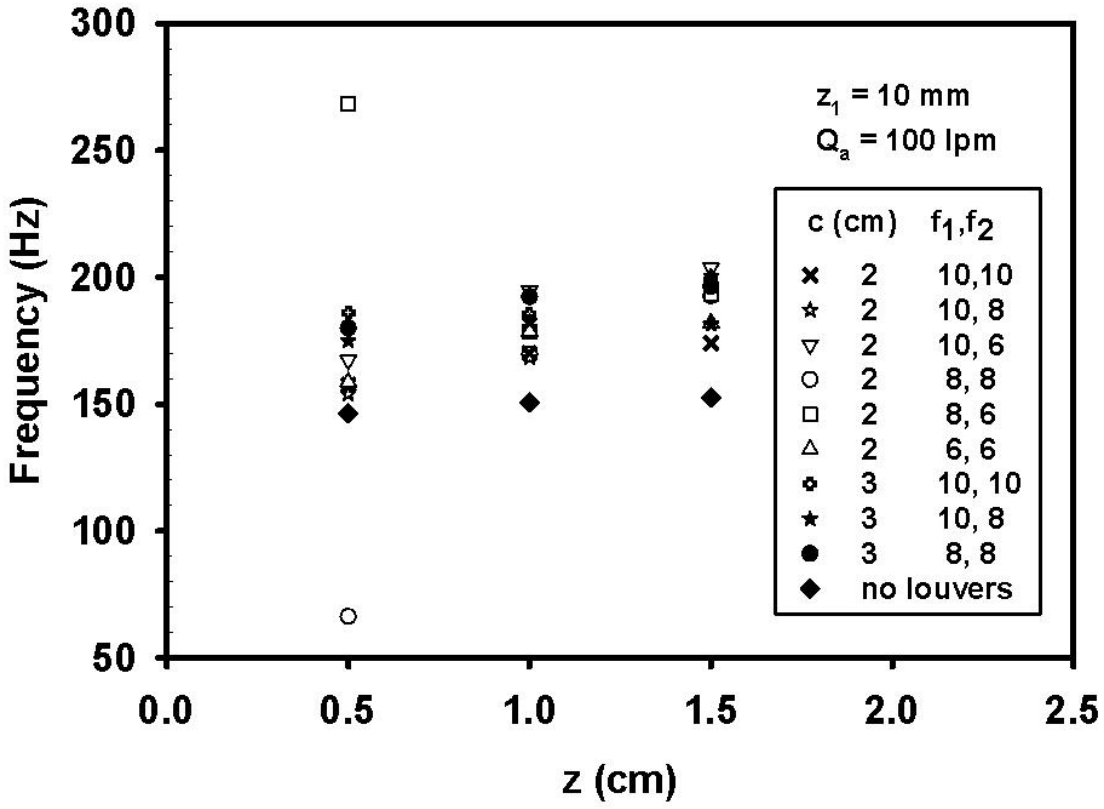

Fig 3.6. Same as Fig 3.5 except only z = 0.5 to 1.5 cm is shown.

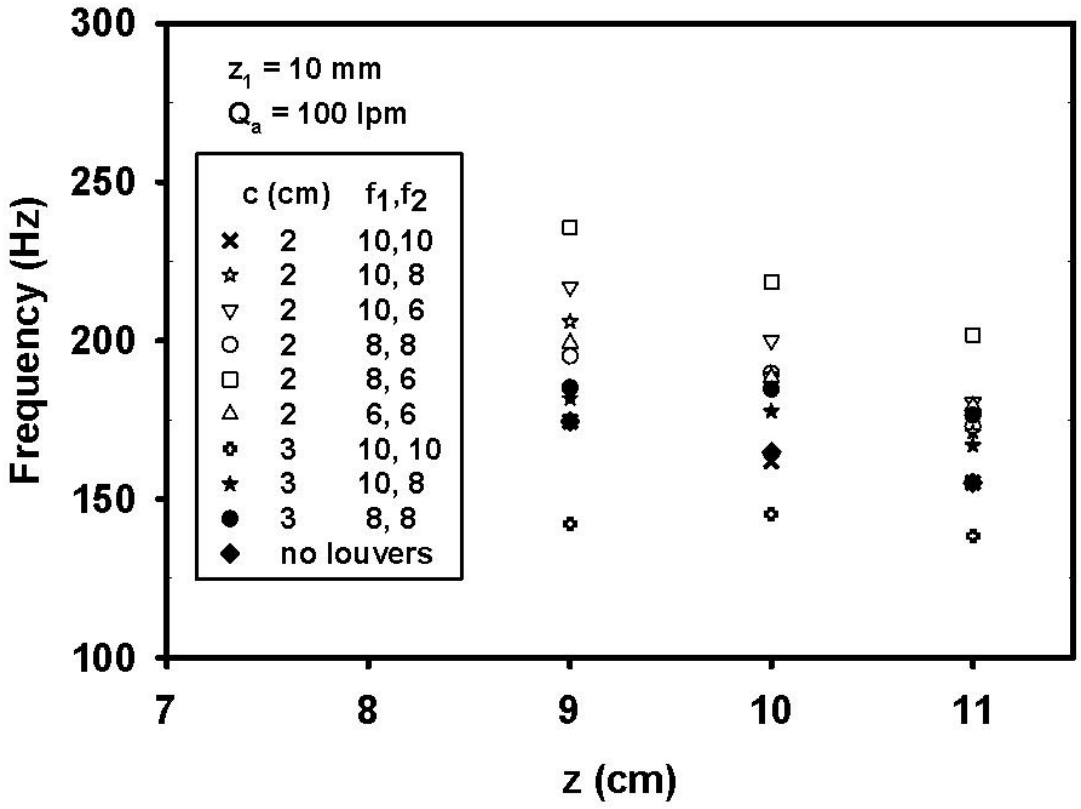

Fig 3.7. Same as Fig 3.5 except only z = 9 to 11 cm is shown.

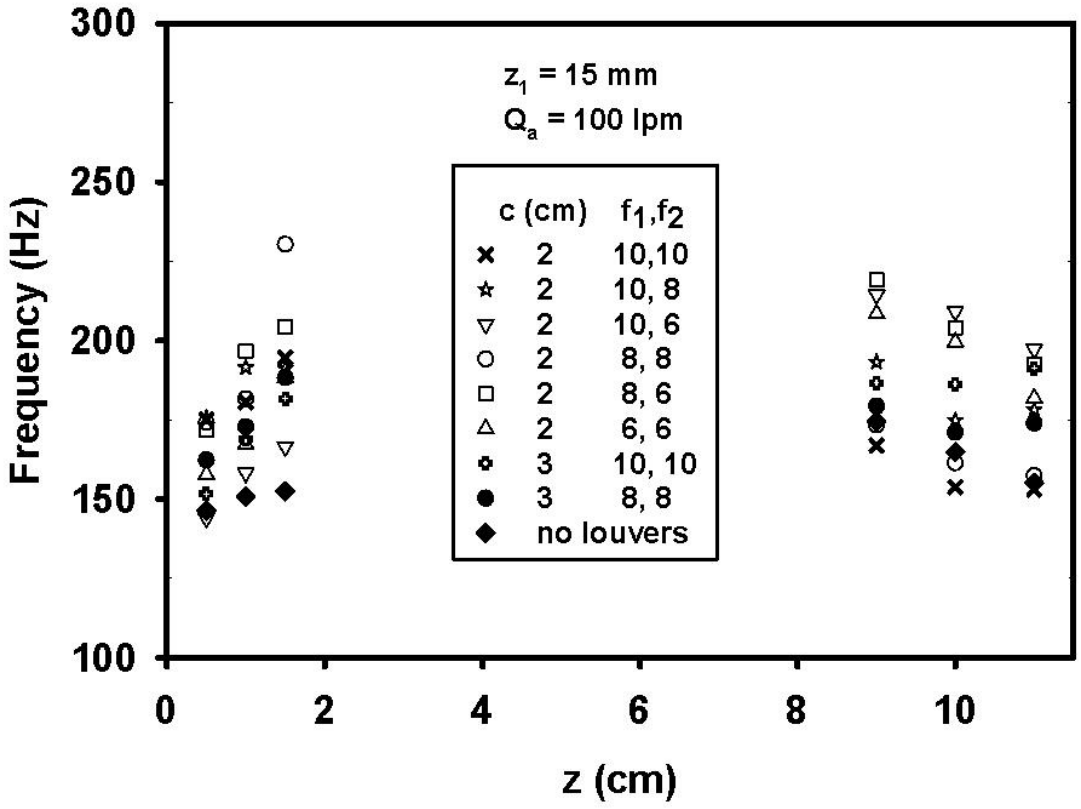

Fig 3.8. Shown is fiber frequency for increasing z distance below the die. Curves are shown for louver configurations f_1,f_2. The leading edge distance was z_1 = 15 mm. The air flowrate was 100 slpm and polymer mass flowrate was 0.5 g/min. Polymer temperature was 230 °C and the air temperature was 300 °C.

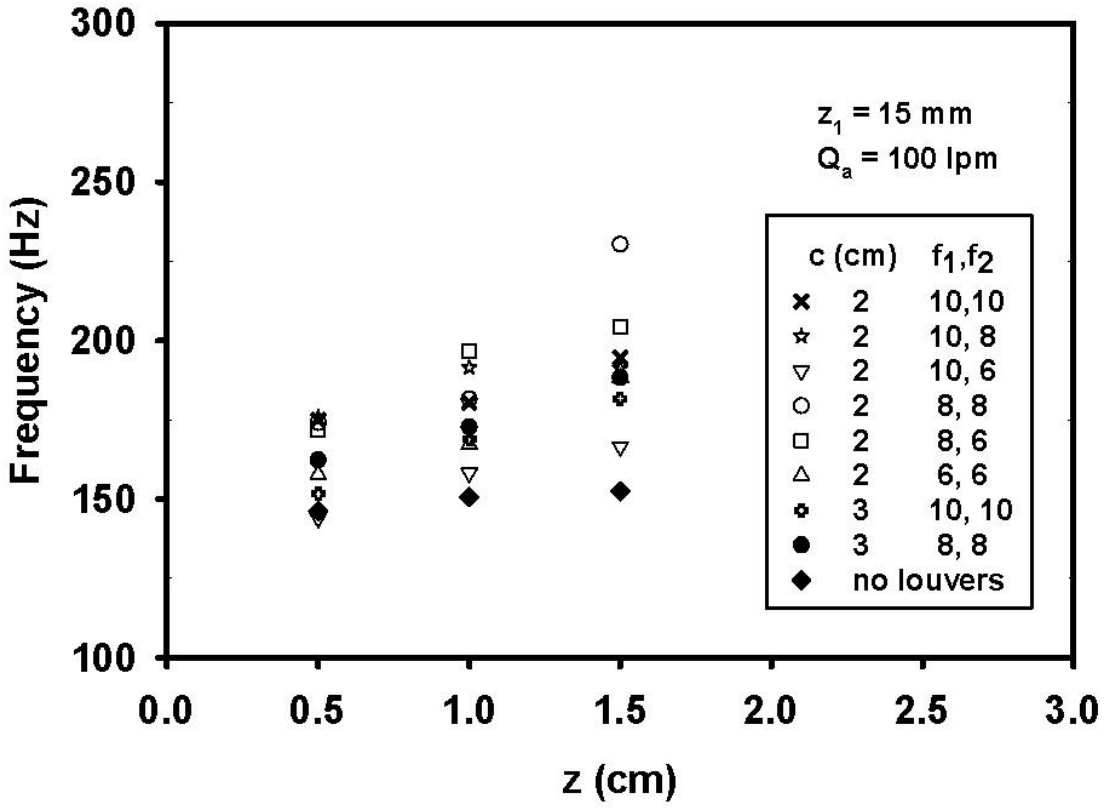

Fig 3.9 Same as Fig 3.8 except only z = 0.5 to 1.5 cm is shown.

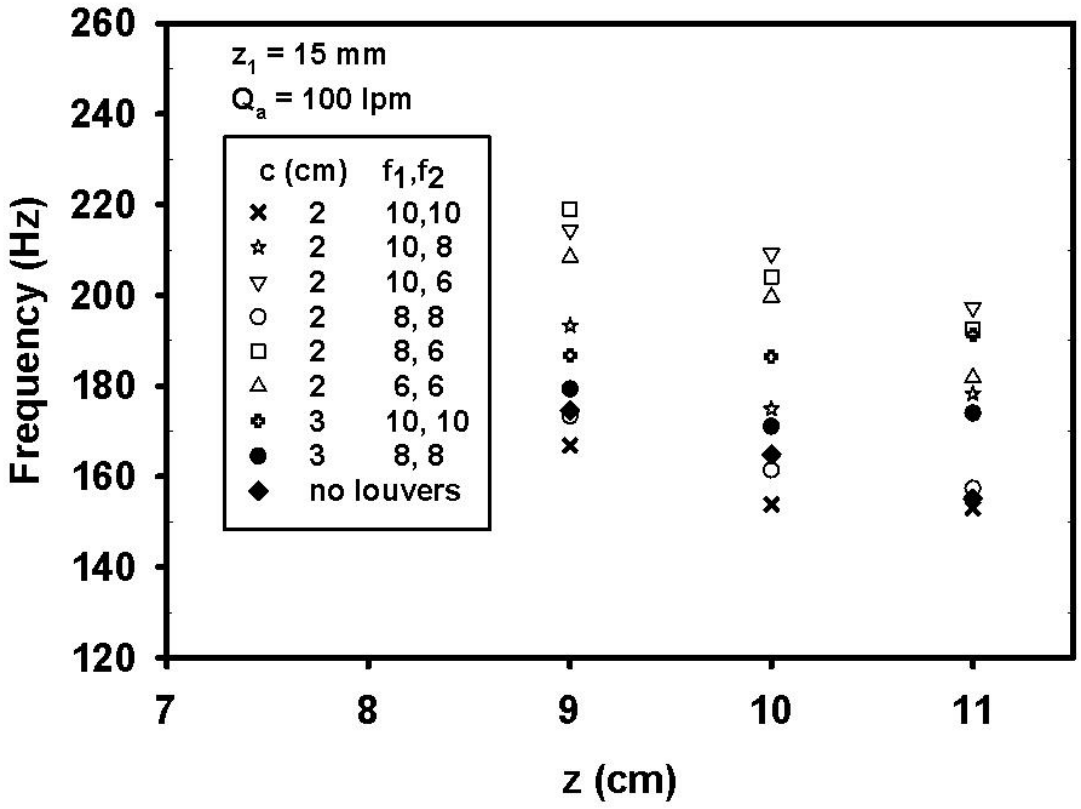

Fig 3.10. Same as Fig 3.8 except only z = 9 to 11 cm is shown.

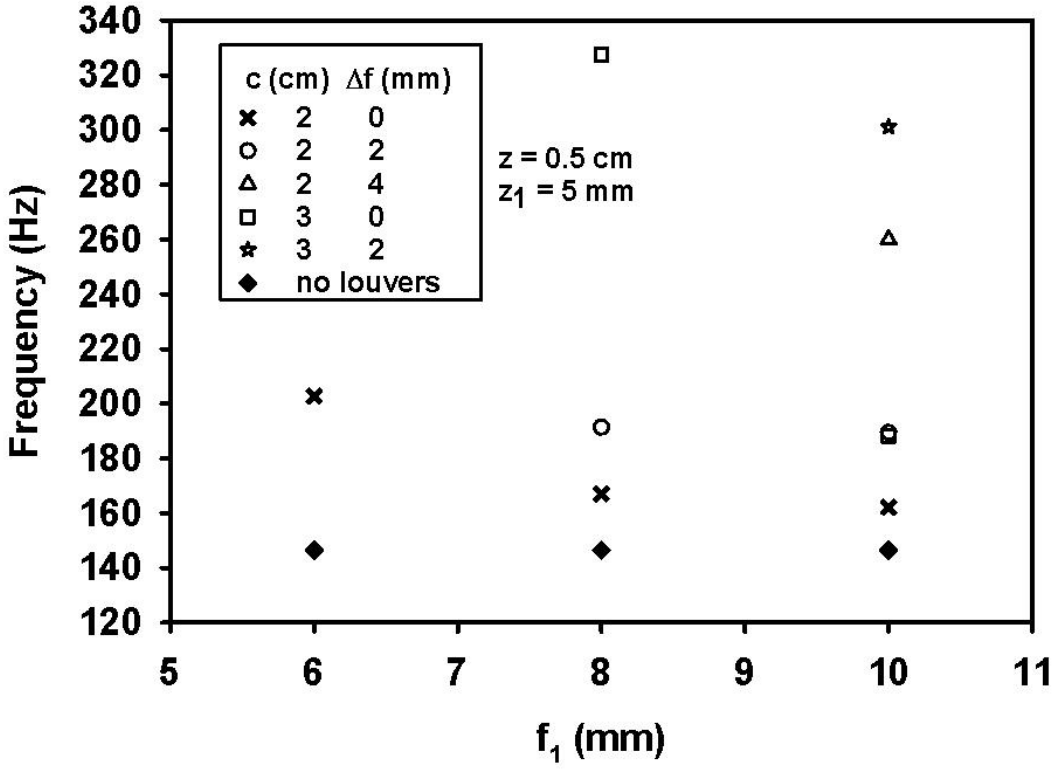

Fig. 3.11. The effect of f_1 on frequency. For this graph, c = 20 mm, z_1 = 5 mm, and air flowrate = 110 L/min. Curves are shown for $\Delta f = f_1 - f_2 = 0$, 2 and 4 mm. The polymer temperature was 230 °C, the air temperature was 300 °C, and the polymer flowrate was 0.5 g/min.

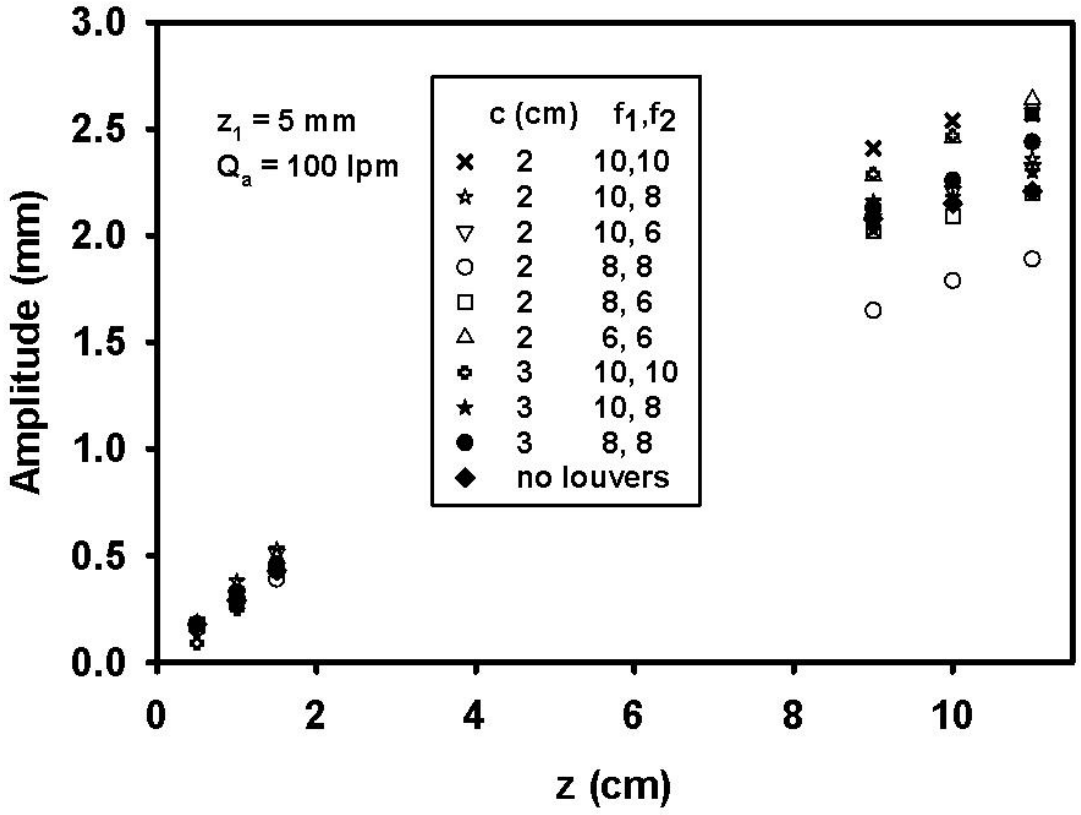

Fig 3.12 Shown is fiber amplitdue for increasing z distance below the die. Curves are shown for louver configurations f_1,f_2. The leading edge distance was z_1 = 5 mm. The air flowrate was 100 slpm and polymer mass flowrate was 0.5 g/min. Polymer temperature was 230 °C and the air temperature was 300 °C.

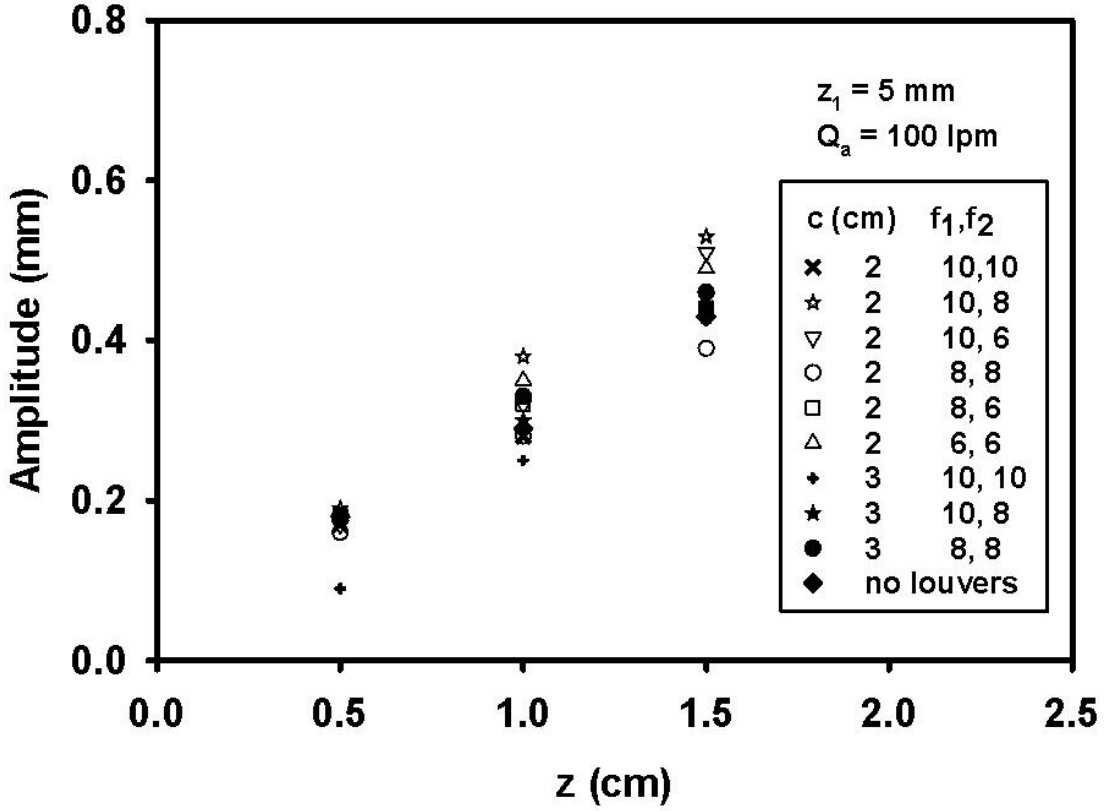

Fig 3.13. Same as Fig 3.12 except only z = 0.5 to 1.5 cm is shown.

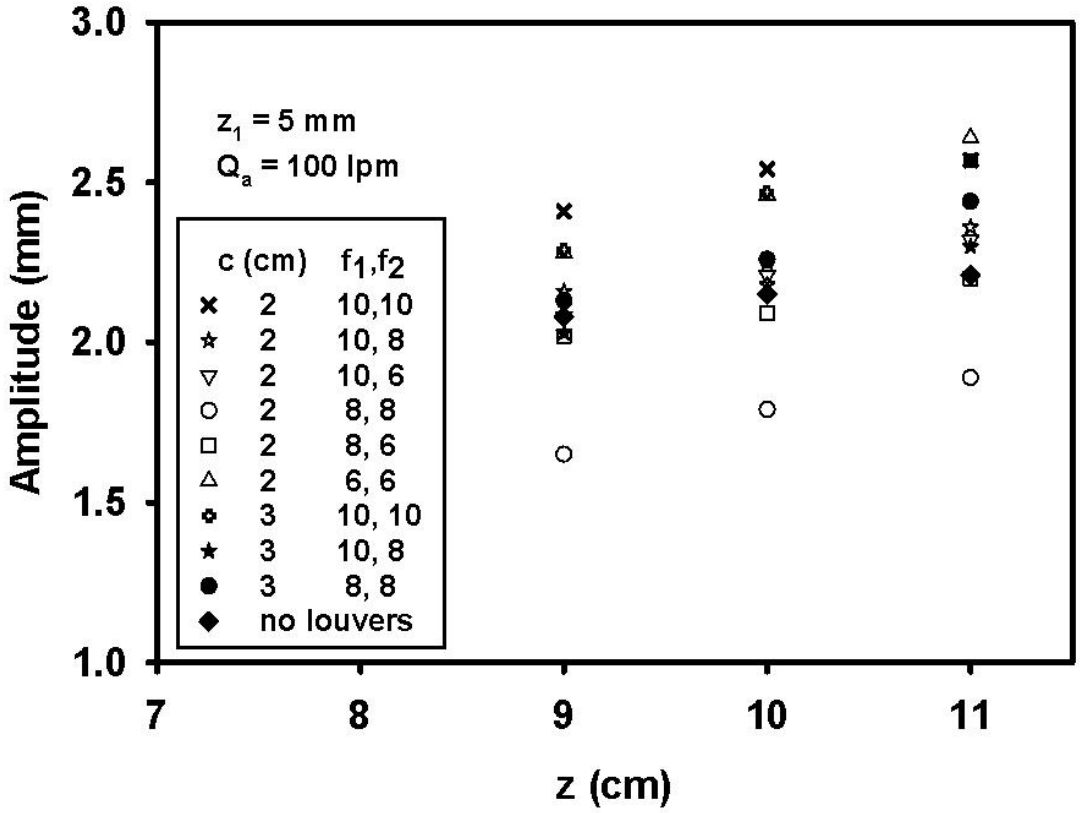

Fig 3.14. Same as Fig 3.12 except only z = 9 to 11 cm is shown.

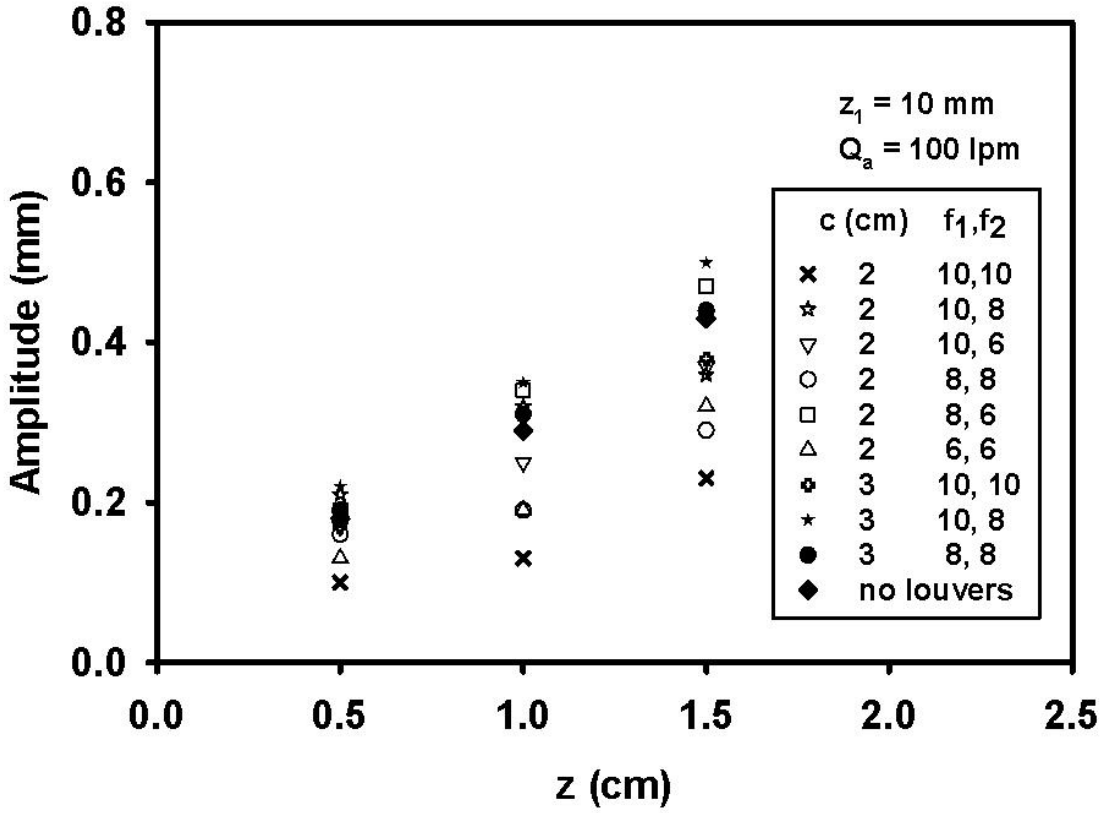

Fig 3.15. Shown is fiber amplitdue for increasing z distance below the die. Curves are shown for louver configurations f_1,f_2. The leading edge distance was z_1 = 10 mm. Show is the z = 0.5 to 1.5 cm range. The air flowrate was 100 slpm and polymer mass flowrate was 0.5 g/min. Polymer temperature was 230 °C and the air temperature was 300 °C.

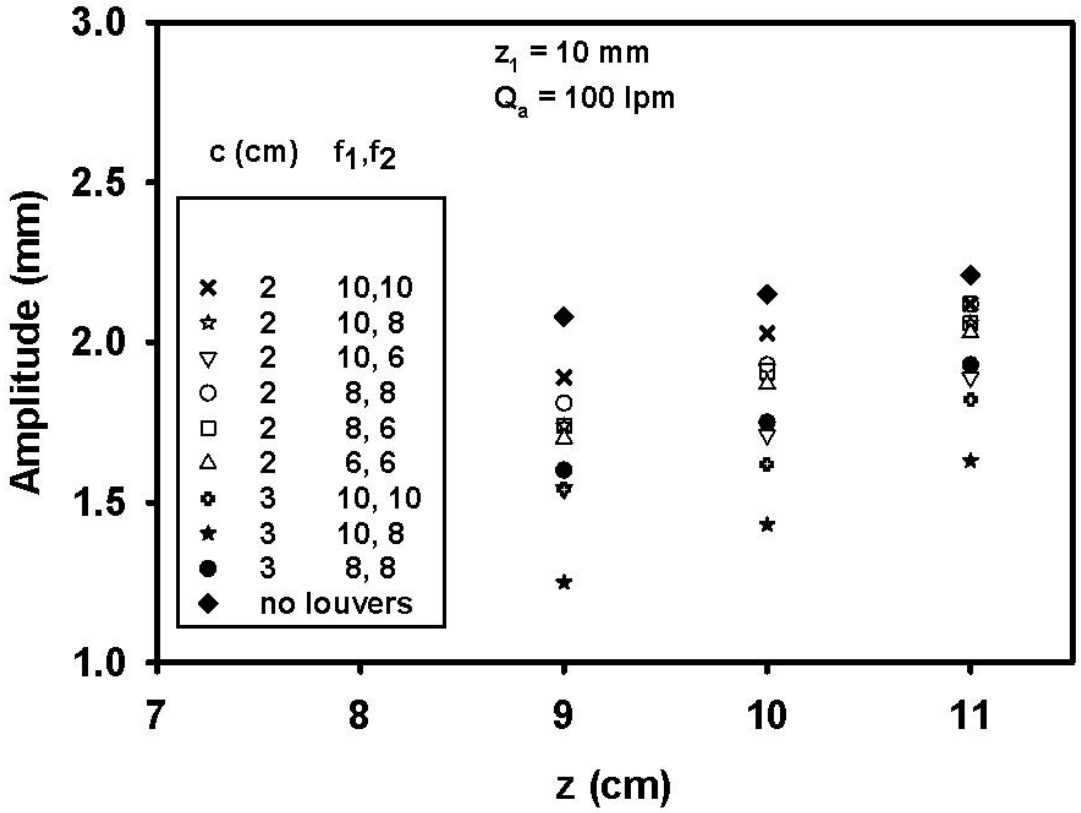

Fig 3.16. Same as Fig 3.15 except the z = 9 to 11 cm range is shown.

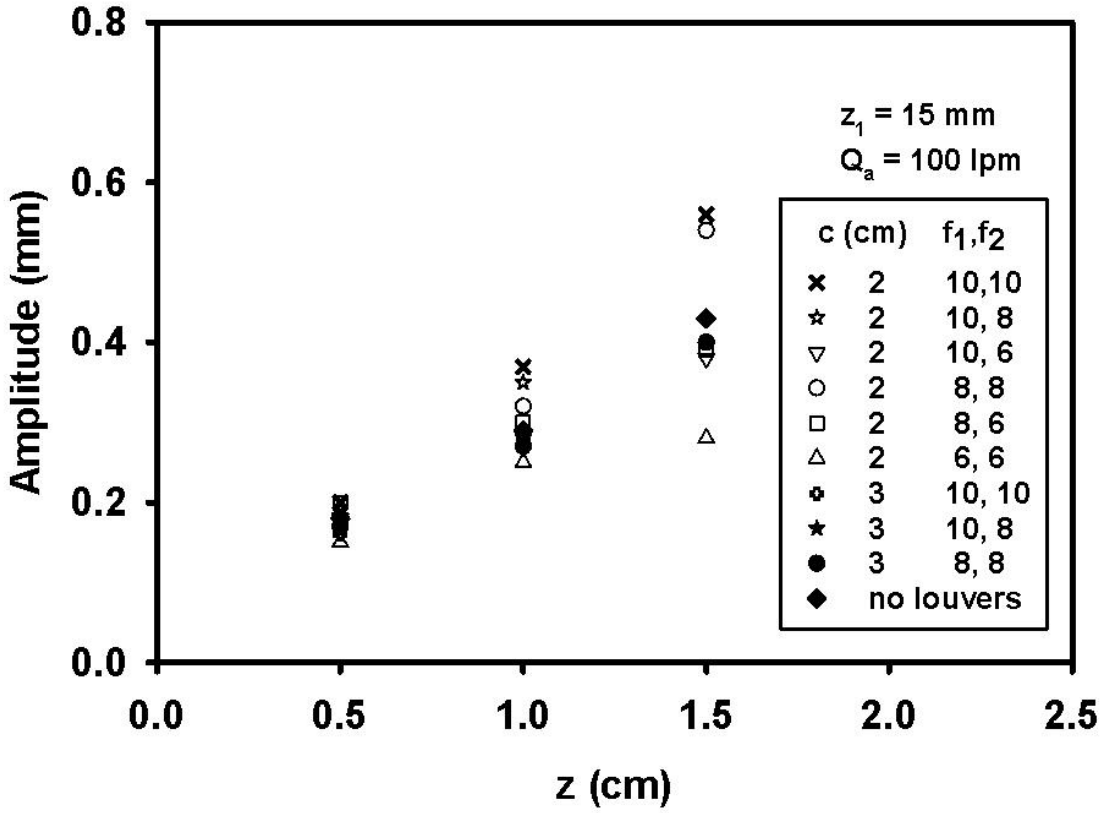

Fig 3.17. Shown is fiber amplitdue for increasing z distance below the die. Curves are shown for louver configurations f_1,f_2. The leading edge distance was z_1 = 15 mm. Show is the z = 0.5 to 1.5 cm range. The air flowrate was 100 slpm and polymer mass flowrate was 0.5 g/min. Polymer temperature was 230 °C and the air temperature was 300 °C.

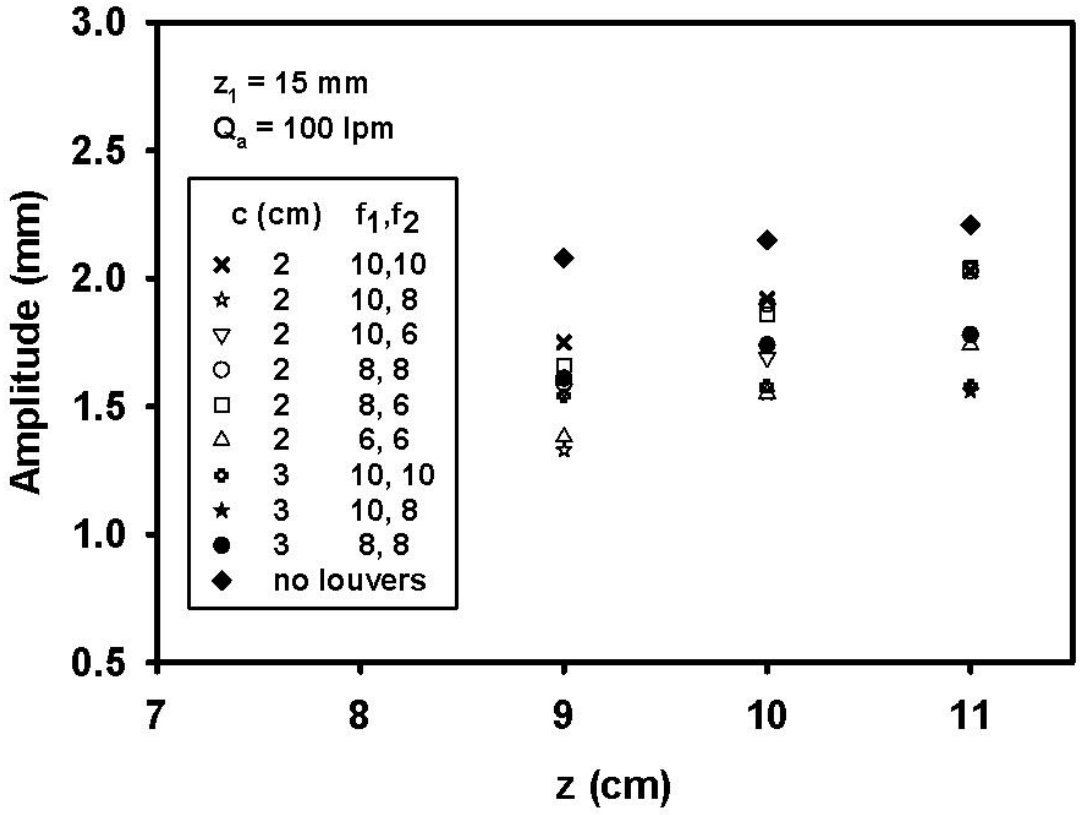

Fig 3.18. Same as Fig 3.17 except the z = 9 to 11 cm range is shown.

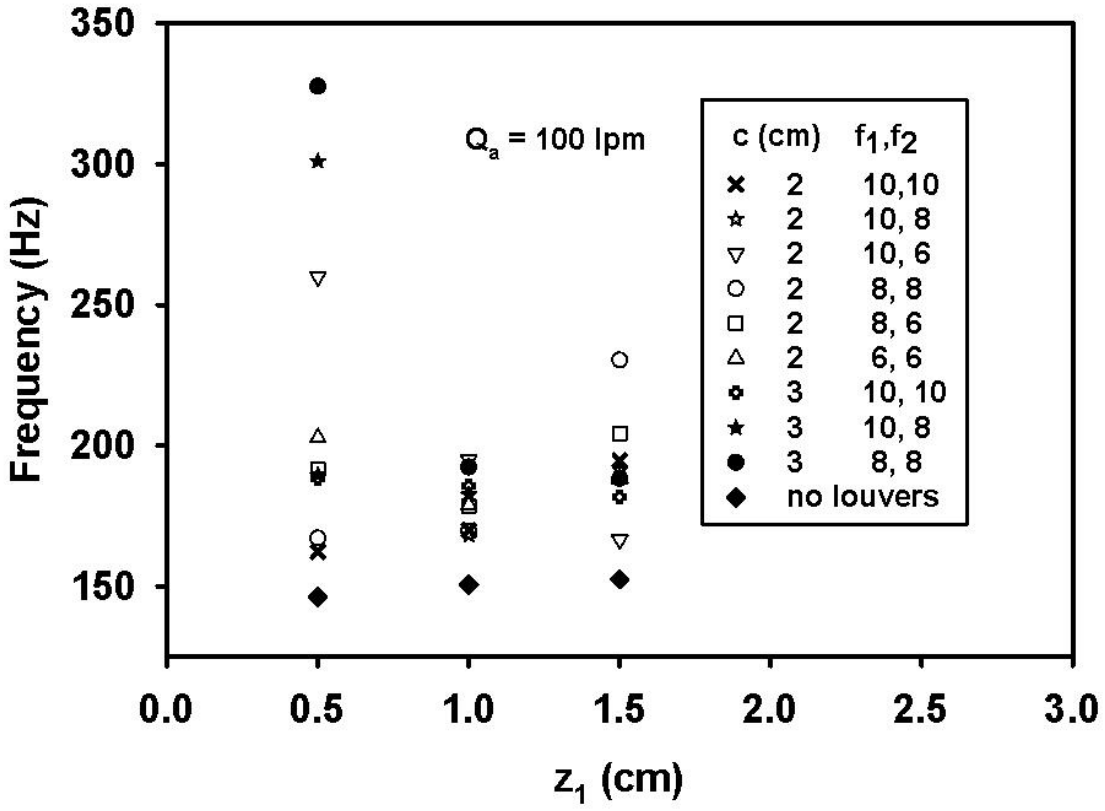

Fig 3.19. The fiber frequency at each of the louver leading edges z_1 is shown. Curves are shown for each f_1,f_2 configuration. The polymer temperature was 230 °C, the air temperature was 300 °C, and the polymer flowrate was 0.5 g/min.

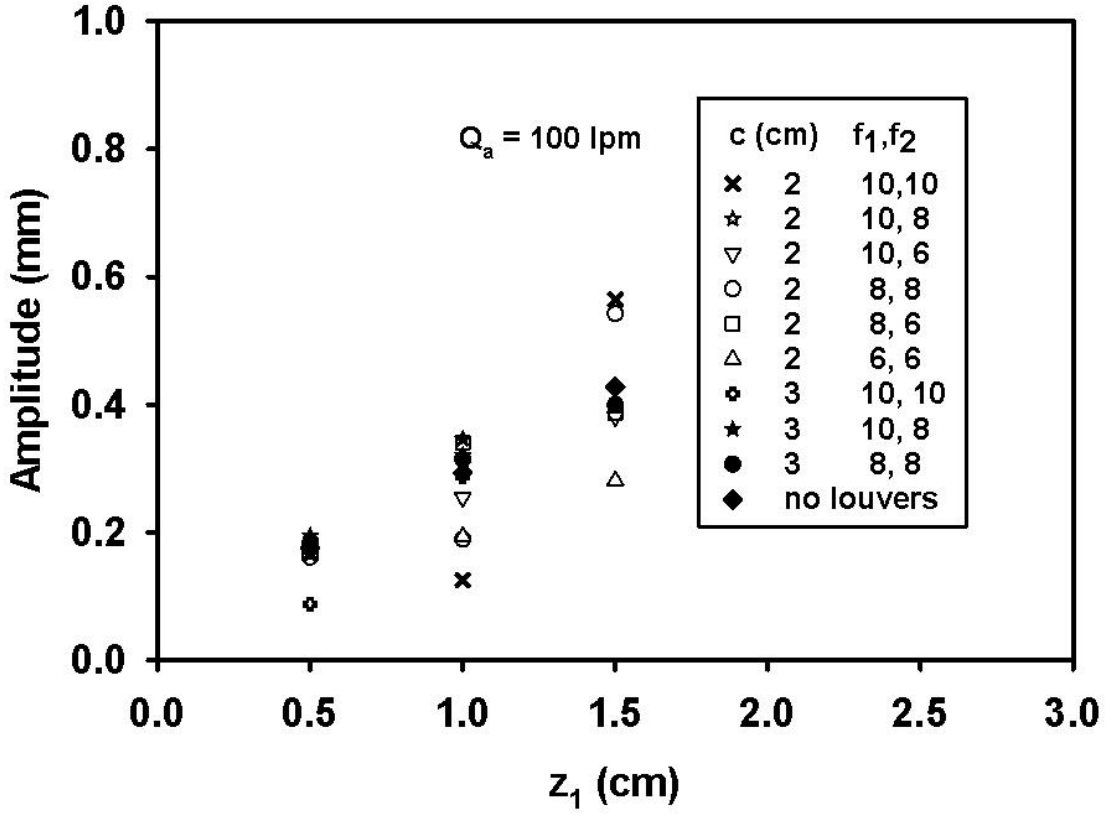

Fig 3.20. The fiber amplitude at each of the louver leading edges z_1 is shown. Curves are shown for each f_1,f_2 configuration. The polymer temperature was 230 °C, the air temperature was 300 °C, and the polymer flowrate was 0.5 g/min.

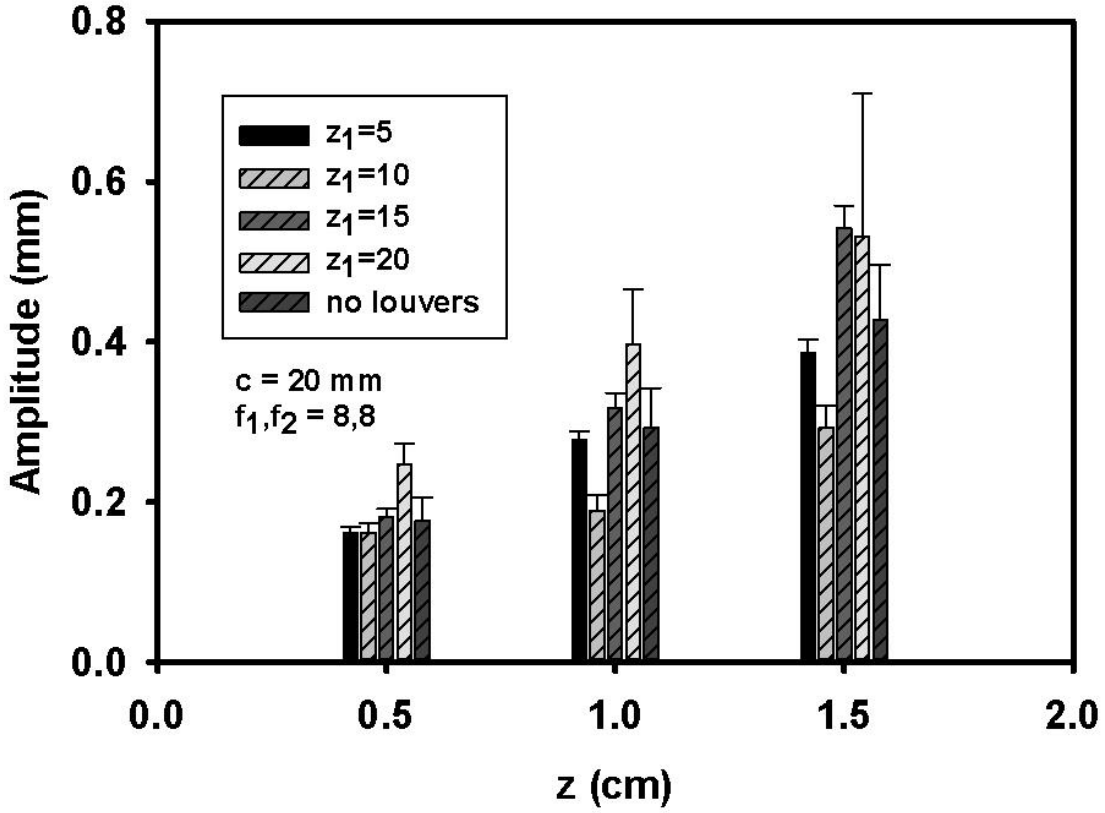

Fig 3.21. Fiber amplitude is shown for increasing z distance below the die for different leading edges z_1. The chord was c= 20 mm with a f_1,f_2 =8,8 configuration. The polymer temperature was 230 °C, the air temperature was 300 °C, and the polymer flowrate was 0.5 g/min.

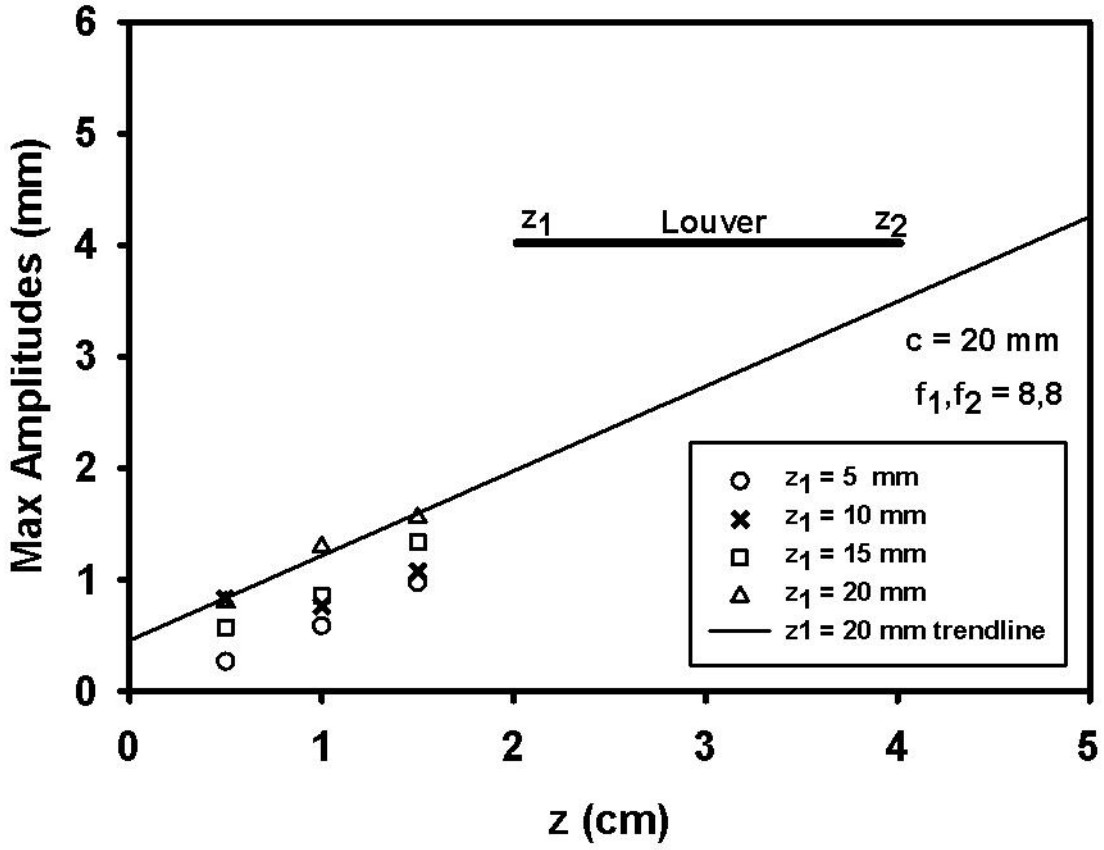

Fig 3.22. Maximum fiber amplitudes are shown for increasing z distance below the die for different leading edges z_1. The chord was c= 20 mm with a f_1,f_2 =8,8 configuration. A represntation of the louver is placed in the figure between z_1 = 2 cm and z_1 = 4 cm. The polymer temperature was 230 °C, the air temperature was 300 °C, and the polymer flowrate was 0.5 g/min.

CHAPTER 4

USE OF AN INFRARED CAMERA IN MEASURING ONLINE FIBER TEMPERATURE WITH LOUVERS IN THE AIR FIELD

4.1 Introduction

As described in Shambaugh et al. (2015) and in Chapter 2 of this work, the louvers physically imposed a plateau in the air field, where air entrainment was prevented, and the fiber velocity was maintained at a constant average value between the louvers. It is expected that the louvers will also approximate a constant air temperature between the louvers by preventing the entrainment of cooler ambient air with the hot air jet. As the constant air velocity between the louvers exposed the melt blown filament to a higher air velocity for longer lengths down the threadline, the constant air temperature is also expected to expose the filament to higher air temperatures. The higher air temperatures will keep the polymer viscosity lower in the region of main attenuation, making it easier for fiber drawing to occur. This "plateau" of constant air temperature and velocity was simulated in the work of B. Shambaugh et al. (2012), and showed higher fiber temperatures maintained for longer distances below the die. These results have not yet been experimentally verified. Therefore, it is of interest to observe the effects of the louvers on the melt blown fiber temperature.

Online fiber temperature has been measured in several different ways in past years. Breese and Ko (2003) used an adjustable-emissivity digital infrared thermometer to measure fiber temperature at different regions below the die. Gohzar et al. (2004), Bansal and Shambaugh (1998), Marla et al. (2007)(2009), and Beard (2006) used infrared photography to image fiber diameters in the melt blowing field. Measurements of the air

temperature field have also been done both experimentally (Tate and Shambaugh, 2004) and through simulations (Krutka et al. 2004). A methodology for measuring online fiber temperature through infrared photography with louvers in the air field will be presented below.

4.2 Proposed Methodology for Temperature Experiments

4.2.1 The Infrared Camera and General Operation

An infrared camera will be used to determine online fiber temperature at different distances below the die. The objective will be to determine if the temperature of the fiber remains higher for longer distances below the die when using louvers compared to the ordinary melt blowing process. The *ThermaCAM® S60* infrared camera developed by FLIR will be used. This camera operates at a spectral range of 7.5 to 13 µm wavelengths. The camera has a 24-degree by 18-degree field of view. The camera has a 320 by 240 detector element grid (similar to pixels). With the primary lens, the camera has a minimum focus distance of 0.3 m. The camera also comes with a 100-degree lens; however, this lens requires a focus distance between 8 and 11 mm. With the current louver bracket system, the camera would not be able to get closer than 13 cm to the fiber at z distances of 8 cm and higher (the region of interest). In the past works of Beard (2006) and Marla et el. (2007) (2009), this lens was required to clearly observe fibers produced at air flowrates greater than 50 liters/min as the fiber diameters were much smaller.

Either the louver bracket will have to be modified to allow for use of the 100-degree lens to observe fiber temperature at the louver tips, or operating conditions that produce larger fibers will need to be used to allow for a better image of the fibers with the primary lens. Note that with the louvers' length (parallel to the die face) of 256 mm,

the 100-degree lens still cannot be used to determine fiber temperature between the louvers, even if the bracket is modified.

The camera is controlled through a IEEE 1394 Firewire connection to a laptop and the software program *ThermaResearcher Pro 2.10* (an updated version of the that used by Beard (2006) to account for Windows 10 driver system). The software allows you to see a real time thermal image of the system, to adjust the camera focus, and determine record settings. Recommended record settings are included in Table 4.1. It is important to note the lens-to-target distance and the initial guessed emissivity in the Object Parameters as these will affect the camera's calculated temperature measurement. If this is forgotten during running, this information can still be inputted for already recorded videos in post-processing.

Videos of the fiber in the field are to be taken with the IR camera and (currently) the primary lens. Videos will be taken for z distances of 0.5, 1, 1.5, 2, 9, 10, 11, and 15 cm below the die with the center of the lens at these locations. Distances of 2.5 to 8.5 cm below the die are currently blocked by the louver bracket. As the IR camera cannot "see" the markings on a ruler, the best way to determine the correct distance below the die head would be to center the lens at each of these locations by measuring the distance between the lens center and the die face.

4.2.2 Online Fiber Diameter Acquisition

Before post-processing of the videos, the online fiber diameters will need to be determined for each louver positional case. The emissivity of the fiber, or the measure of the fiber's radiation emission, is dependent on fiber diameter. Also, the melt blown fibers are small compared to the thermal detectors of the IR camera. As the fiber does not take

up the entire thermal detector view, the camera will under-calculate the measured temperature. Marla (2007) produced correlations to account for the fiber diameter size relative to the larger thermal detectors of the IR camera. These correlations are based on the ratio of camera measured temperature to actual corrected temperature for different ratios of the instantaneous field of view of the camera (IFOV) to the fiber diameter (Fig 4.1). For IFOV/Fiber diameter ratios near to one, the fiber diameter takes up most of the thermal detector view. For larger ratios, the fiber diameter takes up less of the thermal detector view and has a smaller measured temperature to actual temperature ratio.

Marla (2007) also produced correlations for determining emissivity of polypropylene fibers based on fiber diameter (Fig 4.2). These correlations are for fiber diameters between 0.1 and 1 mm range (100 to 1000 μm). As our typical operation conditions are for fiber diameters between the 20 and 80 μm range, these correlations will have to be extended for this range, or the operating conditions need to be changed to account for the difference. The latter choice would be ideal if it were chosen not to modify the louver bracket as the primary-lens for the infrared camera will require fibers with diameters in the 100 to 1000 μm range. Operating conditions that produce fibers with diameters with in this range include mass flowrates of 1 g/min or greater and air flowrates of 80 liters/ min or lower. Table 4.2 shows a listing of fiber diameters produced for different mass and air flowrates for a no louvers case and for 30 mm louvers in parallel with a separation of 8 mm and a leading-edge distance below the die of 5 mm.

A 3200D Nikon camera with a 105 mm Nikon lens can be used to determine fiber diameters online. Images are to be taken at the different z positions below the die head that will be used when taking temperature measurements with the infrared camera.

Appropriate shutter speeds and apertures needed to image the rapidly moving fiber will need to be determined. Faster shutter speeds (i.e. 1/500 to 1/4000 seconds) will be needed to "freeze" motion of the fiber and obtain a crisp image of the fiber without smearing. Additional lighting and a sufficiently large aperture will be needed to see the fiber in the image. However, the aperture will also need to be small enough to allow a depth of field large enough to account for the fiber vibrations in the y direction. The operating conditions used in taking online fiber diameters will need to be the same as those conditions used in taking the online temperature measurements (to be determined).

Fiber images taken with the 3200D Nikon camera will be analyzed with NIH ImageJ software. A photo with a ruler in the field of view will be needed to do calibration in ImageJ. The software creates a calibration based on a known distance between two points in the image, in this case the markings on the ruler. The diameter of the fibers can then be determined by drawing a horizonal line across the fiber. These diameters will then be assumed when determining fiber emissivity and the spatial effect of the camera on the temperature measurements with Figs. 4.1 and 4.2.

4.2.3 Post-Processing with ThermaResearcher

After recording the infrared images, the maximum temperature along a "line" can be recorded for each frame in *ThermaResearcher.* As the camera lens was centered at each z location below the die, a horizontal "line" will be placed at the center of each video at vertical detector element 120. The software will then determine the point of maximum temperature along that line for each frame. (Note: The software also allows you to determine the average and minimum temperatures for the line.)

The software can then plot the maximum temperature for each frame of video. The maximum peaks in the resulting plot are assumed to be the time points where the fiber is in focus. The maximum of these temperature peaks is chosen for determining the uncorrected measured fiber temperature. In this peak's corresponding frame, a "spot" is placed on the fiber. Using the emissivity calculator for this "spot" allows you to determine the camera's measured temperature corrected for fiber emissivity. The emissivity inputted is the emissivity determined from Fig 4.2. This value is then divided by the ordinate value of Fig. 4.1 to correct for the spatial resolution of the camera. This temperature is considered as actual temperature of the fiber.

4.3 Potential Experimentations and Studies

As was described in chapter 1 of this work and the "plateau" simulations of B. Shambaugh et al. (2012), it might be of interest to observe the effect of air flowrate on the fiber temperature in the presence of louvers. Variables of interest include louver leading edge distance below the die z_1, chord length c, louver configurations f_1,f_2, and air flowrates.

Beard (2006) observed that increasing air flowrates resulted lower fiber temperature. They believed this was due to the finer fiber (from the higher air velocity) cooling faster than a larger diameter fiber (produced from a lower air velocity). Although finer fibers are produced with the louvers (as seen in Chapter 2), perhaps of fiber temperatures do not exhibit as sharp of a temperature drop with increasing air flowrate when the louvers are in the air field. However, until the 100-degree lens issue (less working distance) is addressed, the air flowrates will need to stay low for large enough fiber diameters to be produced to detect the fiber on the infrared camera. This should take

a latter priority to the effect of louver distance below the die and chord length until this issue is resolved. Beard (2006) also observed regions of almost constant temperature below the die where it was believed to have online crystallization. It would be interesting to observe if this event still occurs when the louvers are in the air field.

Also of potential interest would be the effect of the louvers on the birefringence of produced fibers to observe final fiber crystallinity. It was predicted by B. Shambaugh (2012) that there would be little change in online crystallinity as the fiber is far too hot for crystallization, even with higher zones of stress. Simulating a quench in the field below the "plateaus" showed little change in crystallization until the temperature drop was large. However, larger temperature drops resulted in poorer fiber attenuation, slightly negating the effects of the "plateau". Understanding effect of the louvers on fiber temperature especially at farther distance below the die might provide insight into ways to increase online crystallization without negating the effect of the louvers. Currently, most crystallization for melt blown fibers occurs at the collector as the fiber slowly cools down (see Bresse and Ko, 2003). However, fine fibers cool faster than coarser fibers. It is possible that the final fiber temperature will be higher when the louvers are in the air field than the base case without the louvers. Hotter fibers at the collector will require more time to cool at the collector than fibers that start out at cooler temperatures, possibly improving offline crystallization.

In the simulated air field model currently being developed, it would be interesting to see if heating or cooling the louvers would significantly affect the air flow between the louvers and the fiber temperature. Currently the louvers are made from aluminum, which

rapidly heats up in the air temperature air field and has a high thermal conductivity. Two questions might be considered:

(1) Is there significant heat loss through the aluminum louvers such that the temperature between the louvers cannot be considered a constant "plateau"?

(2) Is the temperature of the louvers significantly affecting the air flow regime at the louver walls?

If there is indeed significant heat loss through the louvers (question 1), then louvers made of materials of higher thermal resistance can maintain a higher air temperature by reducing the heat loss through the louvers. Heat losses from the interior (inside the louvers) air field through the louvers would consist of three resistances in series (convection on the inside, conduction through the louvers, and convection on the outside of the louvers. For the inside convective resistance, we should consider that there is a boundary layer that develops on each of the louvers as the air flows between the louvers. At the top of the louvers, the boundary layer has a thickness of zero. The boundary layer reaches its thickest value at the bottom of the louvers. Boundary layer calculations were made (see Appendix VI), and for an air flowrate of 100 liters/min, the boundary layer thicknesses (at the bottom of the louvers) ranged from 0.82 mm to 1.35 mm. Since the louvers were 6 to 10 mm apart, a substantial "core" of the airflow passes through the louvers with essentially no heat transfer occurring in a transverse direction to the air flow. Thus, the air flowing between the louvers outside of these boundary layers is expected to remain at the centerline temperature, thus maintaining the air temperature "plateau" at the centerline. As the fiber is most affected by the centerline air velocity and

temperature, this region is of main importance, and there is not significant heat loss from the air in this region.

Question (2) concerns the effect of louver wall temperature on the air flow regime and will be considered here. The temperature of flat plates can affect the critical Reynolds number of the flow regime (Schlichting, 1968; Welty et al., 2008) where hotter plate temperatures will decrease the critical Reynolds number, while cooler plates will increase this value. If the hot louvers are affecting the flow regime (making it more turbulent) that might affect the whipping of the fiber (if the temperature of the louvers are indeed greater than that of the air temperature). Perhaps a cooler louver will help stabilize the flow at the louver walls, reduce drag on the louvers, reduce resulting turbulence fluctuations between the louvers, and thus decrease the possibilities that the fiber will hit and stick to the louvers. It is also easier to remove slightly solidified polymer from the louvers than it is to remove the sticky molten polymer. If the polymer slightly solidifies upon hitting the louvers, it would have a greater chance of detaching from the louvers under the air flow, preventing accumulation of the polymer on the louvers. In this manner, the fiber can "unstick" itself and return to proper operating conditions.

4.4 Conclusion

It is proposed that infrared photography can be used to determine the effects of the louvers on the fiber temperature, and a methodology was presented for the use of infrared photography. Online fiber diameters will need to be obtained to correct for emissivity and spatial resolution effects on the measured temperatures. Issues to be resolved before a complete study can be done include the following:

- selecting proper operating conditions to observe the fiber with the primary lens of the infrared camera
- potentially modifying the louver device or bracket to allow the use of the infrared camera 100-degree lens to observe fiber temperature at higher air flowrates and finer diameter ranges
- determining proper Nikon D3200 camera settings to consistently observe accurate online fiber diameters

Studies on the effects of the louvers with different chord lengths, different leading-edge distances, and different air flowrates are recommended. Additional studies on the birefringence of produced fiber mats to observe crystallization and the effect of "cold" louvers on the air flow field and polymer temperature are also of interest.

REFERENCES

Bansal, V.; Shambaugh, R. L. On-line Determination of Diameter and Temperature during Melt Blowing of Polypropylene. *Ind. Eng. Chem. Res.* 1998, *37*(5), 1799-1806.

Bresse, R. R.; Ko, W. C. Fiber Formation During Melt Blowing. *Int. Nonwovens J.* 2003, 12, 21.

Beard. J. H. Analysis of fiber temperature and motion in the melt blowing process. Thesis (M.S.) University of Oklahoma, 2006.

Golzar, M.; Beyreuther, R.; Brunig, H.; Tandler, B.; Vogel, R. Online Temperature Measurement and Simultaneous Diameter Estimation of Fibers by Thermography of the Spinline in the Melt Spinning Process. *Adv. Polym. Technol*. 2004, *23* (3), 176-185.

Krutka, H. M.; Shambaugh, R. L.; Papavassiliou, D. V. Effects of Temperature and Geometry on the Flow Field of the Melt Blowing Process. *Ind. Eng. Chem. Res.* 2004, *43* (15), 4199

Marla, V. T.; Shambaugh, R. L.; Papavassiliou, D. V. Use of an Infrared Camera for Accurate Determination of the Temperature of Polymer Filaments. *Ind. Eng. Chem. Res.* 2007, *46* (1), 336–334.

Marla, Vishnu T., Shambaugh, Robert L., and Papavassiliou, Dimitrios, Online Measurement of Fiber Diameter and Temperature in the Melt Spinning and Melt Blowing Process. Ind. Eng. Chem. Res., 48 (2009), p 8736

Schlichting, H. *Boundary-Layer Theory*; 6th ed.; McGraw-Hill: New York, 1968; p 494-495.

Shambaugh, R. L.; Krutty, J. D.; Singleton, S. M. Melt Blowing Dies with Louvers. *Ind. Eng. Chem. Res.,* 2015, *54* (51), 12999-13004.

Shambaugh, B. R.; Papavassiliou, D. V.; Shambaugh, R. L. Modifying Air Fields to Improve Melt Blowing. *Ind. Eng. Chem. Res.* 2012, 51, 3472-3483.

Tate, B. D.; Shambaugh, R. L. Temperature Fields below Melt Blowing Dies of Various Geometries. *Ind. Eng. Chem. Res.* 2004, 43 (17), 5405-5410.

J. R. Welty; C. E. Wicks; R.E. Wilson; G. L. Rorrer. *Fundamentals of Momentum, Heat, and Mass Transfer,* 5th ed.; John Wiley & Sons, Inc: New Jersey, 2008; pg 165.

Table 1. Lists the recommended operational settings of the *ThermaCAM S60* infrared camera for taking thermal images of the melt-blown fiber.

IR Camera Recording Settings	
Start Record	Tool button/ F5
Record	At highest speed
Stop Record	After time duration of 33 seconds
File Format	Images in one file
Frame Rate	60 Hz
Emissivity (initial)	0.82
Object to Lens Distance	0.33 m (for Primary Lens) 9 to 10 mm (for 100° Lens)

Table 2. List of fiber diameters for fibers produced at different polymer flowrates and air flowrates. One set of diameters was produced with louvers in the air field. The louvers were c= 30 mm in the f_1,f_2 = 8,8 configuration, with a leading edge of z_1 = 5 mm. The second set of fiber diameters is for normal melt blowing.

Polymer Flowrate (g/min)	Air Flowrate (slpm)	Fiber Diameters (microns)	
		With Louvers	No Louvers
1	60	167	255
1	80	87	170
1.2	60	174	286
1.2	80	103	178

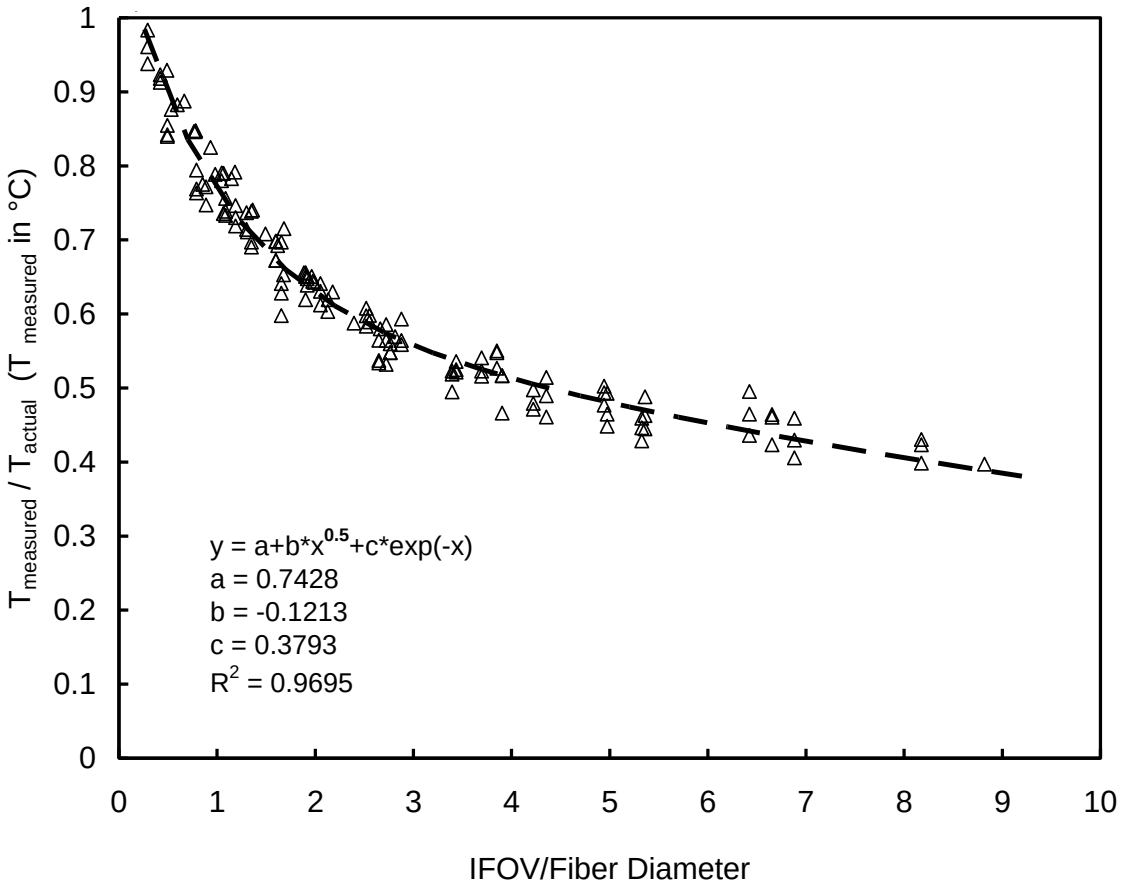

Fig 4.1. Correlation graph to correct measured temperature based on the instantaneous field of view to fiber diameter ratio. This graph was taken from Marla et al (2007).

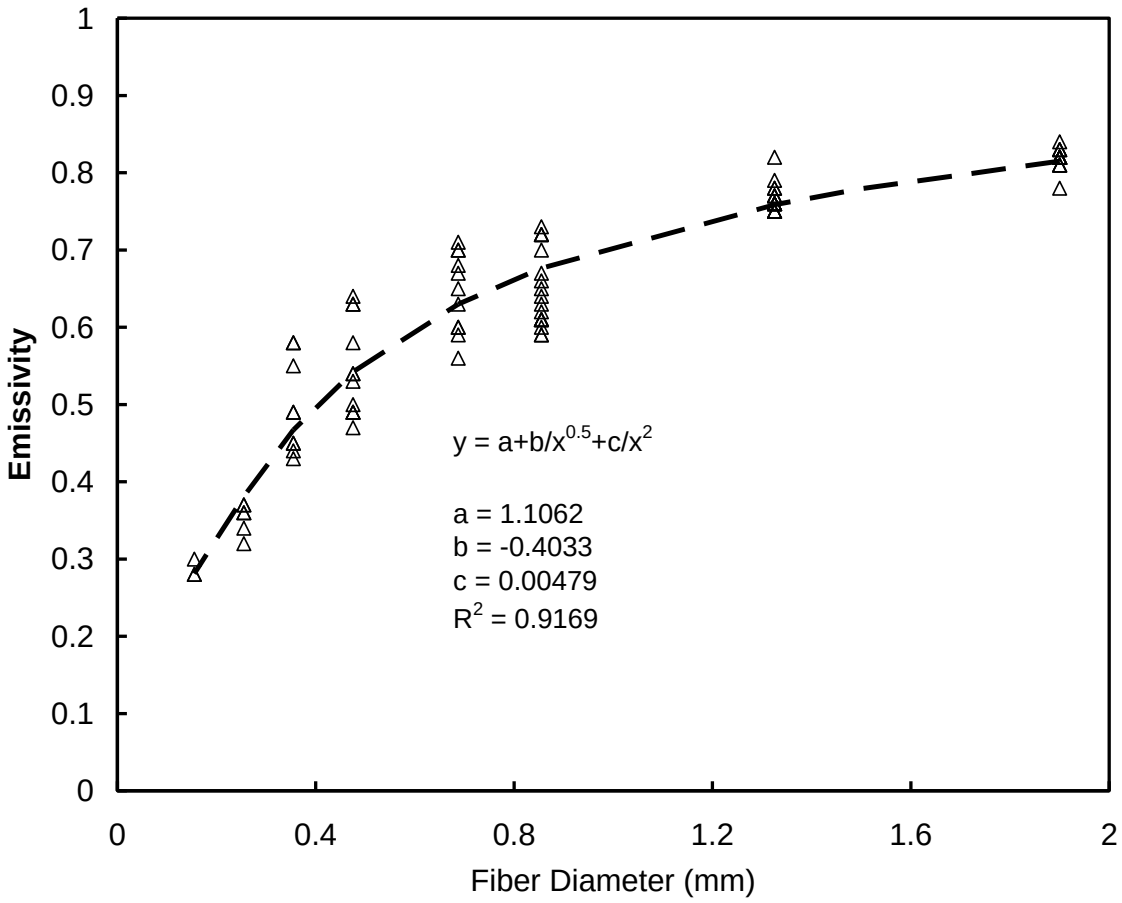

Fig. 4.2. Correlation graph to predict emissivity for polypropylene fibers of fiber diameters between 0.1 and 1 mm. This graph was taken from Marla (2007).

CHAPTER 5

CONCLUSIONS AND DISCUSSION OF FUTURE WORK

5.1 Summary of Work

A physical plateau in the air field below a melt blowing die was imposed by airfoil shaped louvers. These louvers prevented air jet spreading and imposed a constant average air velocity on the polymer filament, resulting in greater attenuation. Fibers were collected and measured offline using optical microscopy. Fiber diameters were found to be significantly reduced when louvers are in the air field compared to normal melt blowing conditions. Longer chords expose longer lengths of the fiber threadline to the nondecaying air velocity, causing a greater forwarding force on the fiber and thus greater attenuation and finer diameters. Angled chords act as a nozzle and expose the fiber to an increasing air velocity. This was found to be more beneficial for shorter chords that expose less of the threadline to the nondecaying air velocity. Louvers placed closer to the die resulted in finer diameters and less fiber sticking.

High Speed Photography was employed to observe the motion of a melt blown polymer filament when louvers were in the air field. Videos of the fiber in the region of the louvers and below the louvers were taken. The position of the fiber over time was tracked at different distances below the die. A code was implemented to calculate the frequency and amplitude of the fiber for various positions, configuration, and louver sizes. Frequency of the fiber in the region near the die was found to be greater for longer chords and angled shorter chords. Below the louvers, the frequency was found to be greater for angled shorter louvers. Longer chords showed little difference in frequency from normal melt blowing below the die. The amplitude of the fibers below the louvers

were found to be less than that of normal melt blowing for greater leading edge distances below the die. Fiber amplitude in the region near the die was similar to normal melt blowing but larger standard deviations in the amplitudes were found when using the louvers. Such larger variances coinciding with fluctuations in air velocity can cause fiber sticking and web defects, particularly for closer chord separations and angled louvers.

5.2 Recommendations for Future Work

A methodology for measuring online fiber temperature with louvers in the air field with infrared photography was presented. As the louver prevent air jet entrainment, the air temperature is expected to not decay between the louvers, exposing the fiber to a higher temperature in the region of main fiber attenuation. Observing the effects of the louvers on the fiber temperature is of interest as maintaining the fiber at higher temperatures will keep the polymer molten and attenable. Online fiber diameter measurements will be needed to correct for emissivity effects and smallness of the fiber compared to the camera thermal detectors.

Online fiber diameter measurements would also provide more insight into the fiber attenuation region and how the louver air field affects this attenuation. If the fiber temperature is maintained for longer distances below the die, then the attenuation range might be extended to longer distances below the die.

The current emissivity correlations for polypropylene developed by Marla et al. (2007) extend to larger fiber diameters (<100 microns). While it would be interesting to observe the effect of the louvers at higher polymer flowrates and lower air flowrates, it would more advantageous to observe online temperature measurements at lower fiber diameter ranges (approximately 20 to 30 microns).

It was also proposed that modifications to the louvers would be advantageous (see Appendix I for a short discussion of such possibilities). Currently the end plates of the louver device and the bracket block the camera line between 2 and 8 cm below the die. Being able to observe fiber frequency, amplitude, and online attenuations in this region would add clarification to the effects of the louvers on the polymer fiber, particularly at the louver tips where the majority of the fiber sticking occurred.

Mentioned in Chapter 2, another common melt spinning process is spunbonding. In this process fibers are extruded from a die and exposed to quenching air to solidify the polymer. The fiber then goes through and attenuating device, usually a venturi, before arriving at a collection screen. It might be beneficial to add louvers immediately below the venturi (see Fig 5.1).

In melt blowing at the nanometer scale, air flowrates are significantly higher, and consequently, so is the potential for detrimental fiber whipping, fiber backfolding, and defects. In their study Chung and Kumar (2012), suggested that one of the factors that lead to fiber backfolding was air jet spreading, and that preventing this spreading could reduce significant whipping and defects. While the air velocities are likely too high for the louver to influence fiber reduction in the nanometer range, the louvers will prevent air jet spreading; therefore, a study with louvers in the melt blowing air field for nanometer fiber production would be of interest.

REFERENCES

Chung, C.; Kumar, S. Onset of Whipping in the melt blowing process. *Journal of Non-Newtonain Fluid Mechanics.* 2013, *192*, 37-47

Marla, V. T.; Shambaugh, R. L.; Papavassiliou, D. V. Use of an Infrared Camera for Accurate Determination of the Temperature of Polymer Filaments. *Ind. Eng. Chem. Res.* 2007, *46* (1), 336–334.

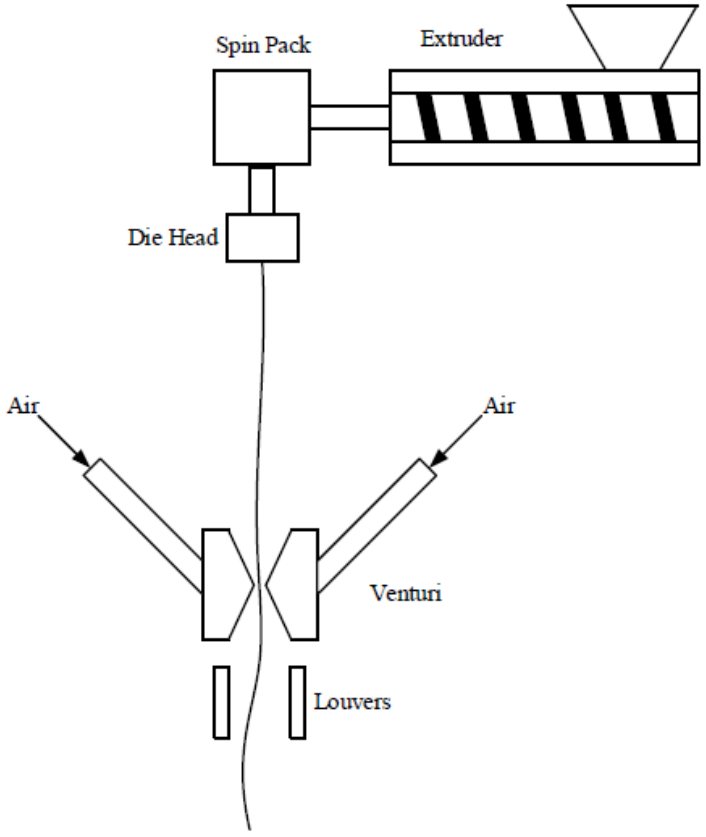

Fig. 5.1. The spunbonding process with louvers below the venturi (attenuation device).

APPENDIX I:

THE LOUVERS

Fig. I.1.a - e and Fig. I.2 are engineering drawings of the louvers and the louver device. The first figure depicts a general louver with a total chord length *c*, a tapered length of 10 mm, a straight length of *x*, and rounded leading-edge of radius 0.794 mm, and a chord thickness of 1.588 mm. The next several figures show the dimensioning for each chord size.

The chords shown in the above figures are then attached to 55 mm long tabs with JB weld with screw holes on the ends. The tabbed louver is then screwed to two end plates with a slot to allow the louvers to be moved to different separations (Fig I.2).

The louver separation was verified by measuring the top separation and the bottom separation with a ruler. The angle of both louvers was also checked with an "angle plate", a wood cutting that was cut at an appropriate angle to act as a level. The "straight" length of the louvers would be aligned up with the appropriate "angled plate" (Fig I.3). The height of the louvers was adjusted by placing wooden planks of certain thickness to raise the louver leading-edges to the appropriate height.

The louvers are then placed on a bracket that is attached to the equipment stand below the die head. Fig I.4. shows the louvers on the louver bracket. Also depicted in the figure is the camera position (both the high speed camera and the infrared camera).

In industry, it would be useful to design a device that can be cranked into correct position so that the louvers do not need to be completely removed to be adjusted. Currently the louvers are adjusted and interchanged by screwing them onto two end plates.

In Chapters 3 and 4 it was recommended that the louver device and bracket be modified to allow better imaging of the fiber in the 2 to 8 cm range below the die. Quickest and easiest modification would be to add a viewing slot on the end plates of the louvers and on the louver bracket. During high speed photography, additional light is needed to image the fiber. The louvers, being solid metal, currently cast shadows at 2 cm and greater in the region with the louvers. A possible solution would be to make louvers out of a transparent material that can still be machined into a simple “airfoil” shape. Borosilicate glass is a possibility as it can tolerate large changes in temperature and is transparent. However, the material would have to be evaluated to determine if it can be machined rather inexpensively and to the correct shape without fracturing.

GENERAL LOUVERS AND NOMENCLATURE

MATERIAL: 1/16" THICK ALUMINUM

NOT TO SCALE

Fig. I.1.a. General Engineering Drawing of the aluminum louvers with a side view and a cross-sectional view. Each louver had a total chord length c, a rounded leading-edge with a radius of 0.794 mm, a tapered trailing-edge of 10 mm, and a chord thickness e of 1.588 mm. Each louver was 256 mm long with an active length of 146 mm. 55 mm of the ends of each side of the louvers had tabs welded to them to allow for the louvers to be attached to the overall louver device.

SIDE VIEW

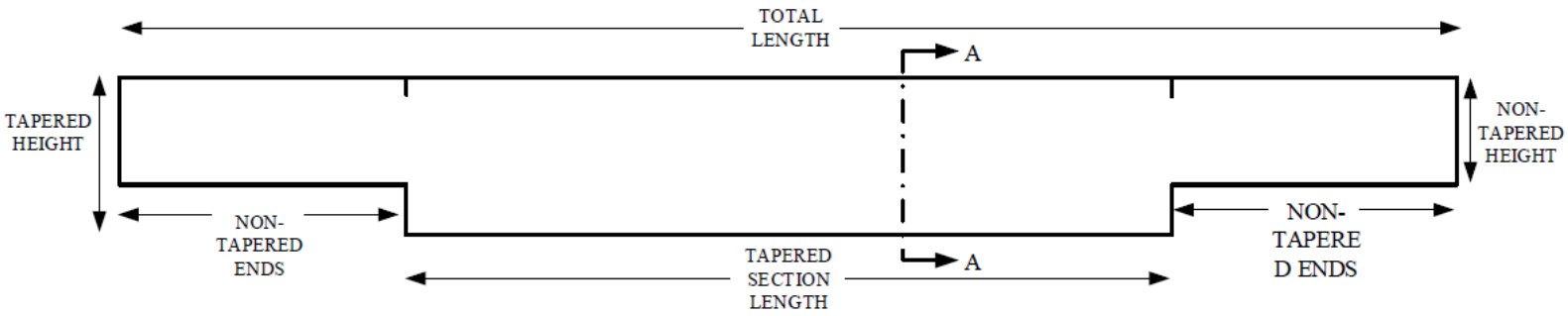

SECTION AA

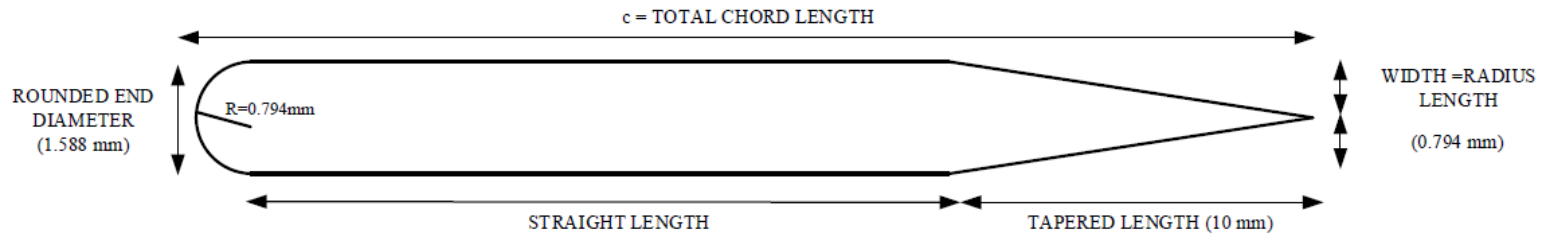

Fig. I.1.b. Engineering drawing of 1.25 cm louvers.

12.5 cm LOUVERS

MATERIAL: 1/16" THICK ALUMINUM

NOT TO SCALE

SIDE VIEW			SECTION AA		
Total Length	256	mm	Total Chord Length	12.5	mm
Tapered Section Length	146	mm	Rounded side Diameter	1.588	mm
Tapered Section Height	12.5	mm	Radius	0.794	mm
Non-tapered Ends Length	55	mm	Straight Length	1.706	mm
Non-tapered Ends Height	20	mm	Tapered Length	10	mm

SIDE VIEW

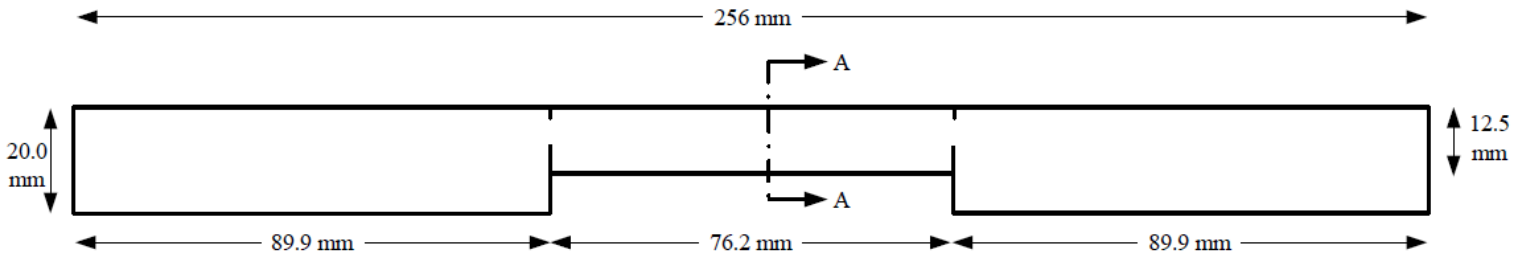

SECTION AA

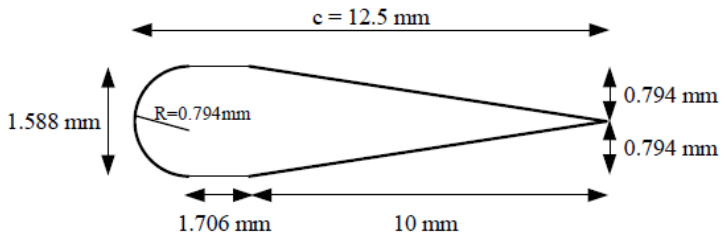

Fig. I.1.c. Engineering drawing of 2 cm louvers

2 cm LOUVERS

MATERIAL: 1/16" THICK ALUMINUM

NOT TO SCALE

SIDE VIEW			SECTION AA		
Total Length	256	mm	Total Chord Length	20	mm
Tapered Section Length	146	mm	Rounded side Diameter	1.588	mm
Non-tapered Ends Length	55	mm	Radius	0.794	mm
Non-tapered Ends Height	20	mm	Straight Length	9.206	mm
			Tapered Length	10	mm

SIDE VIEW

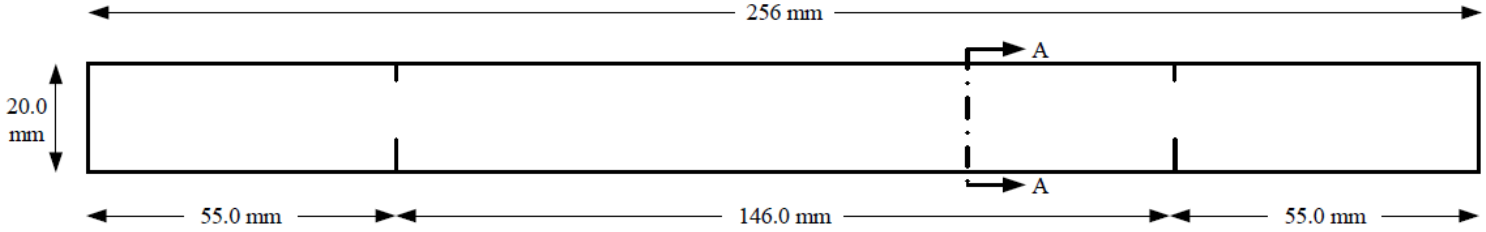

SECTION AA

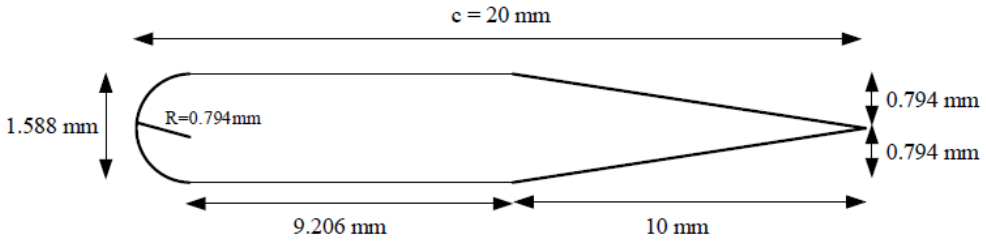

Fig. I.1.d. Engineering drawing of 3 cm louvers

3 cm LOUVERS

MATERIAL: 1/16" THICK ALUMINUM

NOT TO SCALE

SIDE VIEW			SECTION AA		
Total Length	256	mm	Total Chord Length	30	mm
Tapered Section Length	146	mm	Rounded side Diameter	1.588	mm
Tapered Section Height	30	mm	Radius	0.794	mm
Non-tapered Ends Length	55	mm	Straight Length	19.206	mm
Non-tapered Ends Height	20	mm	Tapered Length	10	mm

SIDE VIEW

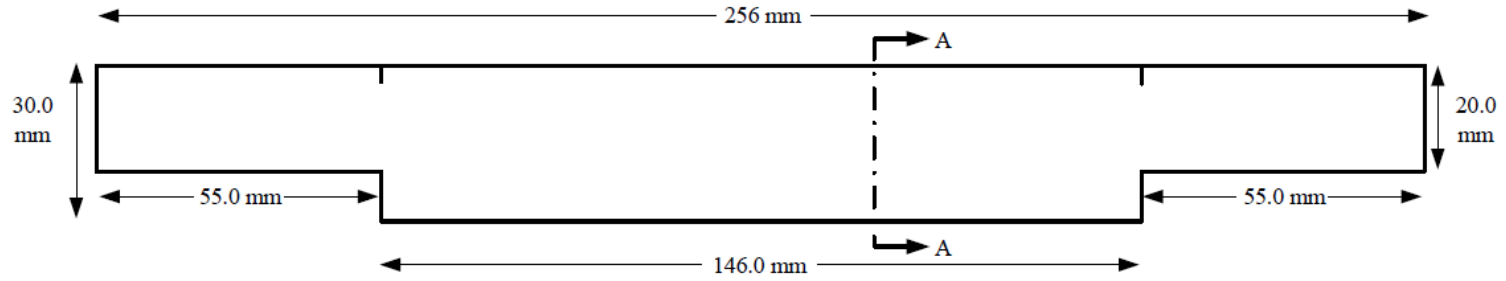

SECTION AA

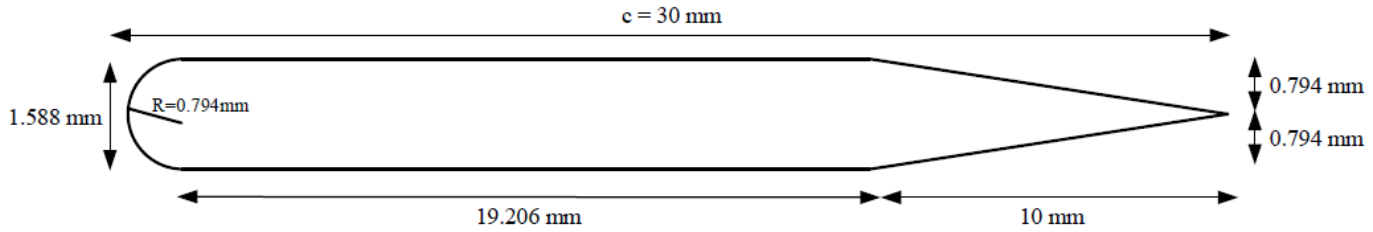

Fig. I.1.e. Engineering drawing 4 cm louvers

4 cmLOUVER

MATERIAL: 1/16" THICK ALUMINUM

NOT TO SCALE

SIDE VIEW			SECTION AA		
Total Length	256	mm	Total Chord Length	40	mm
Tapered Section Length	146	mm	Rounded side Diameter	1.588	mm
Tapered Section Height	40	mm	Radius	0.794	mm
Non-tapered Ends Length	55	mm	Straight Length	29.206	mm
Non-tapered Ends Height	20	mm	Tapered Length	10	mm

SIDE VIEW

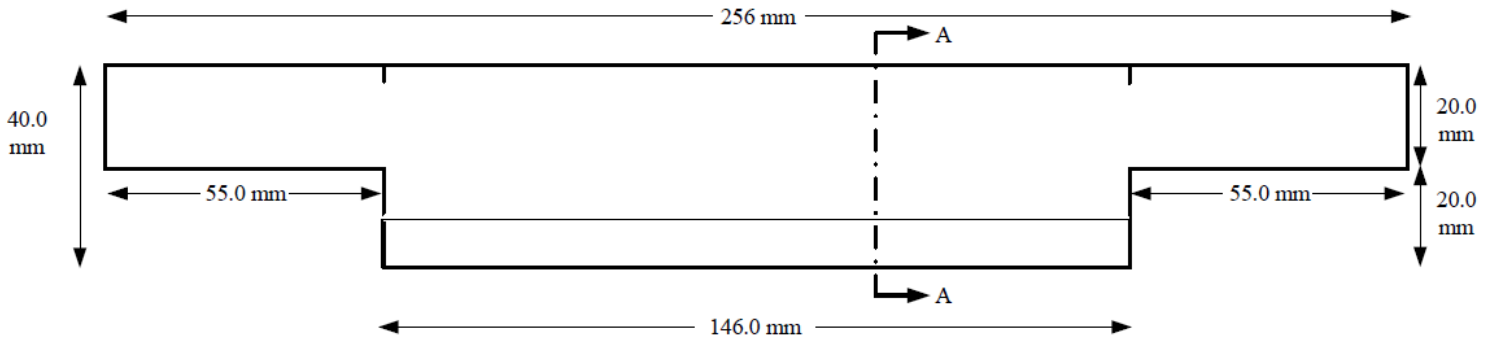

SECTION AA

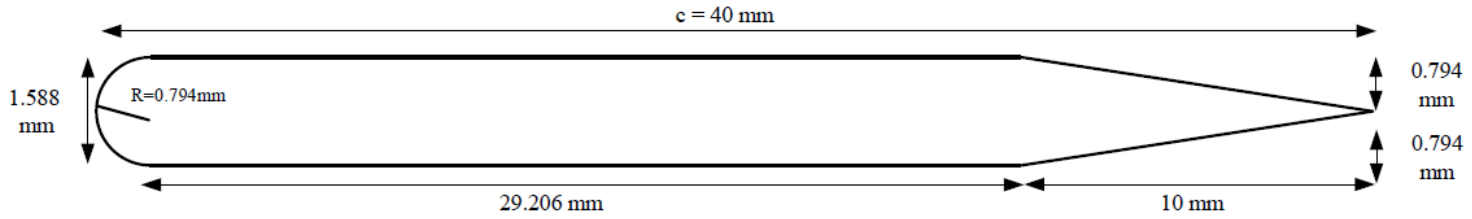

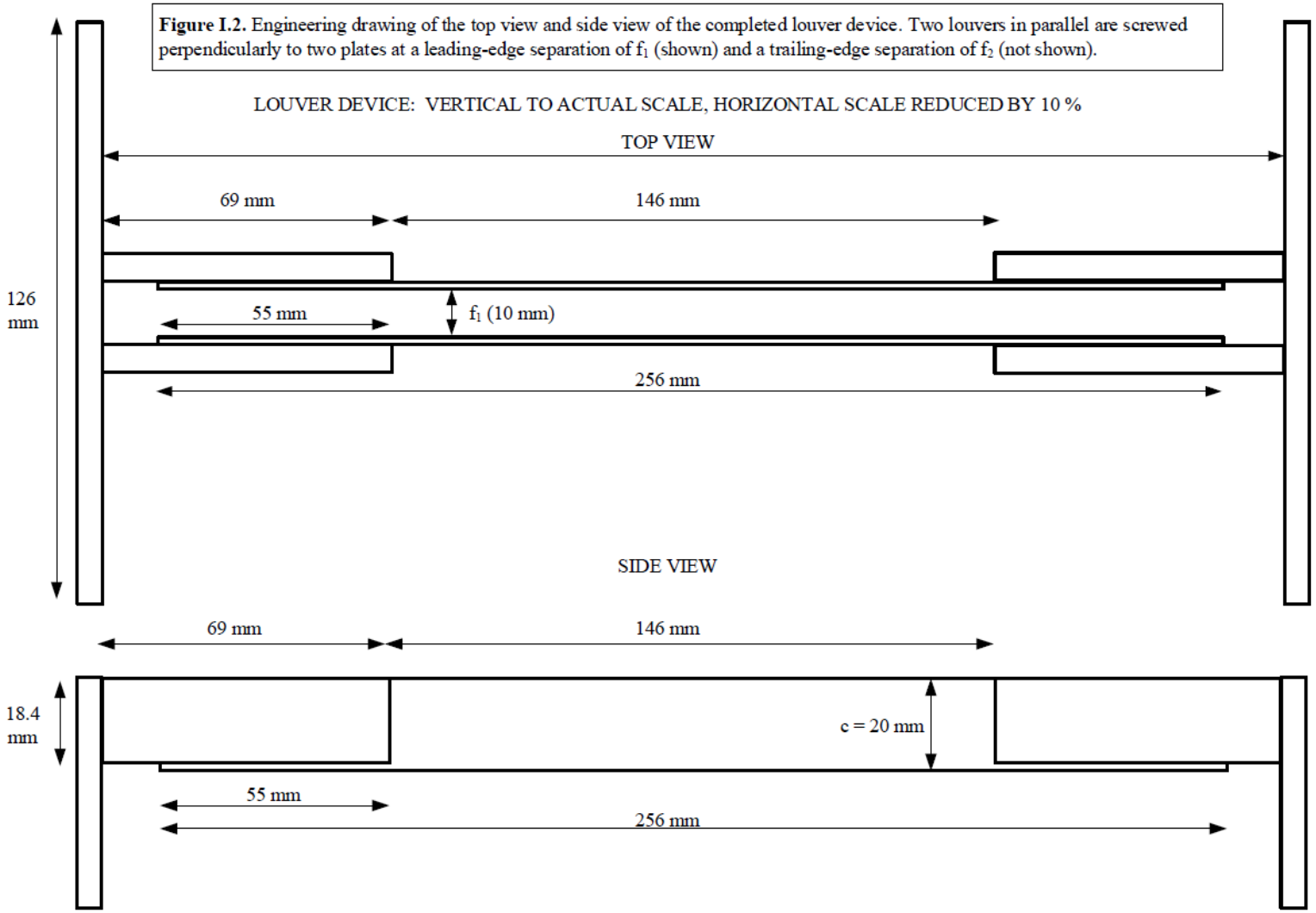

Figure I.2. Engineering drawing of the top view and side view of the completed louver device. Two louvers in parallel are screwed perpendicularly to two plates at a leading-edge separation of f_1 (shown) and a trailing-edge separation of f_2 (not shown).

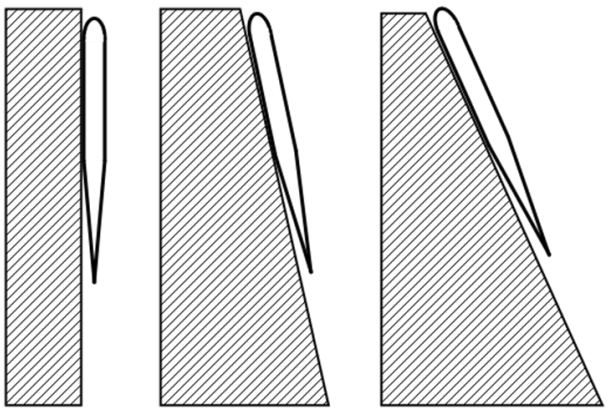

Fig. I.3. General schematic of angle plates used to align the louvers at a desired angle.

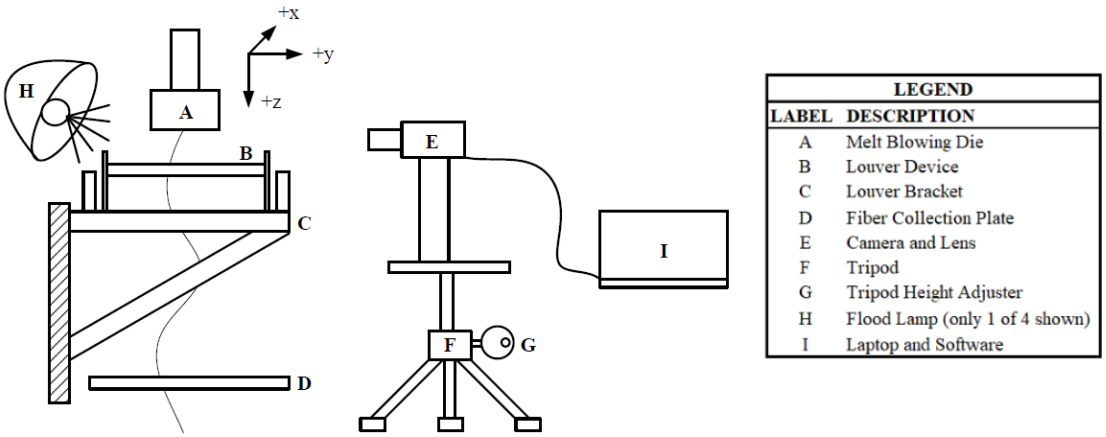

Fig. I.4. Schematic of the louver bracket and louver device below the die head. Also shown is the position of the camera used in chapter 3 and in chapter 4.

APPENIDX II:

MEASURMENT OF FIBER DIAMETERS AND ADDITIONAL RESULTS TO CHAPTER 2

II.1 Further Details on Fiber Collection and Web Defects

Fibers were collected on a mesh screen. A sample of this was cut from the resulting web and placed on a microscope slide. A Nikon Labophot-Pol optical microscope with a micrometer eyepiece was used to measure the fiber diameters offline. For each slide, 15 fiber diameter measurements were taken and averaged. A student T-Test was performed on each collected data set to verify that the fiber diameter obtained with the louvers was significantly different than the fiber diameter obtained without the louvers. The criteria value used was a t value of 0.05. Except for positions two positions, all cases were found to be significantly different. These potions were for 12.5 mm chords with a louver configuration of f_1,f_2 =10,10 at leading edges of z1= 5 and 10 mm for an air flowrate of 110 slpm. The standard deviation of the experiments averaged between 1 to 2 μm for each case.

Table II.1 and II.2 provides a complete list of all the louver positional and air flowrate combinations that were used in experiments. These tables also notate which positions produced webs with defects (signified with *) or were not collectable (signified with **). These defects were the result of the fiber sticking to the louver wall, tangling with more incoming fiber, and then detaching after the filament had cooled. Usually after detaching from the louver walls, the operation would return to normal for a period before the threadline again struck and stuck to the louvers. It is believed that this sticking is a result of fluctuations in the air field which would push the fiber onto the louver walls.

II.2 Additional Fiber Diameter Results

The additional graphs are similar to those presented in chapter 13, but they include the lower air flowrates of 80 and 100 slpm, the 12.5 and 40 mm chords, and the greater leading edges. The graphs in Chapter 2 were selected as they showed the lowest fiber diameters and were operationally the easiest to use, which is preferred for publication. As these graphs are at lower air flowrates, the fiber diameters were larger, 50 to 80 microns compared to the 40 to 20 micron fiber diameters seen in Chapter 2. For the most part, the trends seen in Chapter 2 are seen in these graphs. The effect of louver angle is more emphasized at lower air flowrates (80 and 100 lpm) as well as for shorter chords (c= 12.5 mm). The poorest results are seen for the 12.5 mm chords, likely as they do not expose much of the fiber length to the constant air jet as the longer chords do. There is also less data collected for some of the higher air flowrates and larger leading edge distances due to difficulties with fiber sticking. In total there are 42 graphs (Fig II.1 to Fig II.42). They are listed in the same order as they were in Chapter 2 (effect of z1, effect of f_1, effect of air flowrate, and the effect of chord length). All graphs are for 0.5 g/min polymer mass flowrate. The polymer temperature at the die was 230° C and the air temperature was 300 °C. All graphs are show curves for f_1,f_2 louver configurations.

Table II.1. A compilation of all louver positions and air flowrate combinations experiments were performed for. The top row categorizes the possibilities in leading-edge distances below the die z_1. The left-most column categorizes the possibilities by chord length and air flowrate combinations. The inner boxes represent the leading and trailing edge separation combinations f_1,f_2. A response of N/A means that an experiment at that possible condition was not performed. A response of * means the produced web had defects. A response of ** means that fibers could not be collected at the position.

Possible Run Conditions	$z_1 = 5$	$z_1 = 10$	$z_1 = 15$	$z_1 = 20$
c = 1 cm , Q_a = 80 liters/min	f_1,f_2 = 10,10	10,10	10,10	N/A
	10,8	10,8	10,8	N/A
	10,6	10,6	10,6	N/A
	8,8	8,8	8,8	N/A
	8,6	8,6	8,6	N/A
	6,6	6,6	6,6	N/A
c = 1 cm , Q_a = 100 liters/min	10,10	10,10	10,10	N/A
	10,8	10,8	10,8	N/A
	10,6	10,6	10,6	N/A
	8,8	8,8	8,8	N/A
	8,6	8,6	8,6	N/A
	6,6	6,6	6,6	N/A
c = 1 cm , Q_a = 110 liters/min	10,10	10,10	10,10	N/A
	10,8	10,8	10,8	N/A
	10,6	10,6	10,6	N/A
	8,8	8,8	8,8	N/A
	8,6	8,6	8,6	N/A
	6,6	6,6	6,6	N/A
c = 2 cm , Q_a = 80 liters/min	10,10	10,10	10,10	10,10
	10,8	10,8	10,8	10,8
	10,6	10,6	10,6	10,6
	8,8	8,8	8,8	8,8
	8,6	8,6	8,6	8,6
	6,6	6,6	6,6	6,6
c = 2 cm , Q_a = 100 liters/min	10,10	10,10	10,10	10,10
	10,8	10,8	10,8	10,8
	10,6	10,6	10,6	10,6 **
	8,8	8,8	8,8	8,8
	8,6	8,6	8,6	8,6 **
	6,6	6,6	6,6 **	6,6 **
c = 2 cm , Q_a = 110 liters/min	10,10	10,10	10,10	10,10
	10,8	10,8	10,8	10,8
	10,6 *	10,6 *	10,6 **	10,6 **
	8,8	8,8	8,8	8,8
	8,6	8,6	8,6 **	8,6 **
	6,6	6,6	6,6	6,6 **

Table II.2. A continuation of Table II.1.

Possible Run Conditions	$z_1 = 5$	$z_1 = 10$	$z_1 = 15$	$z_1 = 20$
c = 3 cm , Q_s = 80 liters/min	10,10	10,10	10,10	N/A
	10,8	10,8	10,8	N/A
	10,6	10,6	10,6	N/A
	8,8	8,8	8,8	N/A
	8,6	8,6	8,6	N/A
	6,6	6,6	6,6	N/A
c = 3 cm , Q_s = 100 liters/min	10,10	10,10	10,10	N/A
	10,8	10,8	10,8	N/A
	10,6	10,6	10,6 **	N/A
	8,8	8,8	8,8	N/A
	8,6	8,6 *	8,6 **	N/A
	6,6	6,6	6,6	N/A
c = 3 cm , Q_s = 110 liters/min	10,10	10,10	10,10	N/A
	10,8	10,8	10,8 **	N/A
	10,6 *	10,6 **	10,6 **	N/A
	8,8	8,8	8,8	N/A
	8,6 *	8,6 **	8,6 **	N/A
	6,6 *	6,6 *	6,6 **	N/A
c = 4 cm , Q_s = 80 liters/min	10,10	N/A	N/A	N/A
	10,8	N/A	N/A	N/A
	10,6	N/A	N/A	N/A
	8,8	N/A	N/A	N/A
	8,6	N/A	N/A	N/A
	6,6	N/A	N/A	N/A
c = 4 cm , Q_s = 100 liters/min	10,10	N/A	N/A	N/A
	10,8	N/A	N/A	N/A
	10,6 **	N/A	N/A	N/A
	8,8	N/A	N/A	N/A
	8,6 *	N/A	N/A	N/A
	6,6	N/A	N/A	N/A
c = 4 cm , Q_s = 110 liters/min	10,10 *	N/A	N/A	N/A
	10,8	N/A	N/A	N/A
	10,6 **	N/A	N/A	N/A
	8,8 *	N/A	N/A	N/A
	8,6 *	N/A	N/A	N/A
	6,6 *	N/A	N/A	N/A

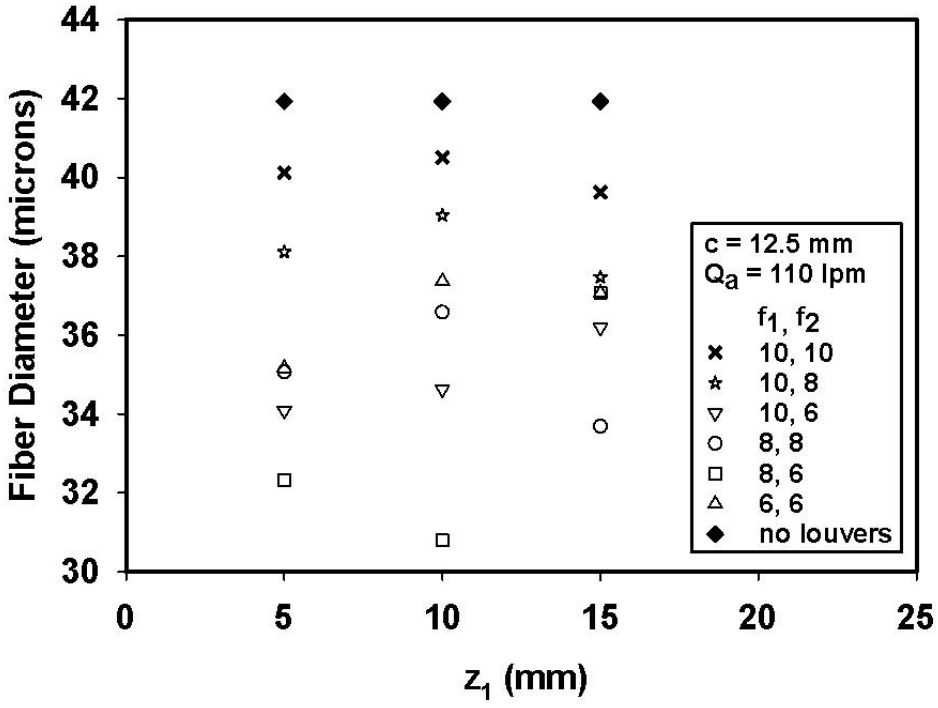

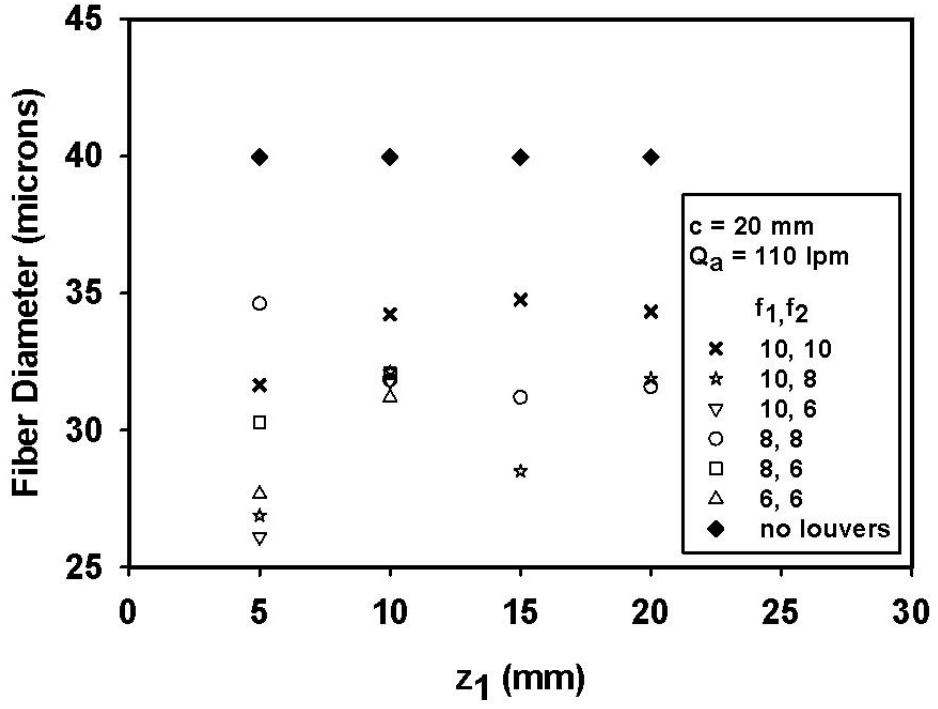

Fig II.1 and II.2. The effect of z_1 on fiber diameter. For these graphs, c = 12.5 and 20 mm and air flowrate = 110 L/min. Curves are shown for each f_1, f_2 configuration.

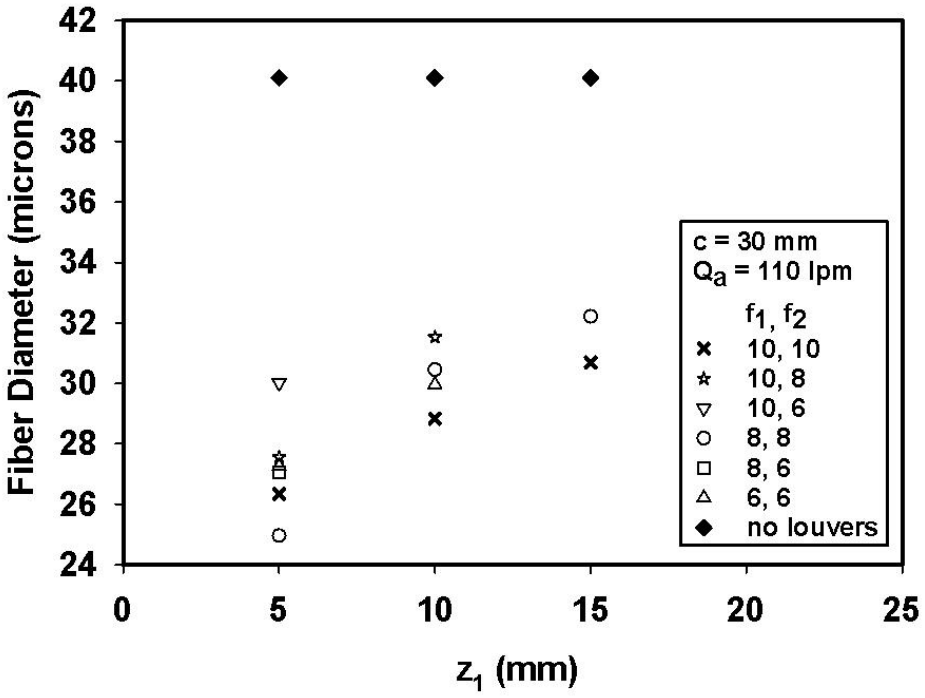

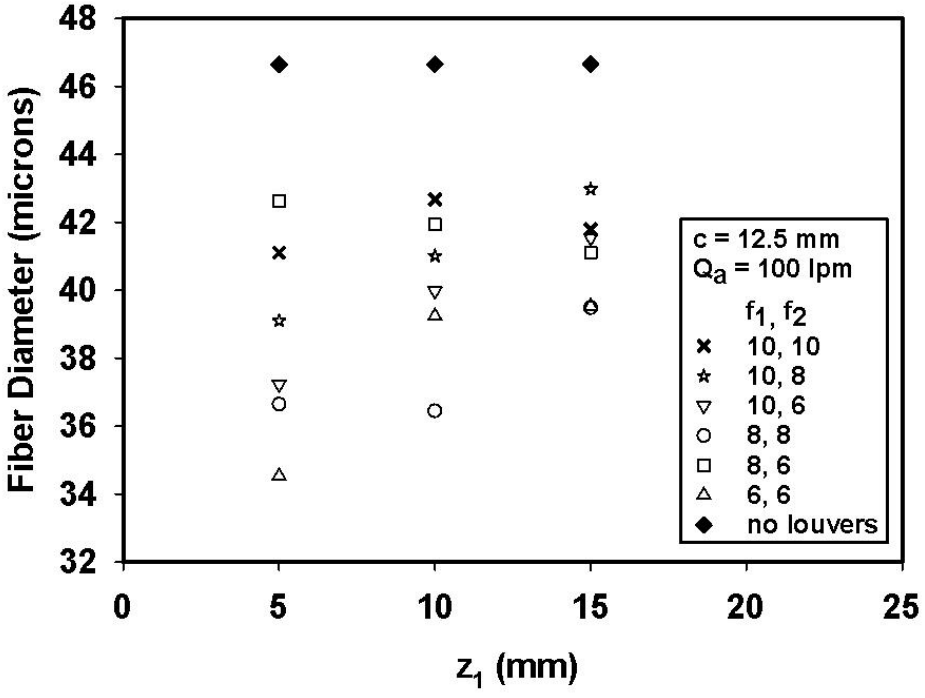

Fig II.3 and II.4. The effect of z_1 on fiber diameter. Fig II.3 is for c = 30 and air flowrate = 110 L/min. Fig II.4 is for c = 12.5 and air flowrate = 100 L/min.

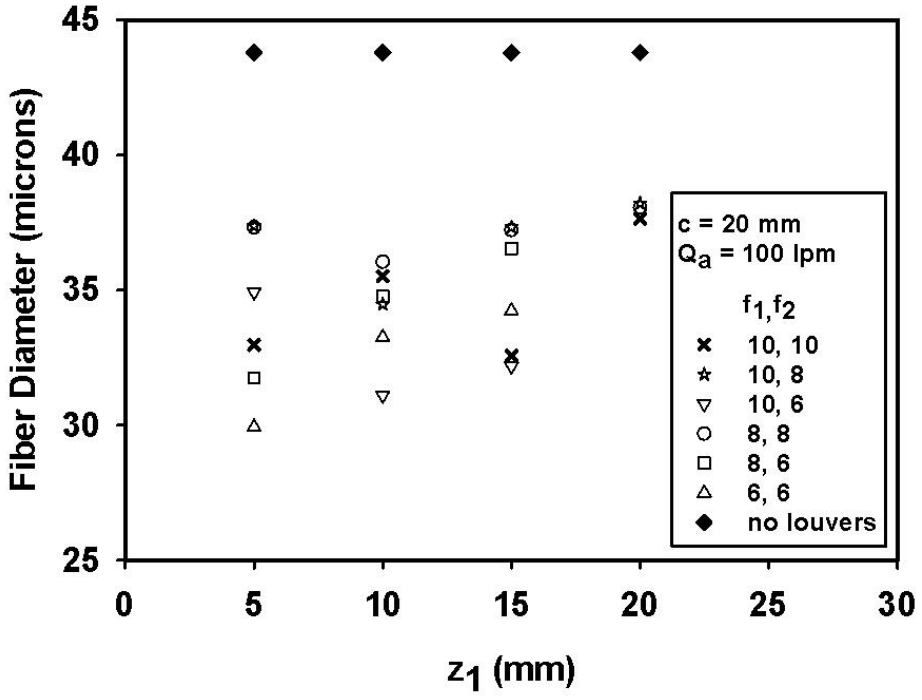

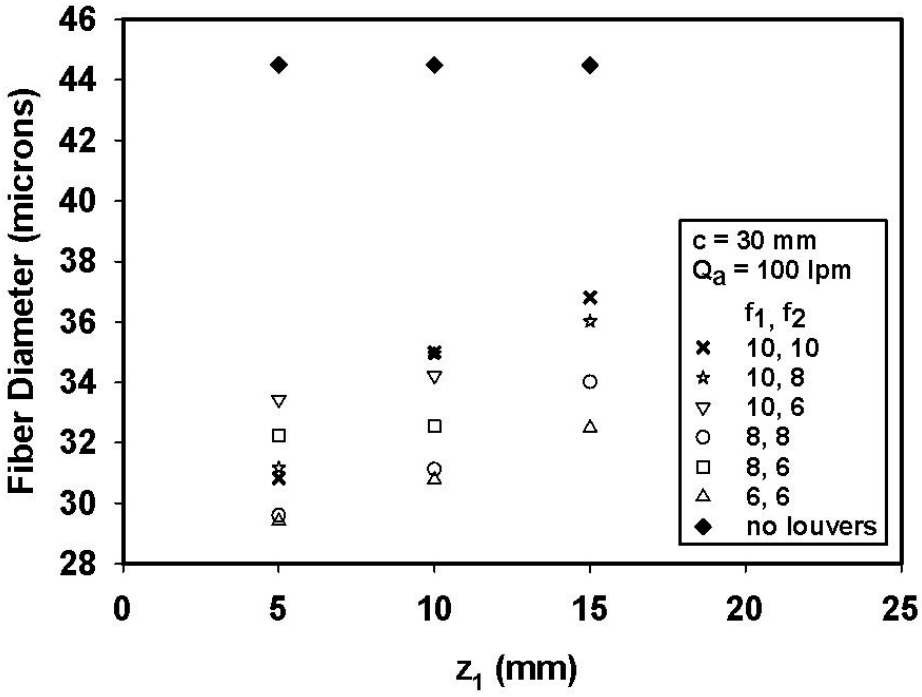

Fig II.5 and II.6. The effect of z_1 on fiber diameter. For these graphs, c = 20 and 30 mm and air flowrate = 100 L/min.

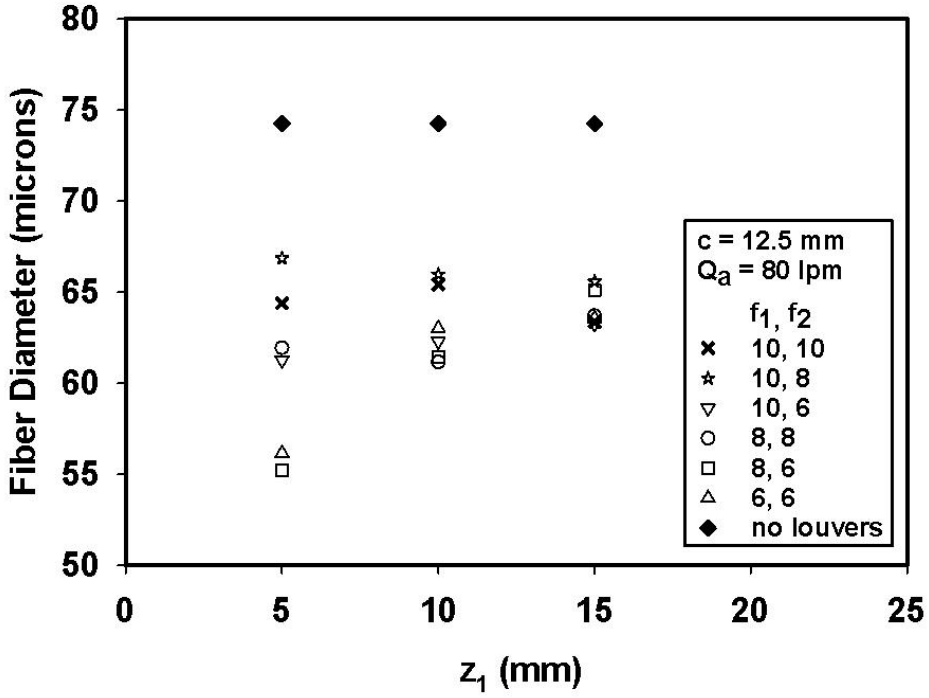

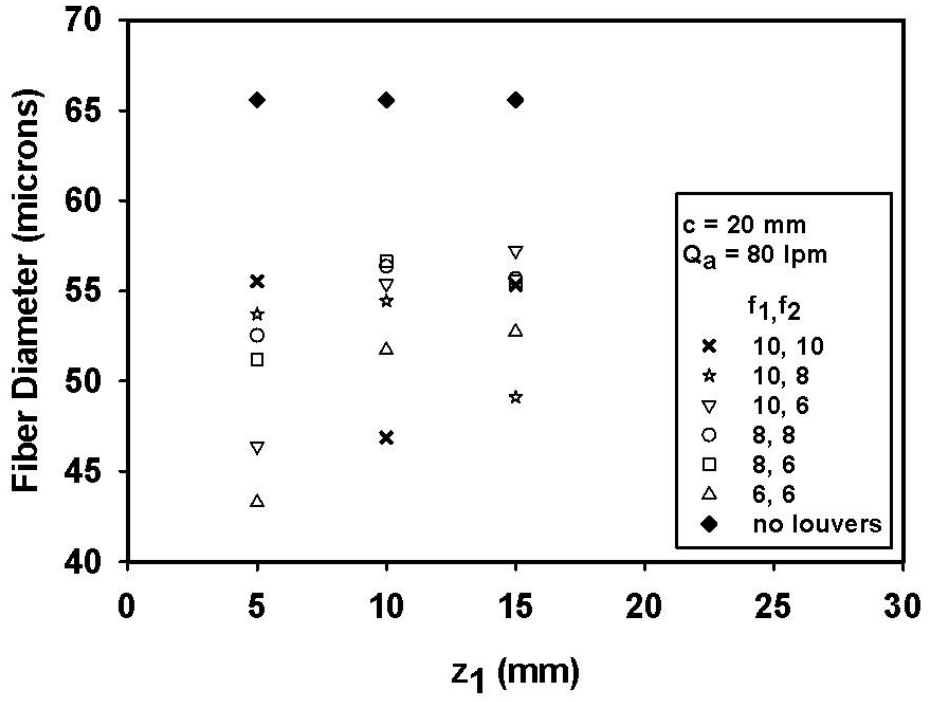

Fig II.7 and II.8. The effect of z_1 on fiber diameter. For these graphs, c = 12.5 and 20 mm and air flowrate = 80 L/min.

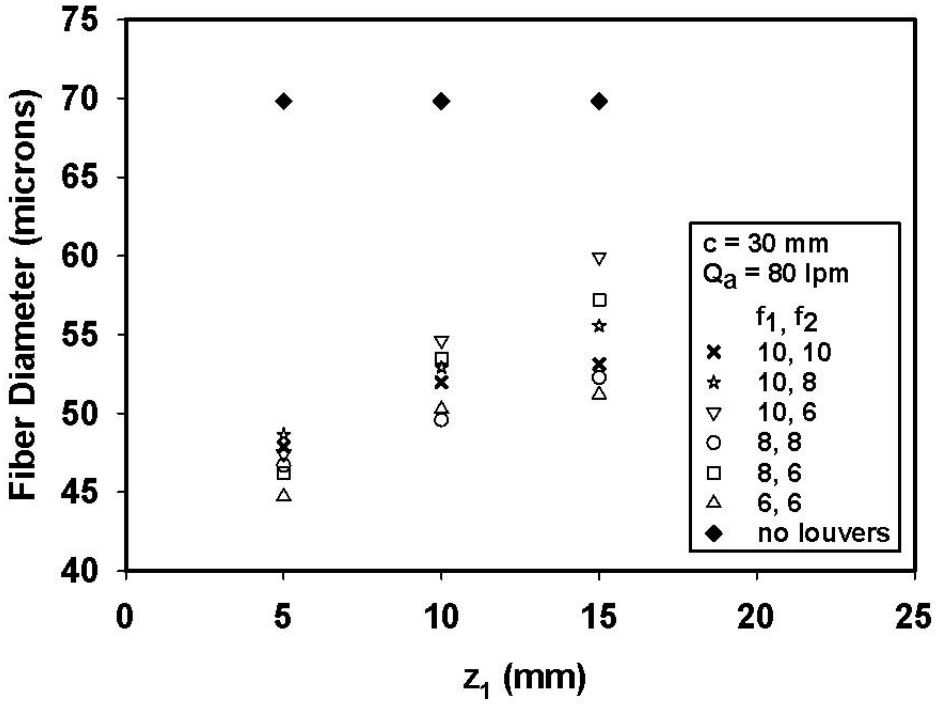

Fig II.9. The effect of z_1 on fiber diameter. For this graph, c = 30 mm and air flowrate = 80 L/min.

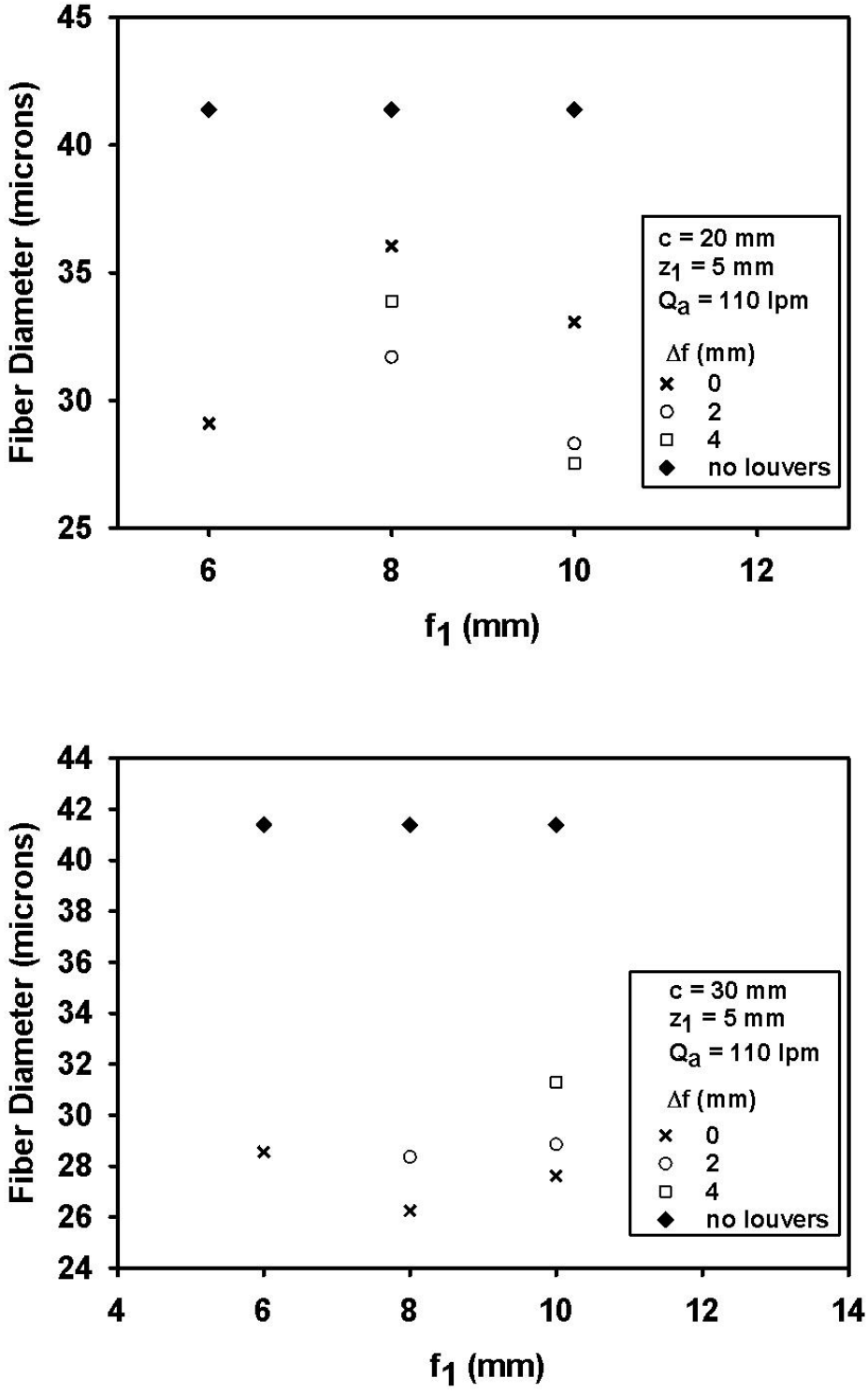

Fig II.10 and II.11. The effect of f_1 on fiber diameter. For these graphs, c = 20 and 30 mm, z_1 = 5 mm, and air flowrate = 110 L/min. Curves are shown for $\Delta f = f_1 - f_2$ = 0, 2 and 4 mm.

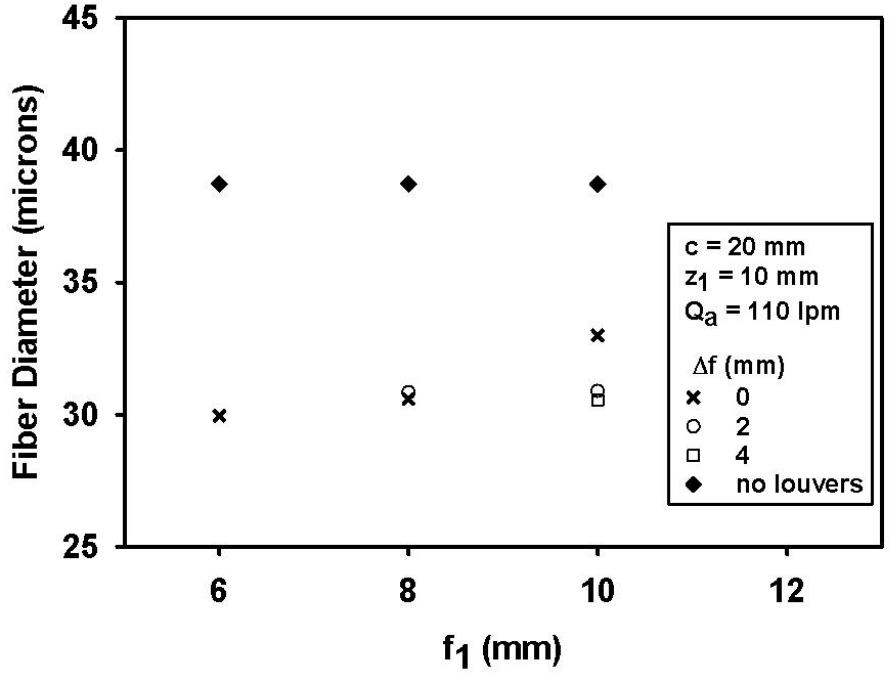

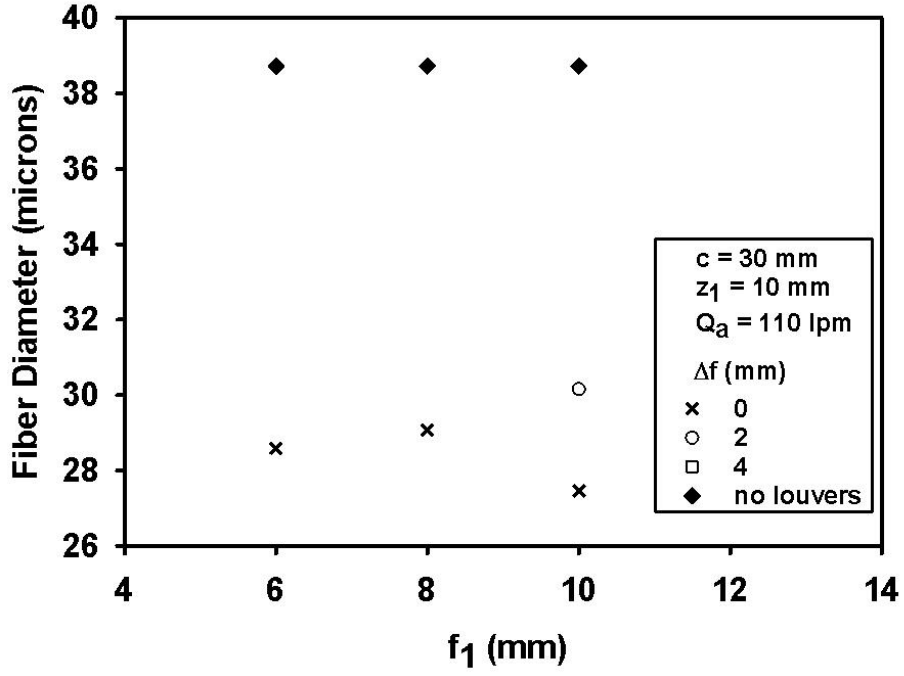

Fig II.12 and II.13. The effect of f_1 on fiber diameter. For these graphs, c = 20 and 30 mm, z_1 = 10 mm, and air flowrate = 110 L/min. Curves are shown for $\Delta f = f_1 - f_2$ = 0, 2 and 4 mm.

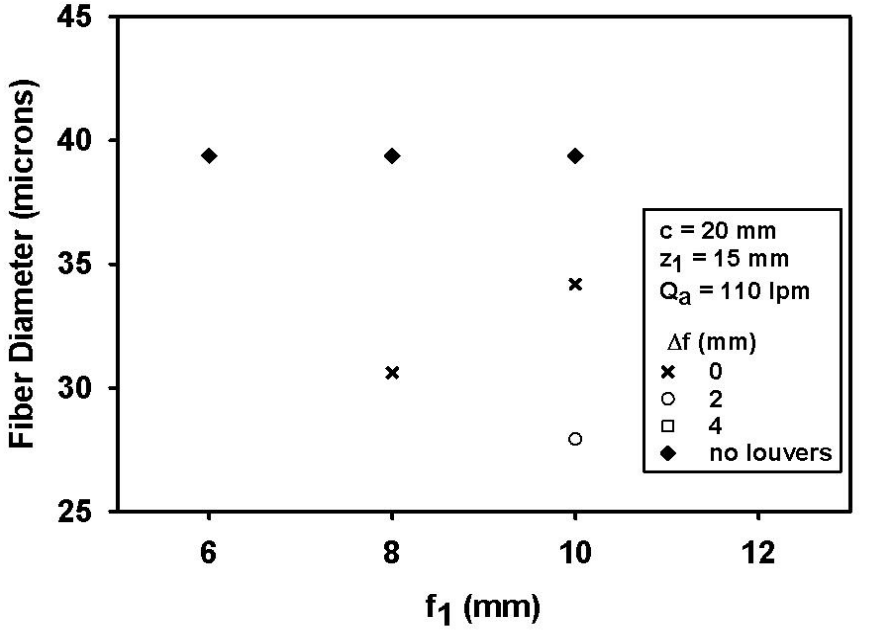

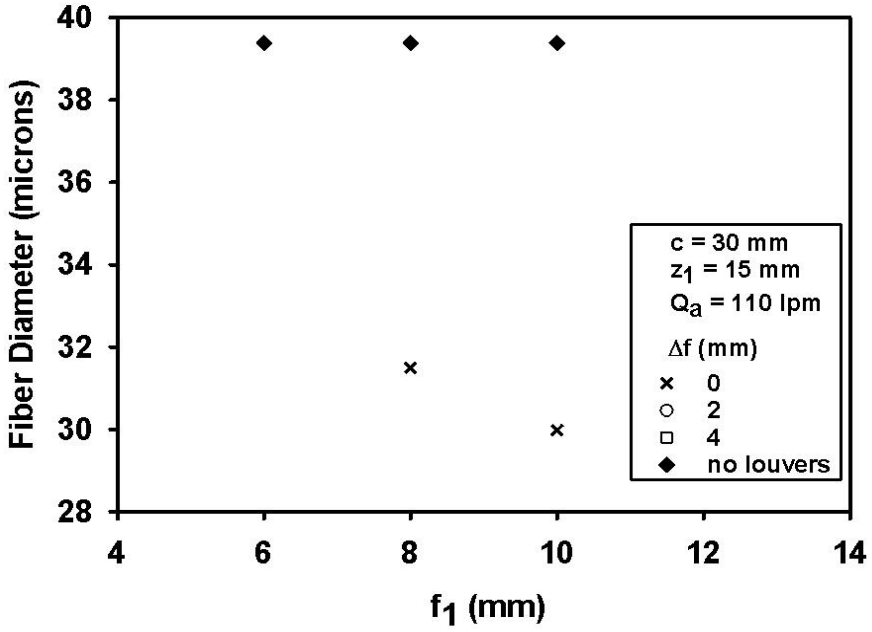

Fig II.14 and II.15. The effect of f_1 on fiber diameter. For these graphs, c = 20 and 30 mm, z_1 = 15 mm, and air flowrate = 110 L/min. Curves are shown for $\Delta f = f_1 - f_2$ = 0, 2 and 4 mm.

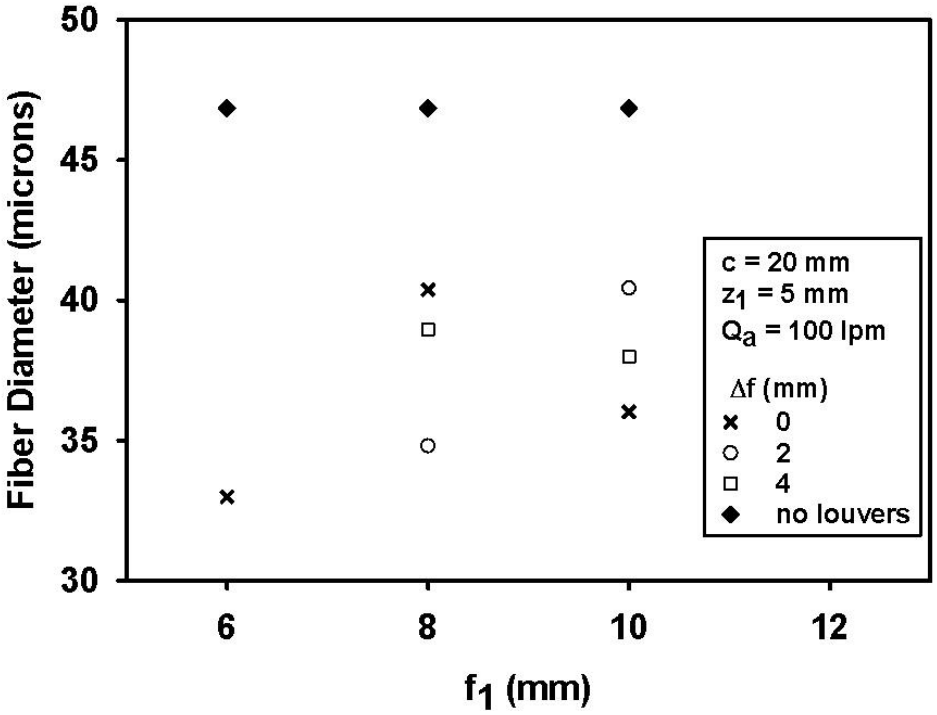

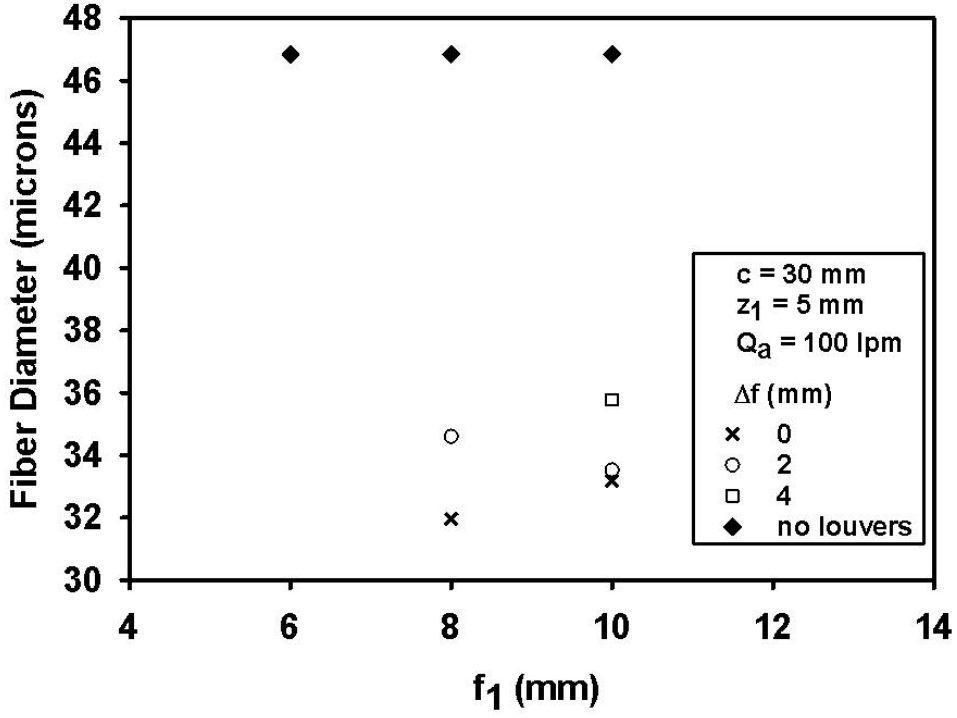

Fig II.16 and II.17. The effect of f_1 on fiber diameter. For these graphs, c = 20 and 30 mm, z_1 = 5 mm, and air flowrate = 100 L/min. Curves are shown for $\Delta f = f_1 - f_2$ = 0, 2 and 4 mm.

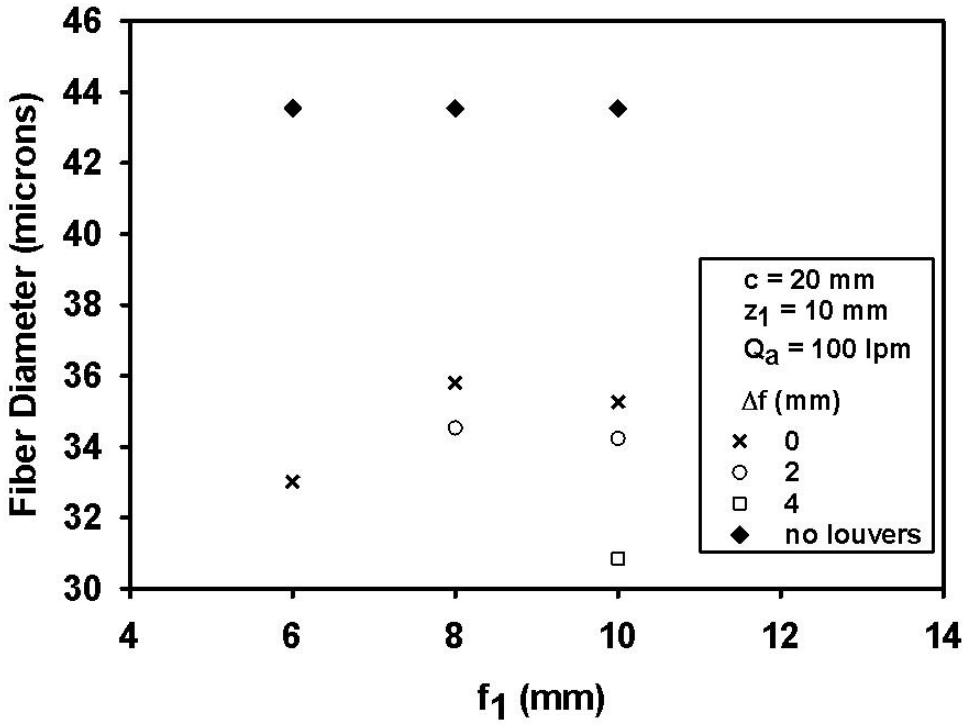

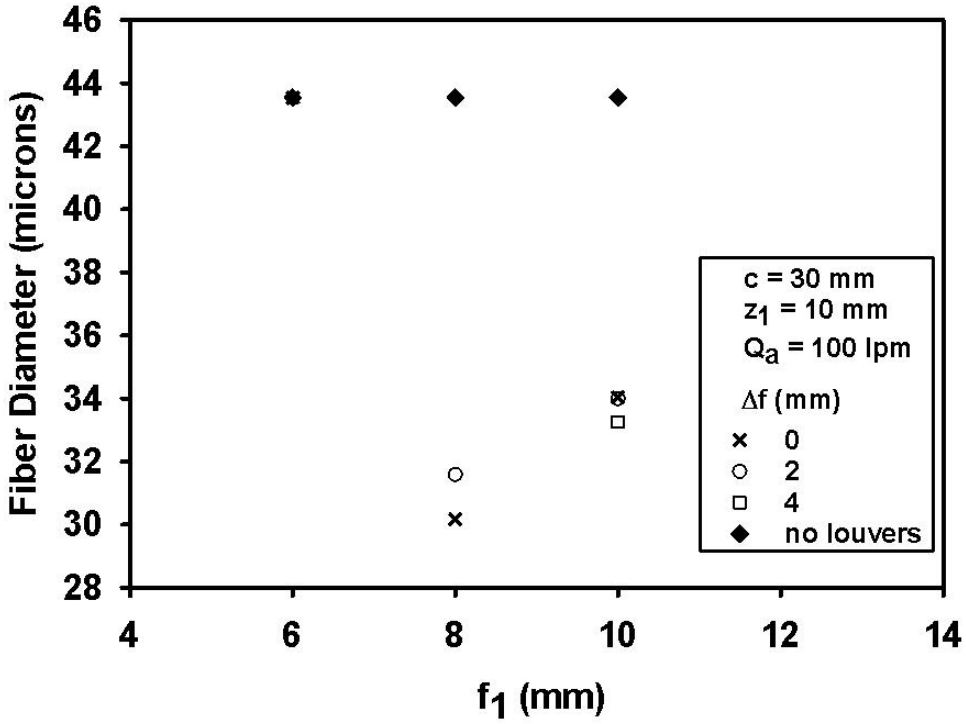

Fig II.18 and II.19. The effect of f_1 on fiber diameter. For these graphs, c = 20 and 30 mm, z_1 = 10 mm, and air flowrate = 100 L/min. Curves are shown for $\Delta f = f_1 - f_2$ = 0, 2 and 4 mm.

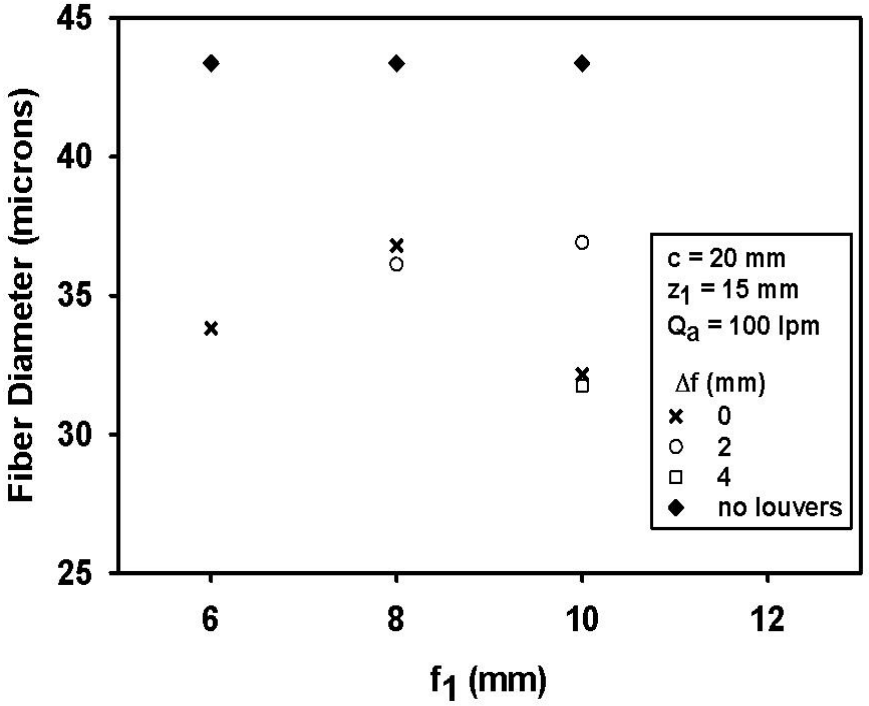

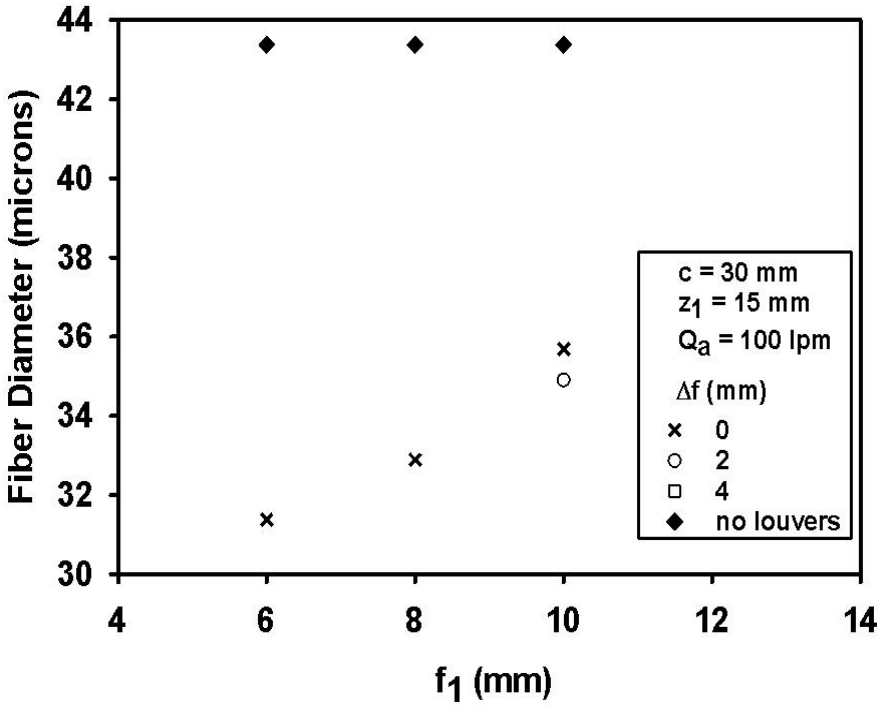

Fig II.20 and II.21. The effect of f_1 on fiber diameter. For these graphs, c = 20 and 30 mm, z_1 = 15 mm, and air flowrate = 100 L/min. Curves are shown for $\Delta f = f_1 - f_2 = 0$, 2 and 4 mm.

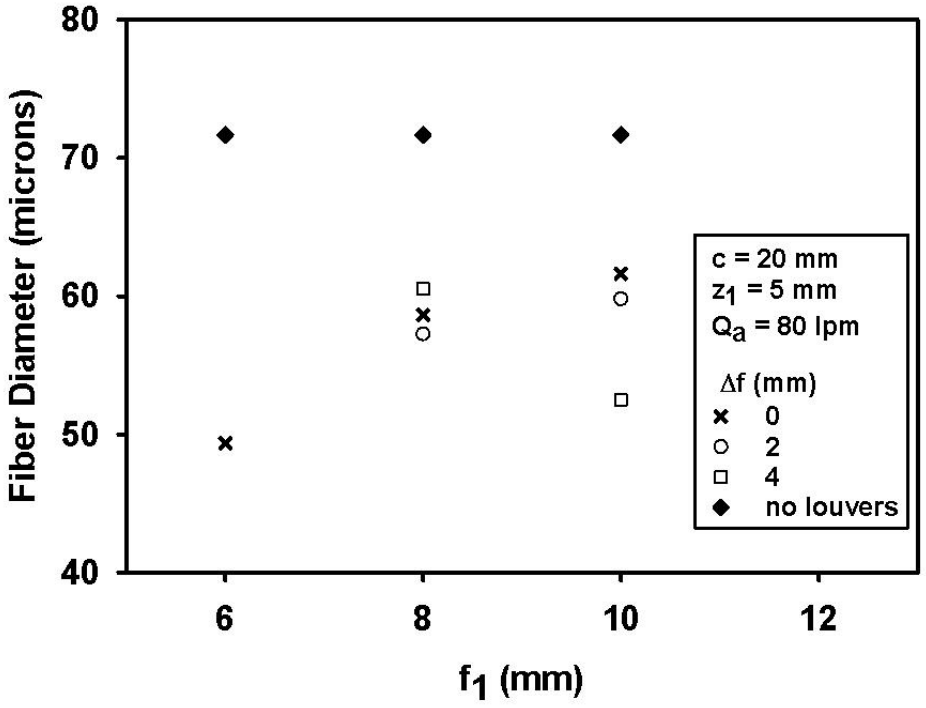

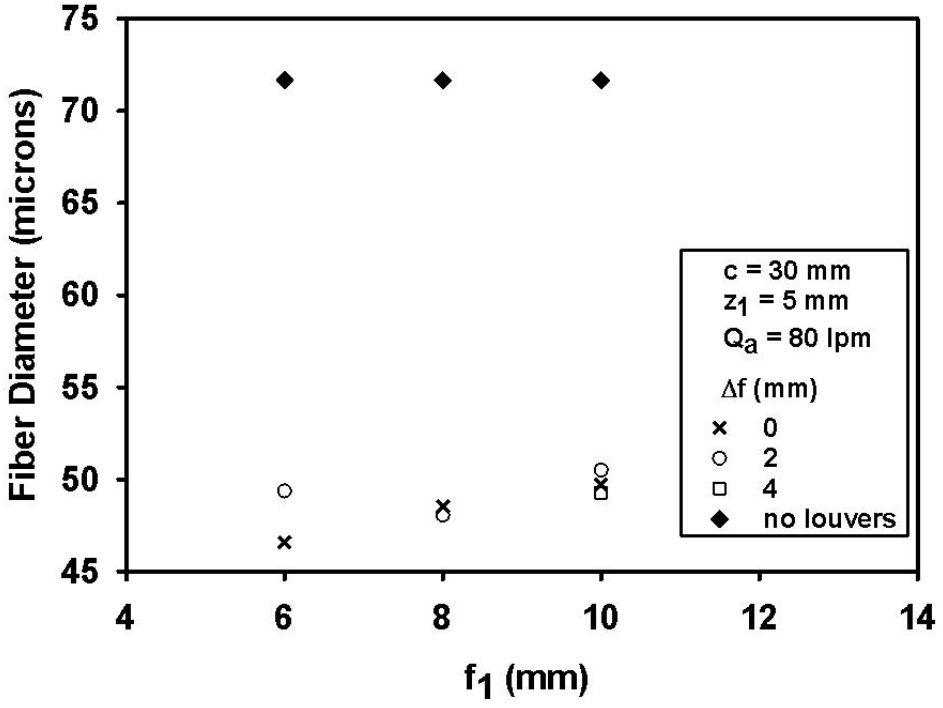

Fig II.22 and II.23. The effect of f_1 on fiber diameter. For these graphs, c = 20 and 30 mm, z_1 = 5 mm and air flowrate = 80 L/min. Curves are shown for $\Delta f = f_1 - f_2$ = 0, 2 and 4 mm.

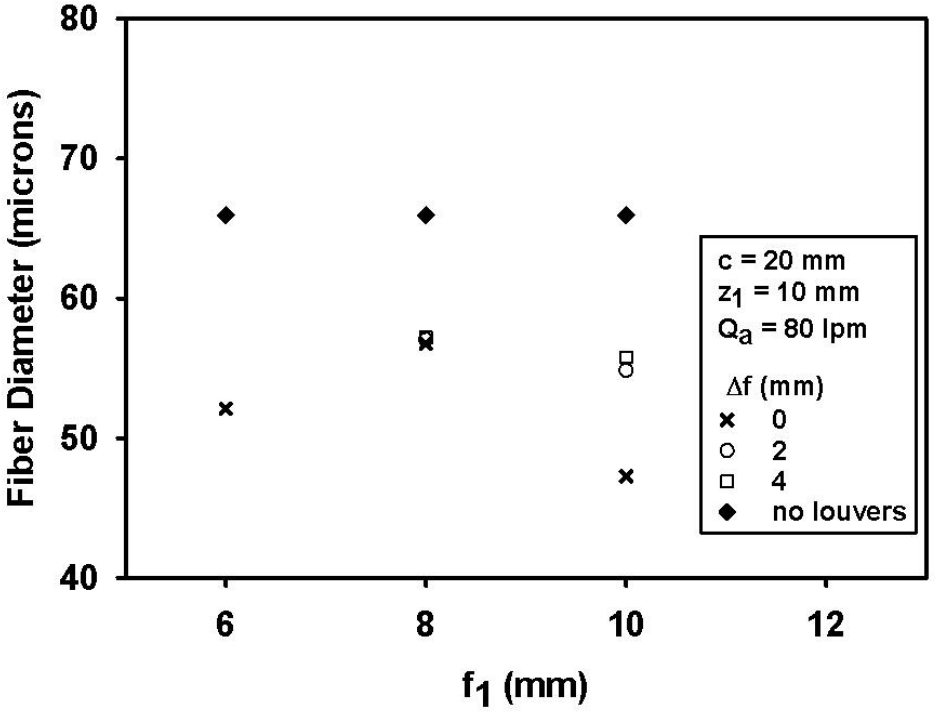

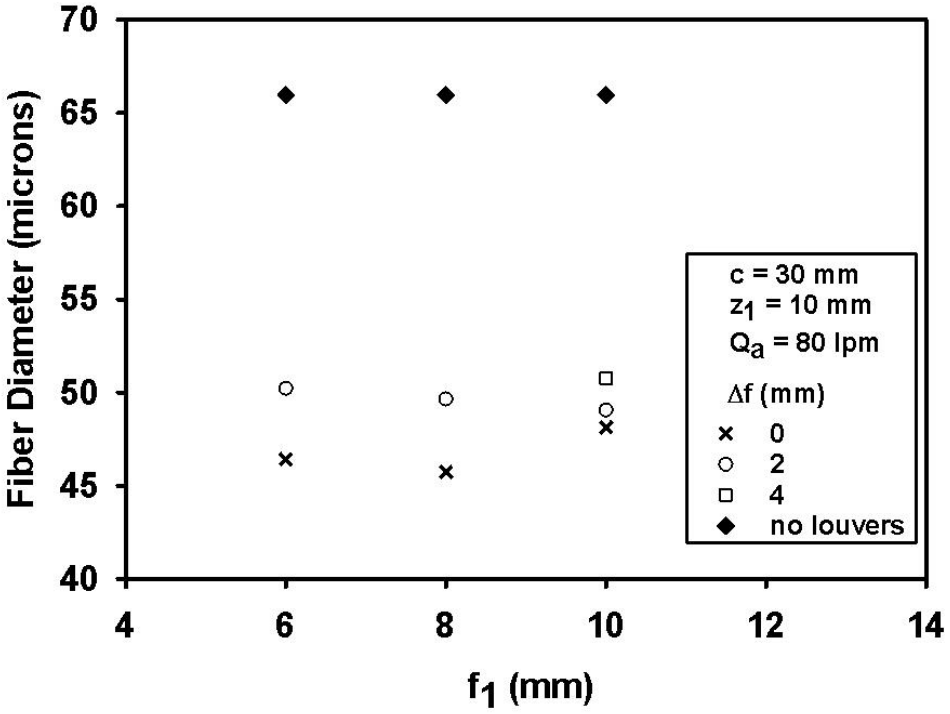

Fig II.24 and II.25. The effect of f_1 on fiber diameter. For these graphs, c = 20 and 30 mm, z_1 = 10 mm and air flowrate = 80 L/min. Curves are shown for $\Delta f = f_1 - f_2$ = 0, 2 and 4 mm.

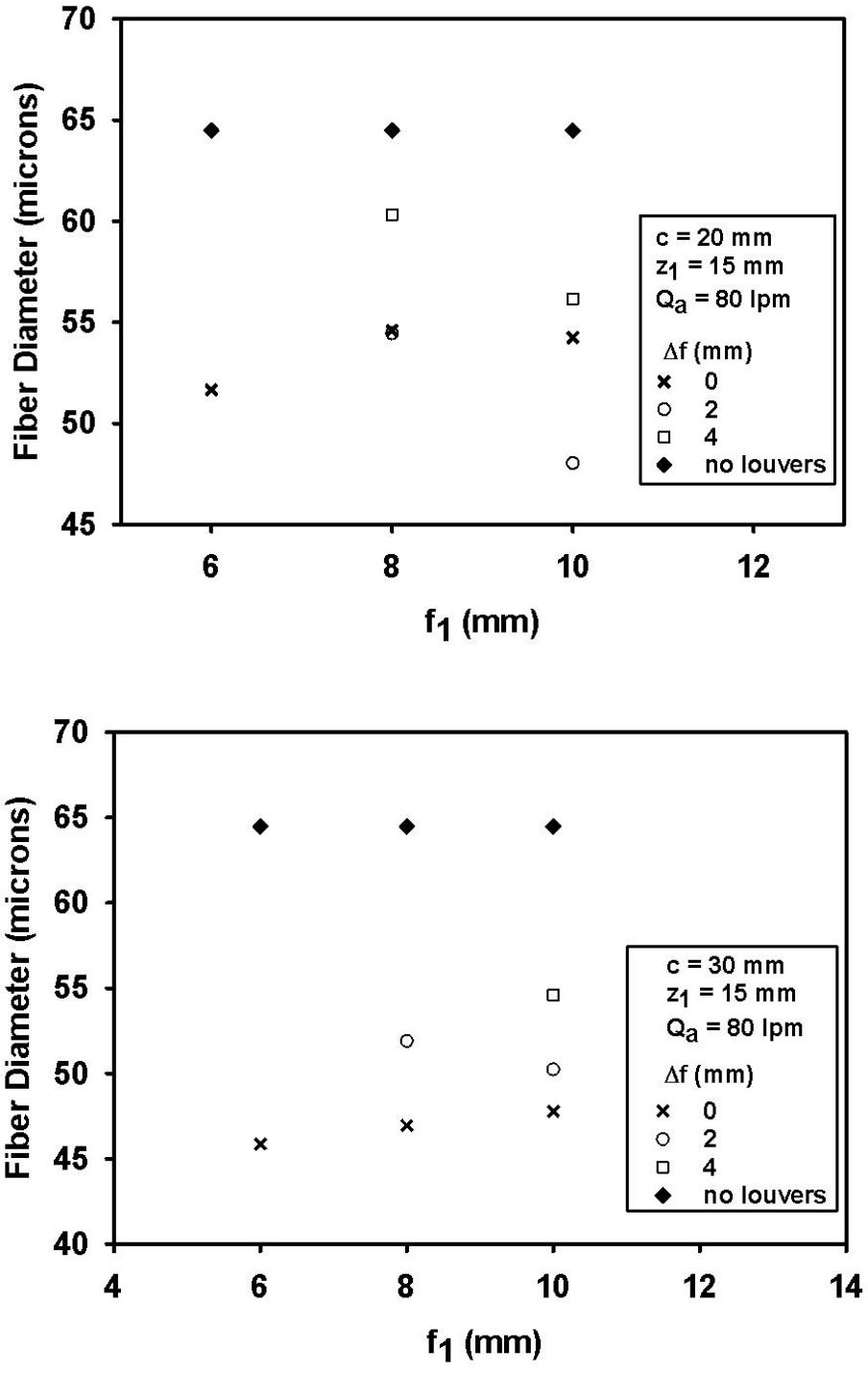

Fig. II.26 and II.27. The effect of f_1 on fiber diameter. For these graphs, c = 20 and 30 mm, z_1 = 15 mm and air flowrate = 80 L/min. Curves are shown for $\Delta f = f_1 - f_2$ = 0, 2 and 4 mm.

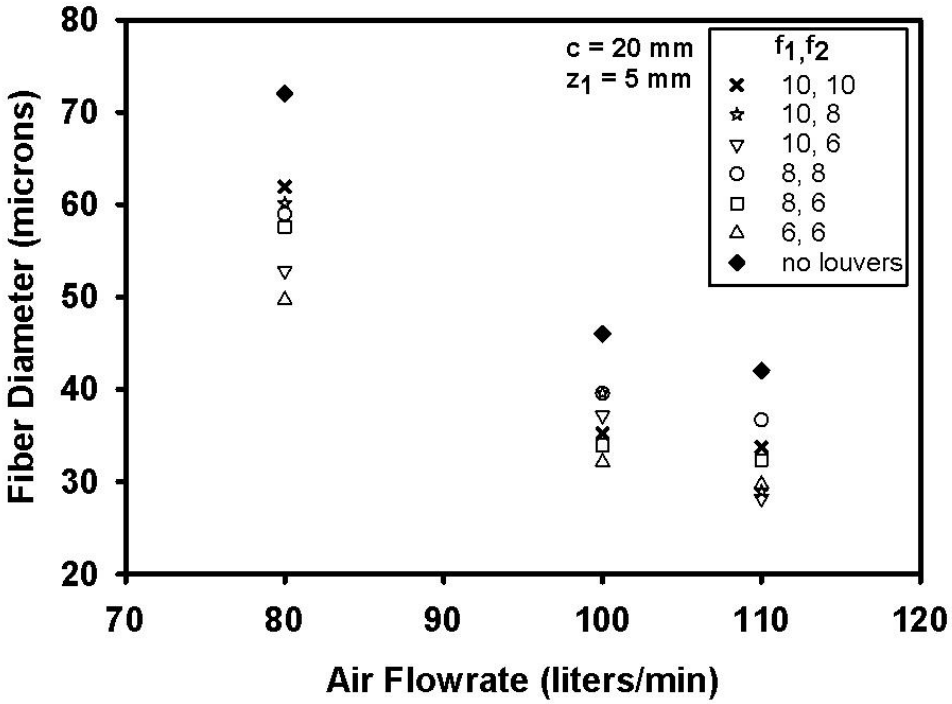

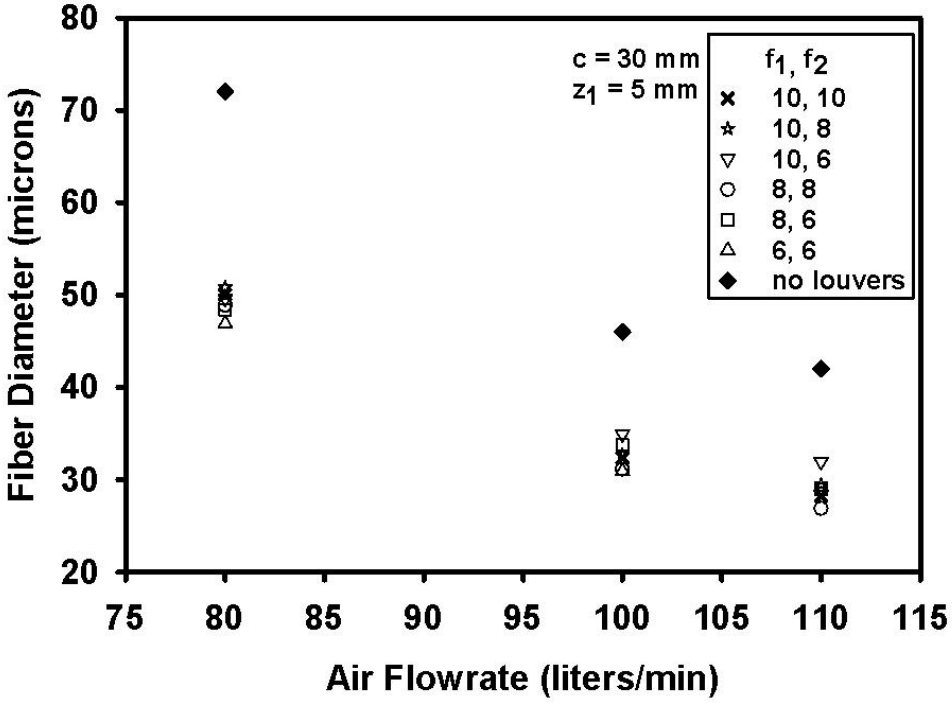

Fig. II.28 and II.29. The effect of air flowrate on fiber diameter. For these graphs, c = 20 and 30 mm and z_1 = 5 mm. Curves are shown for each f_1, f_2 configuration.

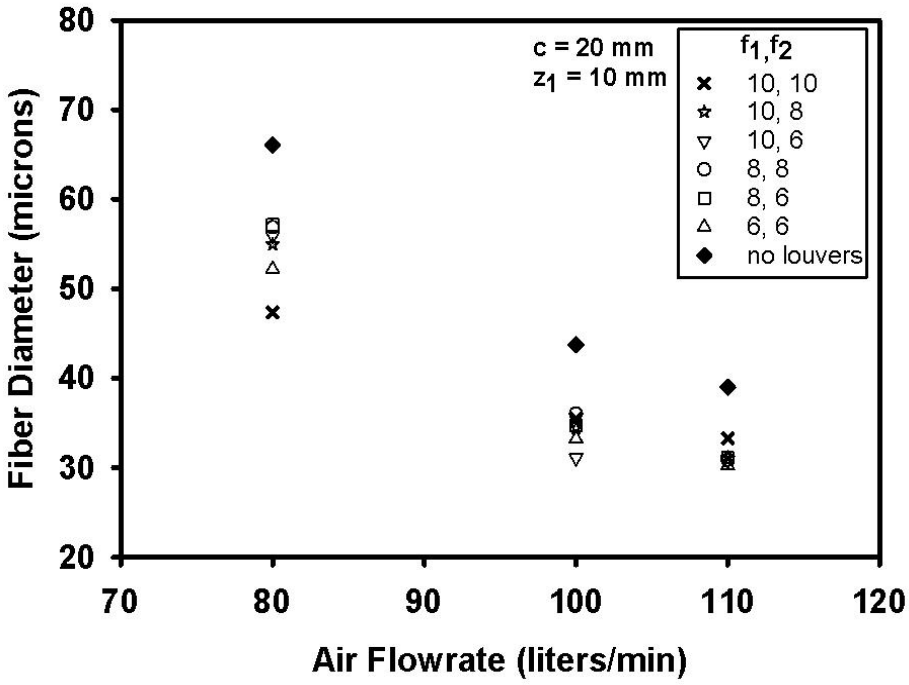

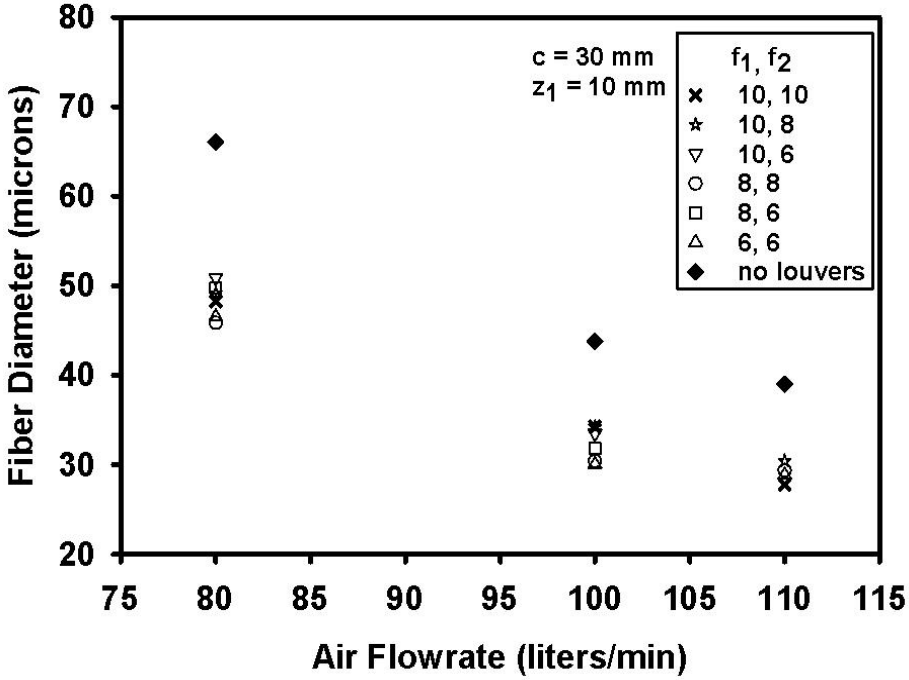

Fig. II.30 and II.31. The effect of air flowrate on fiber diameter. For these graphs, c = 20 and 30 mm and z_1 = 10 mm. Curves are shown for each f_1, f_2 configuration.

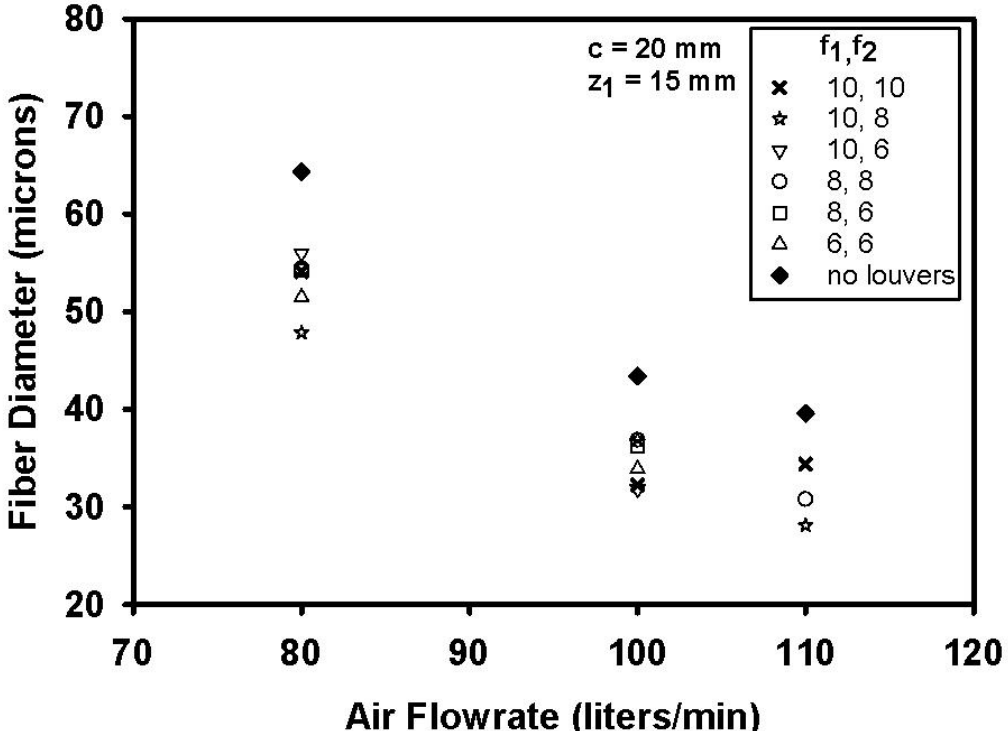

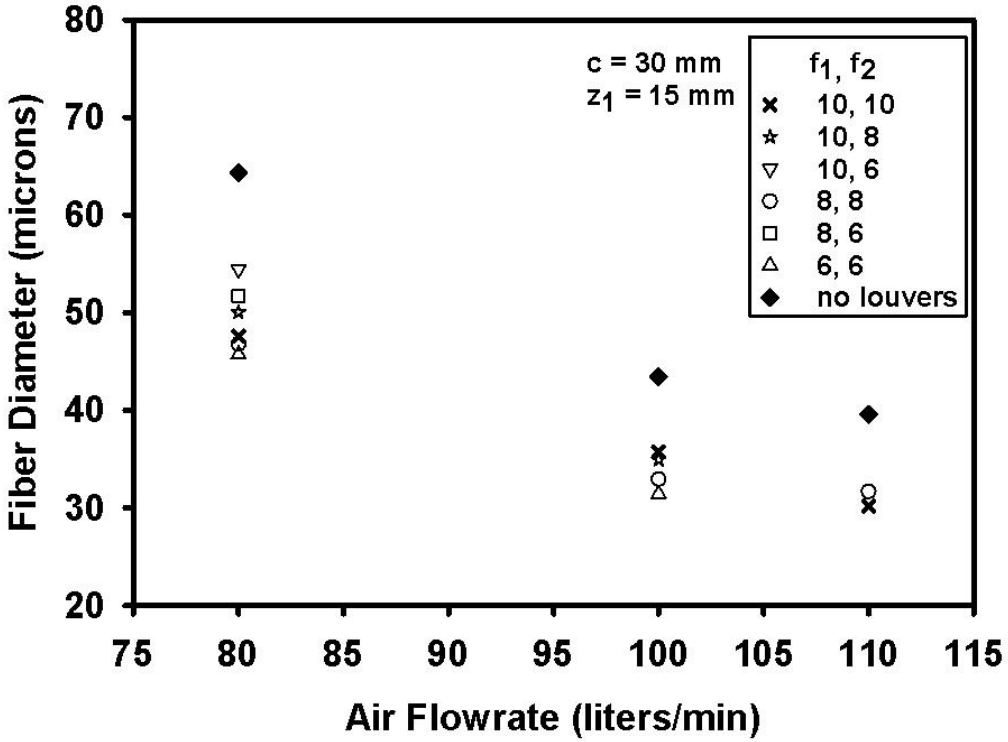

Fig. II.32 and II.33. The effect of air flowrate on fiber diameter. For these graphs, c = 20 and 30 mm and z_1 = 15 mm. Curves are shown for each f_1, f_2 configuration.

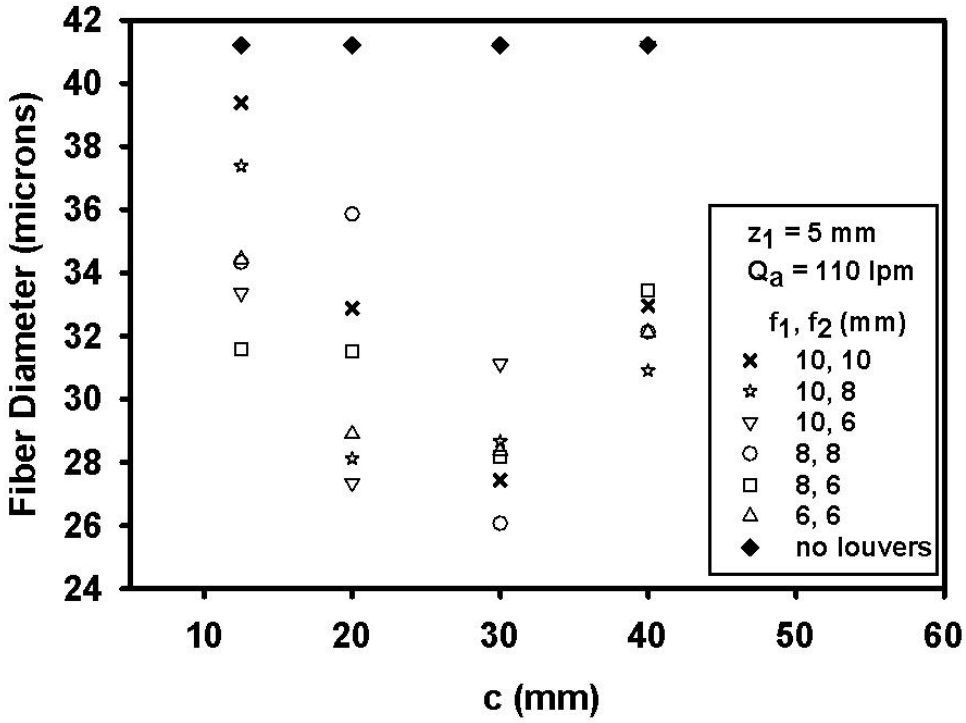

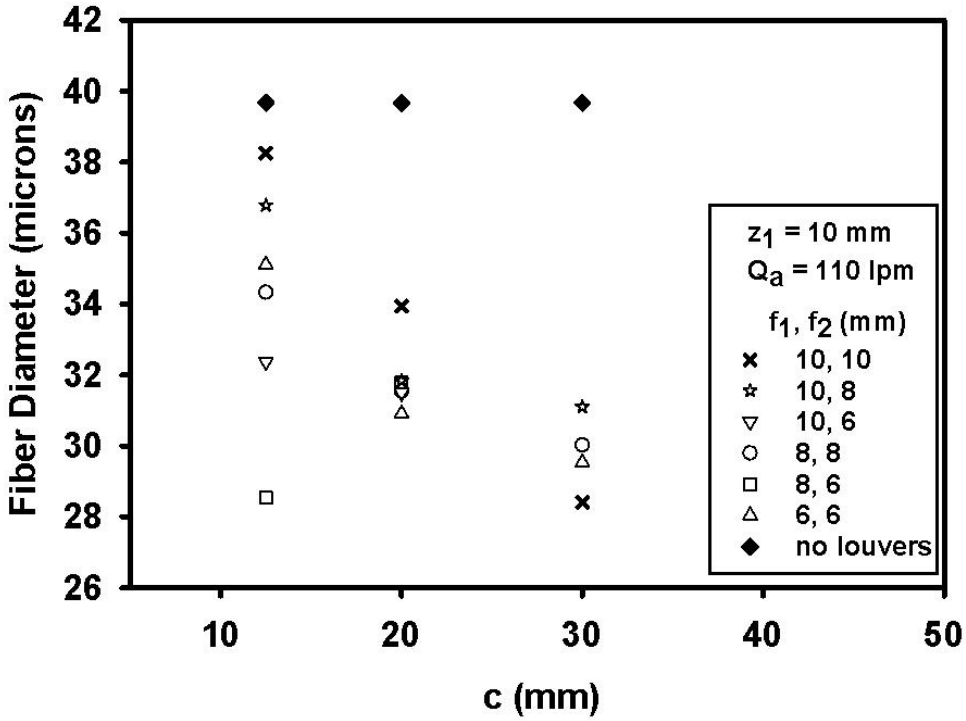

Fig. II.34 and II.35. The effect of chord length c on fiber diameter. For these graphs z_1 = 5 and 10 mm and air flowrate = 110 L/min. Curves are shown for each f_1, f_2 configuration.

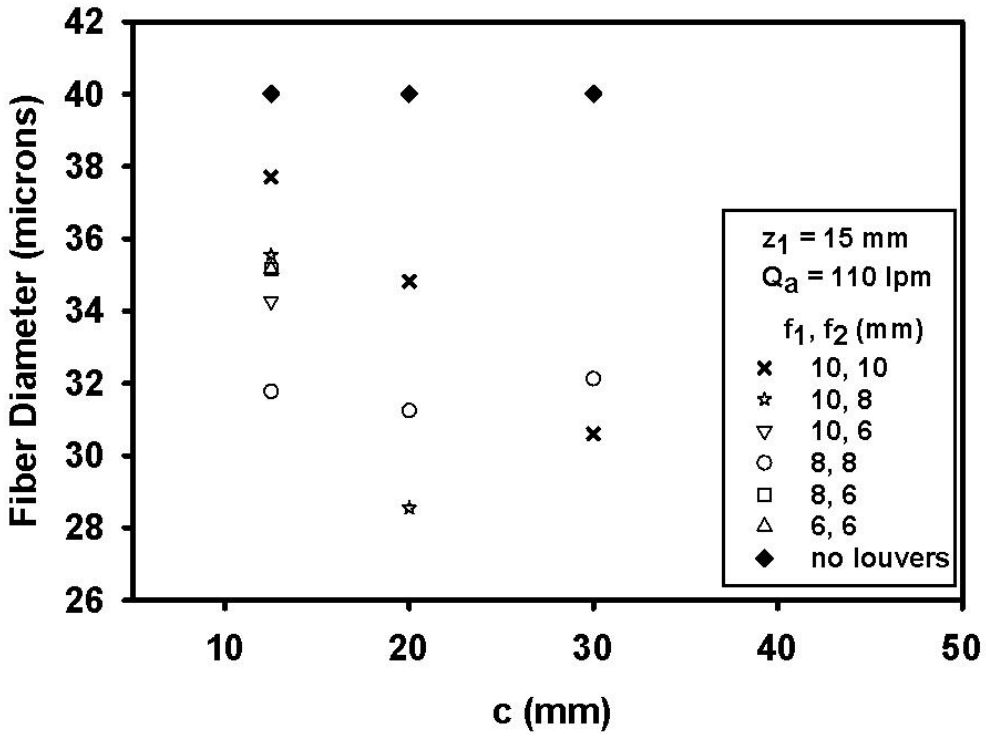

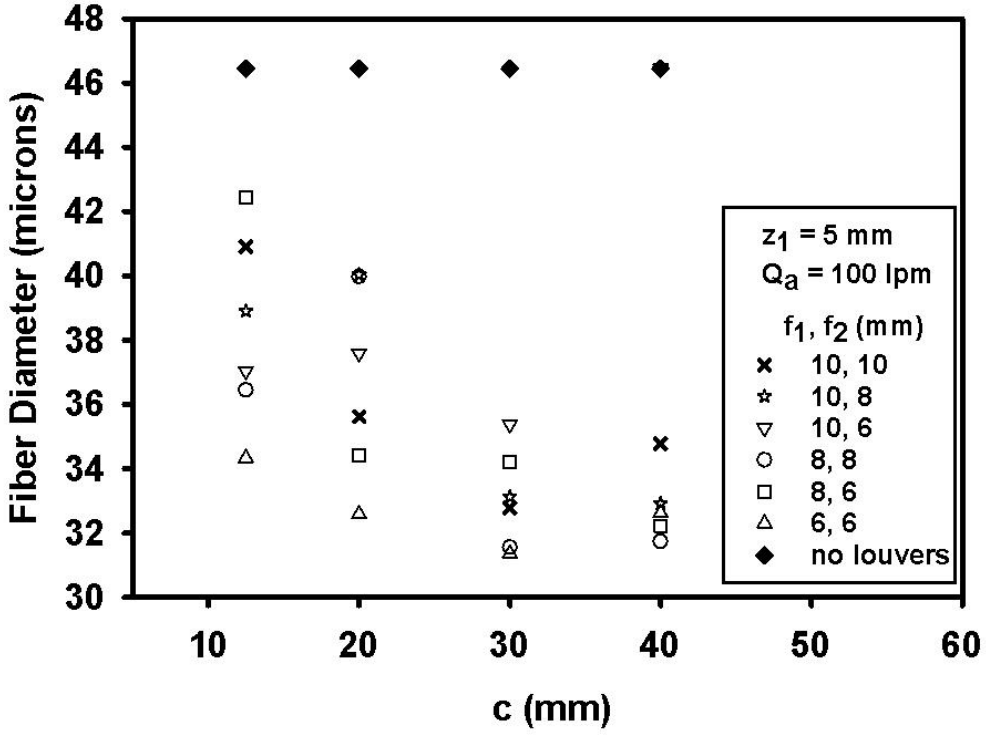

Fig. II.36 and II.37. The effect of chord length c on fiber diameter. Fig II.36 for z_1 = 15 mm and air flowrate = 110 L/min. Fig II.37 for z_1 = 5 mm and air flowrate = 100 L/min. Curves are shown for each f_1, f_2 configuration.

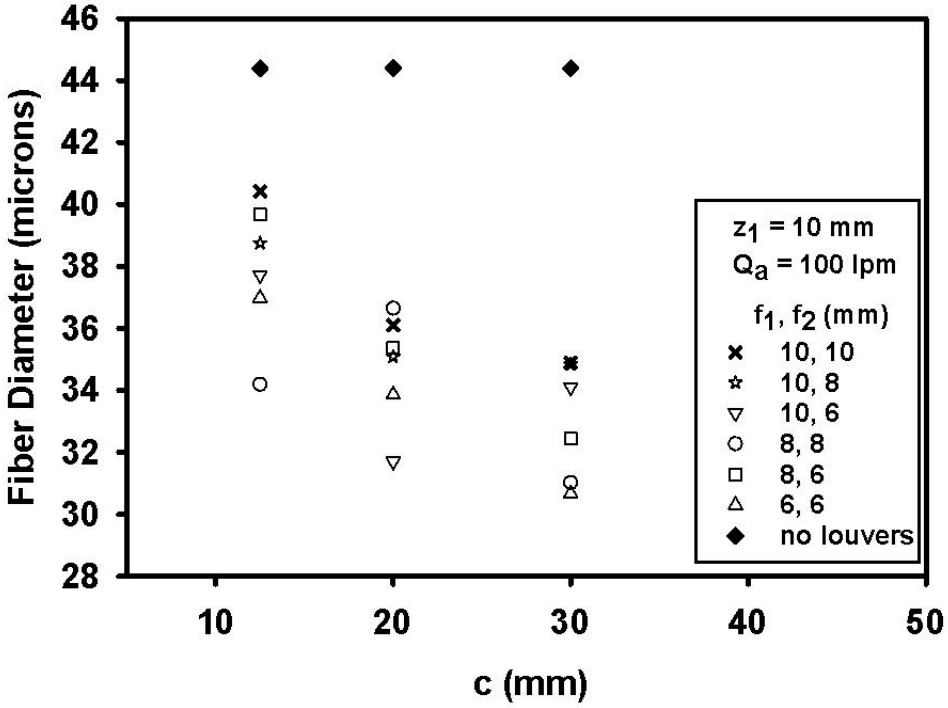

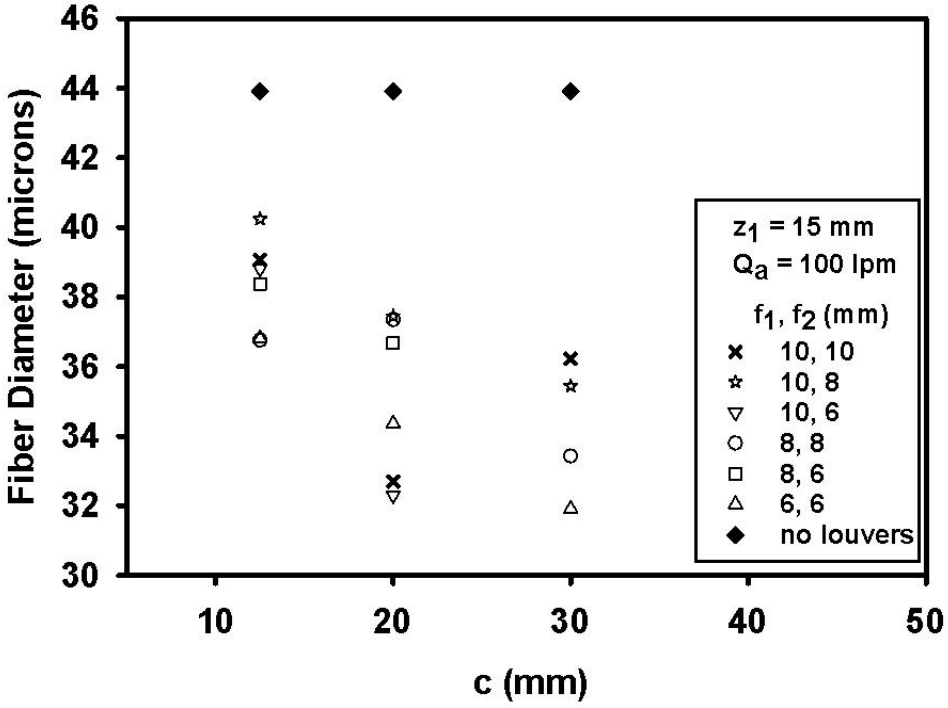

Fig. II.38 and II.39. The effect of chord length c on fiber diameter. For these graphs z_1 = 10 mm and 15 mm and air flowrate = 100 L/min. Curves are shown for each f_1, f_2 configuration.

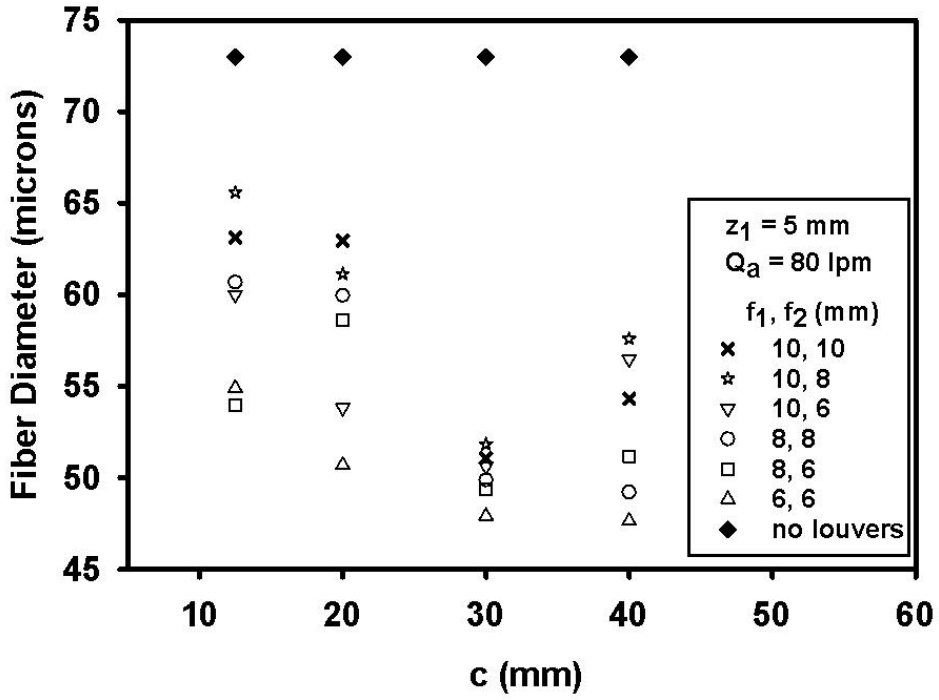

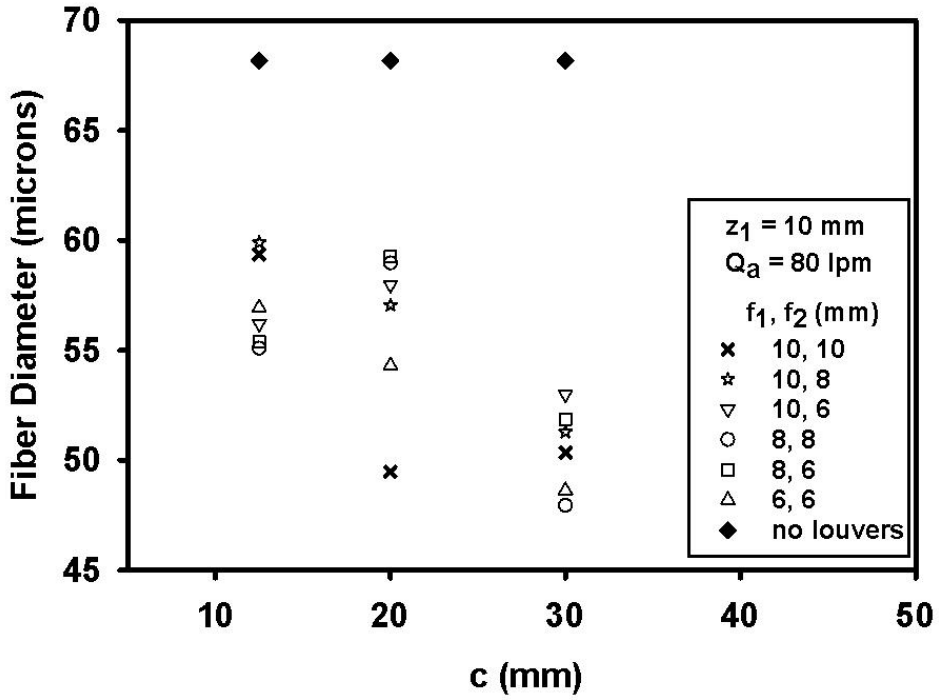

Fig. II.40 and II.41. The effect of chord length c on fiber diameter. For these graphs z_1 = 5 mm and 10 mm and air flowrate = 80 L/min. Curves are shown for each f_1, f_2 configuration.

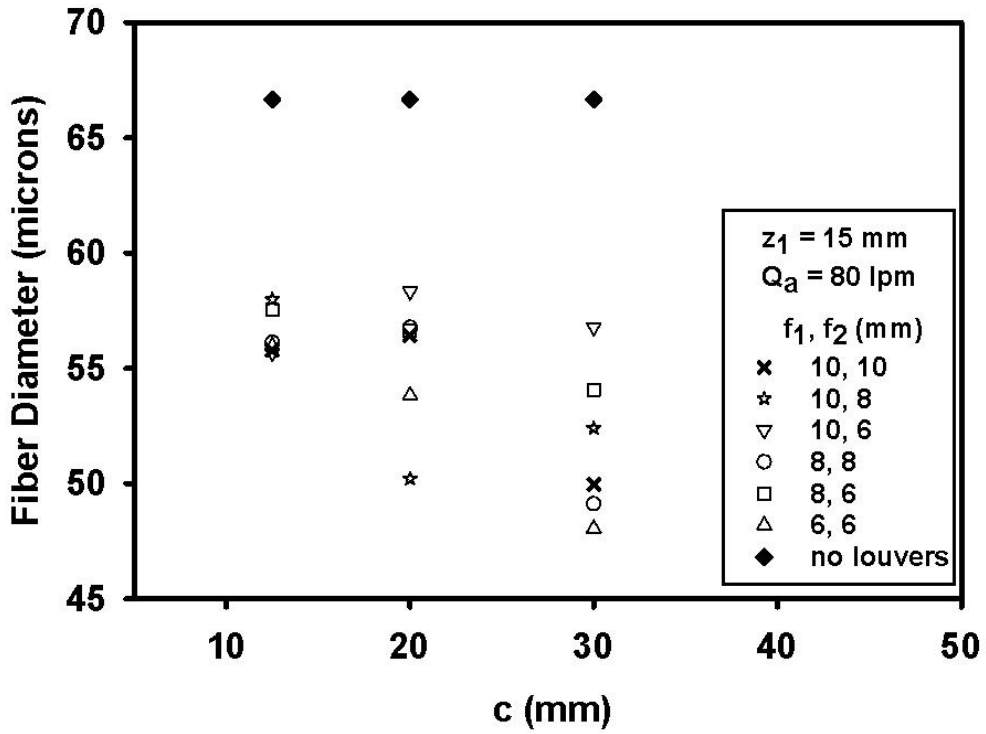

Fig. II.42. The effect of chord length c on fiber diameter. For this graph z_1 = 15 mm and air flowrate = 80 L/min. Curves are shown for each f_1, f_2 configuration.

APPENDIX III:

MOTION STUDIO AND PROANALYST

The software *MotionStudio* is the upgraded version of *MotionPro* used previously by Beard et al. (2007). There is little difference between the two software packages for our purposes; however, digital drivers for use in a Windows 10 laptop were only found for *MotionStudio*. As the analysis software *ProAnalyst* supported *.avi* files, additional converter software was not required as was the case with Beard et al (2007).

Once the videos captured and saved in *MotionStudio*, they were uploaded to *ProAnalyst*. This software used a multi-file saving system where any changes made, such as applying filters to change contrast settings or adding annotations, would be saved separately. This allowed for the original video file to remain unaltered. Once a video is processed, it would have several separate files including calibration, line tracker, annotation, and graph files saved in a folder along with the original video file and a *ProAnalyst* project file. Each of the individual files would have the same file name followed by a different file type (mcl, *.ltc*, *.cal* etc).

Videos uploaded to *ProAnalyst* first had a calibration applied to it. At the beginning of an experiment, a ruler would be held up to the die head and the camera moved to the "above" and "below" positions described in Chapter 3. A single frame video would be taken at each of these positions to be later uploaded to the analysis software. In *ProAnalyst*, a calibration file is created by selecting two points in the photo and specifying the distance between the points. In this case, the points were placed on the 1 cm and 2 cm marks on the ruler in the picture and specifying that there are 10 mm between the points. *ProAnalyst* then determines how many pixels per millimeter there are. Although this

calibration was done for every experiment, the calibration was approximately 13 pixels per millimeter each time.

An annotation file was also created outlining the ruler in the calibration photo. This annotation would then be applied to the corresponding fiber videos that did not have a ruler in the field to determine the location of the tracker lines. Tracker lines were then placed at the specified *z* distances. They were placed in the plane perpendicular to the melt-blown fiber, and would be used to track the change in position of the fiber in the x-axis with time. The software did this by searching for the point of highest pixel intensity along that line. In this case, the "white" fiber on a "dark grey" background. For cases where the fiber was in shadow, the background was significantly brightened such that the fiber was "black" and the background "white". A "reverse" filter would then be applied, allowing for the fiber to be tracked. At times the tracker would miss the fiber and the fiber position would have to be determined manually after the automatic tracking had been completed. This was done by selecting the point on the line where the fiber was located and pressing set point.

Data would then be exported to excel. The data exported from *ProAnalyst* includes frame number, its corresponding time point, the X and Y coordinates of the location of the tracker point, the coordinates of the tracker line endpoints, and other miscellaneous information. In all, there would be 6000 data points; one for each frame of the video.

APPENDIX IV:

FREQUENCY AND AMPLITUDE CALCULATION EXPLAINATION AND CODE

IV.1. Code Explanation

Similar to Beard et al. (2007), the amplitude and frequency were calculated by finding the absolute extrema between the zeros point. However, Beard et al (2007) manually did these calculations by hand.

A code was written in *Visual Basic* to automate the calculation of the frequency and amplitude of the vibrating fiber in the air field below the melt blowing die. An explanation of the code will be presented here with the fiber x-position over time data at z= 9 cm data between time points 0.90 to 1.20 seconds for 20 mm chords at a leading edge of z_1 = 5 mm, an f_1,f_2 = 8,8 configuration, and an air flowrate of 100 slpm (Fig. IV.1). The code begins with a user form which allows the user to input experimental conditions and information and have that information inputted to the spreadsheet (Fig IV.2). It also allows the user to begin the calculations. The exported data is first normalized by taking the average of all the X coordinates and of the Y coordinates, then subtracting each X and Y coordinate by these averages. This allowed the data to be centered around x= 0 mm and y= 0 mm (Fig IV.3). Next, the "zeros" points where the fiber crosses the x-axis are found. This allows for the following subroutine to determine the absolute maxima and minima found between our adjacent "zeros". Only one absolute maximum or minimum is picked between these "zero" points. Fig IV. 4 is a truncation of Fig IV. 3 and will be used to demonstrate the collection of extrema points.

As the fiber often crossed the x-axis between time points, the point immediately after the sign change was chosen as our "zero" and was designated as either a positive (+)

or a negative (-) “zero” (Fig IV.4). For example, points A, D, H, K, and N were positive “zeros” and points B, G, J, L, and P were negative “zeros”. Between the adjacent “zeros” it was determined if the range would have a maximum or a minimum based on the signs of the “zeros” at the beginning and the end of each evaluation range. For the range A to B, as the sign changes from (+) to (-), the range was determined to have a maximum. The absolute maximum was then chosen from that range, including the points A and B. In this case, the maximum is located at point A. In the range from B (-) to D (+), the range will contain a minimum, which in this case is point C. Table IV.1 Summarizes the extrema determination for Figure IV.4.

As only one absolute extrema point between the zeros is used in determining the frequency and amplitude of the vibrating fiber, an additional subroutine is used to eliminate any repeating absolute extrema within the “zeros” range. For example, in range D to G, the interval contains two maximums of the same positional value, points E and F. Point E is chosen as the maximum and point F is eliminated by the subroutine. Finally, the frequency and amplitude were calculated. The amplitude was found by taking the average of the absolute value of all x-positions at each extrema point. The frequency was determined by finding the difference in time between extrema points and taking its average. This value would be multiplied by 2 to determine the cycle period and then inversed producing the frequency in Hertz.

The amplitude and frequency of several data sets were calculated by hand in the manner described above to verify the accuracy of the code. It was found that the frequency and amplitude values determined with the automated code were no more than 5 percent

different from the frequency and amplitude values determined by hand and were consistently higher than the hand-determined values.

IV.2 Visual Basic Code for Fiber Frequency and Amplitude Calculations

```
Attribute VB_Name = "Module1"
'Main Sub: FrequencyAndAmplitude -massive call for all component subs

Sub ClearSheet()
Range("A1:ZZ10000").ClearContents
End Sub

Sub ClearAllButPROAnalyst()
Range("K1:ZZ10000").ClearContents
Range("H22:J10000").ClearContents
End Sub


'Needed to start the userform, assigned to button on sheet
Sub FreqAmpCalcUserForm()
UserForm1.Show
End Sub
'''''''''''''''''''''''''''''''''''''''''''''''''''''''''''''''''''''''''''''''''''''''''''''''''''''''''''''''''''''''''''''''''
Sub FrequencyAndAmplitudeUserFormVersion() 'Userform calls this when pressing the "calculate" button

Call ExperimentInfoUserForm  'Allows for Inputing experimental conditions
Call NormalizeData           'Centers the data about the x-axis
Call FindingZeros            'Finds all locations where the position crosses the x-axis
Call ZerosFreq               'Does a quick frequency calculation based on the zeros as a quick check
Call FindingExtremaNEW       'Finds the absolute extrema between adjacent zeros
Call EliminatingRepeats      'Sometimes more than one maximum or a minimum of the same value occurs between a zeros range.
                             'The first occuring of these values is selected while the remainder of the repeats are eliminated .
Call CalcFreqAmp             'Finally the ampliutde and frequency is calculated. The frequency here is compared to the frequency
                             'calculated in ZerosFreq as a check to make sure all repeated extrema are eliminated.

Freq = Range("M18").Value
amp = Range("M19").Value

MsgBox "The Frequency is " & Freq & "Hz and the amplitude is " & amp & " mm."

End Sub
'''''''''''''''''''''''''''''''''''''''''''''''''''''''''''''''''''''''''''''''''''''''''''''''''''''''''''''''''''''''''''''''''
Sub ExperimentInfoUserForm()

Range("L2:M20").Clear

Range("L2").Value = "Experimental Information"
Range("L3").Value = "Date:"
Range("L5").Value = "Mass Flowrate (g/min):"
Range("L6").Value = "Air Flowrate (lpm):"
Range("L8").Value = "Chord Length (mm):"
Range("L9").Value = "f1 (mm):"
Range("L10").Value = "f2 (mm):"
Range("L11").Value = "z1 (mm):"
Range("L13").Value = "Camera Position: "
Range("L14").Value = "Tracker Line z (cm): "
Range("L15").Value = "Louvers Used?"
Range("L17").Value = "Calculations"
Range("L18").Value = "Frequency (Hz):"
Range("L19").Value = "Amplitude (mm):"
Range("L20").Value = "Notes"

'UserForm inputs
Range("M3").Value = UserForm1.TextBox1.Value   'Date

Range("M5").Value = UserForm1.TextBox2.Value   'Mass Flowrate
```

```
Range("M6").Value = UserForm1.TextBox3.Value   'Air Flowrate

Range("M8").Value = UserForm1.TextBox4.Value   'Chord
Range("M9").Value = UserForm1.TextBox5.Value   'f1 Leading Edge Separation
Range("M10").Value = UserForm1.TextBox6.Value  'f2 Trailing Edge Separation
Range("M11").Value = UserForm1.TextBox7.Value  ' Distance Below Die head z1

Range("M13").Value = UserForm1.TextBox8.Value  ' General Camera Position
Range("M14").Value = UserForm1.TextBox9.Value  'Tracker line distance below die head z
Range("M15").Value = UserForm1.TextBox10.Value 'Louvers Used
Range("M20").Value = UserForm1.TextBox11.Value 'Any notes
End Sub
''''''''''''''''''''''''''''''''''''''''''''''''''''''''''''''''''''''''''''''''''''''''''''''''''''''''''''''''''''''''''''''''
Sub NormalizeData()
Range("H22:K10000").Clear
'Formats
Range("H23").Value = "t"
Range("I23").Value = "X"
Range("J23").Value = "Y"
Range("K23").Value = "Frame"
Range("H22").Value = "Avg:"

FrameRange = Range(Cells(24, 1), Cells(15000, 1))
noframes = WorksheetFunction.Count(FrameRange)
'MsgBox noframes

xrange = Range(Cells(24, 3), Cells(noframes - 1 + 24, 3))
yrange = Range(Cells(24, 4), Cells(noframes - 1 + 24, 4))

xavg = WorksheetFunction.Average(xrange)
yavg = WorksheetFunction.Average(yrange)

Range("I22").Value = xavg
Range("J22").Value = yavg

i = 0

Do Until i = noframes
t = Range("B24").Offset(i, 0).Value
x = Range("C24").Offset(i, 0).Value
y = Range("D24").Offset(i, 0).Value
Frame = Range("A24").Offset(i, 0).Value

Range("H24").Offset(i, 0).Value = t
Range("I24").Offset(i, 0).Value = x - xavg
Range("J24").Offset(i, 0).Value = y - yavg
Range("K24").Offset(i, 0).Value = Frame
i = i + 1

Loop

End Sub
''''''''''''''''''''''''''''''''''''''''''''''''''''''''''''''''''''''''''''''''''''''''''''''''''''''''''''''''''''''''''''''''
Sub FindingZeros()

Range("L22:O10000").Clear

'Formating
Range("L22").Value = "Finding Zeros Subroutine"
Range("L22").Offset(1, 0).Value = "Frames"
Range("L22").Offset(1, 1).Value = "t"
Range("L22").Offset(1, 2).Value = "X"
Range("L22").Offset(1, 3).Value = "Type of CrossOver"

'Determing how many times the loop interates
noptsrange = Range(Cells(24, 8), Cells(15000, 8))
    nopts = WorksheetFunction.Count(noptsrange)
```

```
    'MsgBox nopts & "nopts"
i = 0

Do Until i = nopts

'- to + Zero
If Range("I25").Offset(i, 0).Value > 0
And Range("I25").Offset(i - 1).Value < 0 _
Then
t = Range("H25").Offset(i, 0).Value
x = Range("I25").Offset(i, 0).Value
FrameNo = Range("K25").Offset(i, 0).Value
entry = Range("L24:L8000")
k = WorksheetFunction.Count(entry)
Range("L24").Offset(k, 0).Value = FrameNo
Range("M24").Offset(k, 0).Value = t
Range("N24").Offset(k, 0).Value = x
Range("O24").Offset(k, 0).Value = "- to +"
'MsgBox "- to +" ''Debugging tool

'+ to - Zero
ElseIf Range("I25").Offset(i, 0).Value < 0 _
And Range("I25").Offset(i - 1).Value > 0 _
Then
t = Range("H25").Offset(i, 0).Value
x = Range("I25").Offset(i, 0).Value
FrameNo = Range("K25").Offset(i, 0).Value
entry = Range("L24:L8000")
k = WorksheetFunction.Count(entry)
Range("L24").Offset(k, 0).Value = FrameNo
Range("M24").Offset(k, 0).Value = t
Range("N24").Offset(k, 0).Value = x
Range("O24").Offset(k, 0).Value = "+ to -"
'MsgBox "+ to -" ''Debugging tool

'To "End" the Sub
ElseIf IsEmpty(Range("I25").Offset(i, 0).Value) = True _
Then
t = Range("H25").Offset(i, 0).Value
x = Range("I25").Offset(i, 0).Value
FrameNo = Range("K25").Offset(i, 0).Value
entry = Range("L24:L8000")
k = WorksheetFunction.Count(entry)
Range("L24").Offset(k, 0).Value = FrameNo
Range("M24").Offset(k, 0).Value = t
Range("N24").Offset(k, 0).Value = x
Range("O24").Offset(k, 0).Value = "End"
'MsgBox "end" ''Debugging tool
Else
End If

 i = i + 1
Loop

End Sub
''''''''''''''''''''''''''''''''''''''''''''''''''''''''''''''''''''''''''''''''''''''''''
''''''''''''''''''''''''''''''''''''''
Sub ZerosFreq()
Range("P18:P10000").Clear

'Formating
Range("P24").Value = "tdiff"
Range("P19").Value = "Freq"
Range("P21").Value = "Avg"

'count number of interations loop will go through
    noptsrange = Range(Cells(24, 13), Cells(15000, 13))
    nopts = WorksheetFunction.Count(noptsrange)
    'MsgBox nopts
```

```
i = 0

Do Until i = nopts - 1

   h = Range("M25").Offset(i, 0).Value
   j = Range("M25").Offset(i - 1, 0).Value
   TimeDiff = h - j
   Range("P25").Offset(i, 0) = TimeDiff
    i = i + 1
Loop

avgtimerange = Range(Cells(25, 16), Cells(25 + nopts - 1, 16))
avgtime = WorksheetFunction.Average(avgtimerange)
multi2 = avgtime * 2
inverse = 1 / multi2
Frequency = inverse

Range("P22").Value = avgtime
Range("P20").Value = Frequency

End Sub
''''''''''''''''''''''''''''''''''''''''''''''''''''''''''''''''''''''''''''''''''''''''''''''''''''''''''''''''''''''''''''''''''''''''''''''''''''''''''
'NOW need to determine the amplitude by finding absolute extrema
Sub FindingExtremaNEW()
Range("R20:Y80000").Clear
'Format
Range("R23").Value = "Frame"
Range("R23").Offset(0, 1).Value = "t"
Range("R23").Offset(0, 2).Value = "x"
Range("R23").Offset(-1, 0).Value = "Normalized Data"

Range("V23").Value = "Frame"
Range("V23").Offset(0, 1).Value = "t"
Range("V23").Offset(0, 2).Value = "x"
Range("V23").Offset(-1, 0).Value = "FindingExtrema"

'First copy&paste normalize data frame, t, x
'Loop interactions
    noptsrange = Range(Cells(24, 8), Cells(15000, 8))
    nopts = WorksheetFunction.Count(noptsrange)
    'MsgBox nopts ''Debugging Tool

    Do Until i = nopts
    Range("R24").Offset(i, 0).Value = 0 + i                           'Frame #
    Range("R24").Offset(i, 1).Value = Range("H24").Offset(i, 0).Value 't
    Range("R24").Offset(i, 2).Value = Range("I24").Offset(i, 0).Value 'x
    i = i + 1
    Loop
''''''''''''''''''''''''''''''''''''''''''''''''''''''''''''''''''''''''''''''''''''''''''''''''''''''''''''''''''''''''''''''''''''''''''''''''''''''''''
aint = Range("S24").Value 'initial time, start of range
bint = Range("M24").Value 'end of range
dint = Range("B25")
eint = Range("B24")
fint = dint - eint
nint = (bint - aint) / fint
mint = Round(nint, 0)

'MsgBox mint & "number of cells" ''Debugging tool

ERint = Range(Cells(24, 20), Cells(24 + mint, 20))

If Range("O24").Value = "+ to -" _
Then
Max = WorksheetFunction.Max(ERint)
Min = 0
'MsgBox Max ''Debugging Tool

```

```
ElseIf Range("O24").Value = "- to +" _
Then
Min = WorksheetFunction.Min(ERint)
Max = 0
'MsgBox Min ''Debugging Tool

End If

i = 0
Do Until i = mint

'Max Case
If Range("T24").Offset(i, 0).Value = Max _
Then
Frame = Range("T24").Offset(i, -2).Value
t = Range("T24").Offset(i, -1).Value
amp = Range("T24").Offset(i, 0).Value
entry = Range("V24:V8000")
k = WorksheetFunction.Count(entry)
Range("V24").Offset(k, 0).Value = Frame
Range("V24").Offset(k, 1).Value = t
Range("V24").Offset(k, 2).Value = amp
Range("V24").Offset(k, 3).Value = "Max"

'Min Case
ElseIf Range("T24").Offset(i, 0).Value = Min _
Then
Frame = Range("T24").Offset(i, -2).Value
t = Range("T24").Offset(i, -1).Value
amp = Range("T24").Offset(i, 0).Value
entry = Range("V24:V8000")
k = WorksheetFunction.Count(entry)
Range("V24").Offset(k, 0).Value = Frame
Range("V24").Offset(k, 1).Value = t
Range("V24").Offset(k, 2).Value = amp
Range("V24").Offset(k, 3).Value = "Min"

End If

i = i + 1

Loop
''''''''''''''''''''''''''''''''''''''''''''''''''''''''''''''''''''''''''''''''
'Btw each zeros range
'loop inerations

    noptsrange = Range(Cells(25, 13), Cells(15000, 13))
    nopts = WorksheetFunction.Count(noptsrange)
    'MsgBox nopts & "nopts" ''Debugging Tool

y = 0
i = 0
Do Until i = nopts

a = Range("M25").Offset(i - 1, 0).Value 'start of range
b = Range("M25").Offset(i, 0).Value 'end of range
d = Range("B25")
e = Range("B24")
f = d - e
n = (b - a) / f

m = Round(n, 0)

ER = Range(Cells(24 + mint + y, 20), Cells(24 + mint + m + y, 20))

If Range("O24").Offset(i, 0).Value = "- to +" _
Then
Max = WorksheetFunction.Max(ER)
Min = 0
```

```
ElseIf Range("O24").Offset(i, 0).Value = "+ to -" _
Then
Min = WorksheetFunction.Min(ER)
Max = 0
End If
'''''''''''''''''''''''''''''''''''''''''''''''''''''''''''''''
p = 0
    Do Until p = m

    'Max Case
    If Range("T24").Offset(mint + y + p, 0).Value = Max _
    Then
    Frame = Range("T24").Offset(mint + y + p, -2).Value
    t = Range("T24").Offset(mint + y + p, -1).Value
    amp = Range("T24").Offset(mint + y + p, 0).Value
    entry = Range("V24:V8000")
    k = WorksheetFunction.Count(entry)
    Range("V24").Offset(k, 0).Value = Frame
    Range("V24").Offset(k, 1).Value = t
    Range("V24").Offset(k, 2).Value = amp
    Range("V24").Offset(k, 3).Value = "Max"

    'Min Case
    ElseIf Range("T24").Offset(mint + y + p, 0).Value = Min _
    Then
    Frame = Range("T24").Offset(mint + y + p, -2).Value
    t = Range("T24").Offset(mint + y + p, -1).Value
    amp = Range("T24").Offset(mint + y + p, 0).Value
    entry = Range("V24:V8000")
    k = WorksheetFunction.Count(entry)
    Range("V24").Offset(k, 0).Value = Frame
    Range("V24").Offset(k, 1).Value = t
    Range("V24").Offset(k, 2).Value = amp
    Range("V24").Offset(k, 3).Value = "Min"

    ElseIf i = nopts Then GoTo LastPart

    End If

    p = p + 1
    Loop
y = y + m
i = i + 1

Loop
'''''''''''''''''''''''''''''''''''''''''''''''''''''''''''''''''''''''''''''''''''''''''''''''''
'Evaluating last point range
LastPart:

i = nopts

 dataptsrange = Range(Cells(25, 19), Cells(15000, 19))
    datarangepts = WorksheetFunction.Count(dataptsrange)

afinal = Range("M25").Offset(i - 1, 0).Value 'last cross-over
bfinal = Range("S25").Offset(datarangepts - 1, 0).Value 'last time point
dfinal = Range("B25")
efinal = Range("B24")
ffinal = dfinal - efinal
nfinal = (bfinal - afinal) / ffinal
mfinal = Round(nfinal, 0)
ERfinal = Range(Cells(24 + mint + y, 20), Cells(24 + mint + mfinal + y, 20))

If Range("O24").Offset(i - 1, 0).Value = "+ to -" _
Then
Max = WorksheetFunction.Max(ERfinal)
Min = 0
```

```
401
402   ElseIf Range("O24").Offset(i - 1, 0).Value = "- to +" _
403   Then
404   Min = WorksheetFunction.Min(ERfinal)
405   Max = 0
406   End If
407
408   p = 0
409       Do Until p = mfinal
410
411       'Max Case
412       If Range("T24").Offset(mint + y + p, 0).Value = Max _
413       Then
414       Frame = Range("T24").Offset(mint + y + p, -2).Value
415       t = Range("T24").Offset(mint + y + p, -1).Value
416       amp = Range("T24").Offset(mint + y + p, 0).Value
417       entry = Range("V24:V8000")
418       k = WorksheetFunction.Count(entry)
419       Range("V24").Offset(k, 0).Value = Frame
420       Range("V24").Offset(k, 1).Value = t
421       Range("V24").Offset(k, 2).Value = amp
422       Range("V24").Offset(k, 3).Value = "Max"
423
424       'Min Case
425       ElseIf Range("T24").Offset(mint + y + p, 0).Value = Min _
426       Then
427       Frame = Range("T24").Offset(mint + y + p, -2).Value
428       t = Range("T24").Offset(mint + y + p, -1).Value
429       amp = Range("T24").Offset(mint + y + p, 0).Value
430       entry = Range("V24:V8000")
431       k = WorksheetFunction.Count(entry)
432       Range("V24").Offset(k, 0).Value = Frame
433       Range("V24").Offset(k, 1).Value = t
434       Range("V24").Offset(k, 2).Value = amp
435       Range("V24").Offset(k, 3).Value = "Min"
436
437       Else
438
439       End If
440       p = p + 1
441       Loop
442
443   End Sub
444
445   Sub EliminatingRepeats()
446   Range("AA15:AI80000").Clear
447
448   'Formats
449   Range("AA22").Value = "EliminatingRepeats"
450   Range("AA23").Value = "Frame"
451   Range("AA23").Offset(0, 1).Value = "t"
452   Range("AA23").Offset(0, 2).Value = "x"
453   Range("AA23").Offset(0, 3).Value = "Max/Min?"
454
455   'First copy&paste "FindingExtrema" data frame, t, x
456   'Loop interactions
457       noptsrange = Range(Cells(24, 22), Cells(15000, 22))
458       nopts = WorksheetFunction.Count(noptsrange)
459
460       Do Until i = nopts
461       Range("AA24").Offset(i, 0).Value = Range("V24").Offset(i, 0).Value 'Frame
462       Range("AA24").Offset(i, 1).Value = Range("W24").Offset(i, 0).Value 't
463       Range("AA24").Offset(i, 2).Value = Range("X24").Offset(i, 0).Value 'x
464       Range("AA24").Offset(i, 3).Value = Range("Y24").Offset(i, 0).Value  'Max/Min
465       i = i + 1
466       Loop
467   i = 0
468   Do Until i = nopts
469
```

```
470   If Range("AC25").Offset(i - 1, 0).Value = Range("AC25").Offset(i, 0).Value _
471   Then
472   Range("AA25:AD25").Offset(i, 0).Clear
473   Else
474   End If
475
476   i = i + 1
477   Loop
478
479   'Now to eliminate those blank cells
480   'Formats
481   Range("AF22").Value = "EliminatingBlanks"
482   Range("AF23").Value = "Frame"
483   Range("AF23").Offset(0, 1).Value = "t"
484   Range("AF23").Offset(0, 2).Value = "x"
485   Range("AF23").Offset(0, 3).Value = "Max/Min?"
486
487   'Pasting Data without blanks
488   i = 0
489   Do Until i = nopts
490
491   test = WorksheetFunction.CountA(Cells(24 + i, 27))
492
493   If test > 0 Then
494       Frame = Range("AA24").Offset(i, 0).Value
495       t = Range("AA24").Offset(i, 1).Value
496       amp = Range("AA24").Offset(i, 2).Value
497       MaxMin = Range("AA24").Offset(i, 3).Value
498       entry = Range("AF24:AF8000")
499       k = WorksheetFunction.Count(entry)
500       Range("AF24").Offset(k, 0).Value = Frame
501       Range("AF24").Offset(k, 1).Value = t
502       Range("AF24").Offset(k, 2).Value = amp
503       Range("AF24").Offset(k, 3).Value = MaxMin
504
505   Else
506
507   End If
508   k = k + 1
509   i = i + 1
510   Loop
511
512   End Sub
513
514   Sub CalcFreqAmp()
515
516   Range("AK15:AL80000").Clear
517
518   'Formating
519   Range("AK18").Value = "Freq:"
520   Range("AK21").Value = "Avg tdiff"
521   Range("AL21").Value = "Avg amp"
522   Range("AK24").Value = "tdiff"
523   Range("AL23").Value = "AbsAmp"
524
525   'count number of interations loop will go through
526       noptsrange = Range(Cells(24, 32), Cells(15000, 32))
527       nopts = WorksheetFunction.Count(noptsrange)
528
529   i = 0
530
531   Do Until i = nopts - 1
532
533      h = Range("AG25").Offset(i, 0).Value
534      j = Range("AG25").Offset(i - 1, 0).Value
535      TimeDiff = h - j
536      Range("AK25").Offset(i, 0) = TimeDiff
537       i = i + 1
538   Loop
```

```
i = 0
Do Until i = nopts
   amp = Range("AH24").Offset(i, 0).Value
   v = Abs(amp)
   Range("AL24").Offset(i, 0) = v

   i = i + 1
Loop

avgtimerange = Range(Cells(25, 37), Cells(25 + nopts - 1, 37))
avgtime = WorksheetFunction.Average(avgtimerange)
multi2 = avgtime * 2
inverse = 1 / multi2
Frequency = inverse

Range("AK22").Value = avgtime
Range("AK19").Value = Frequency

avgamprange = Range(Cells(24, 38), Cells(24 + nopts, 38))
avgamp = WorksheetFunction.Average(avgamprange)
Range("AL22").Value = avgamp

Range("M18").Value = Frequency
Range("M19").Value = avgamp

'Checking Frequency Calculation

g = Range("M18").Value
f = Range("P20").Value

percentdiff = 100 * Abs(g - f) / WorksheetFunction.Average(g, f)

If percentdiff < 3 Then Exit Sub
If percentdiff > 3 Then Call ExtraElimination

End Sub

Sub ExtraElimination()

Range("AN15:AT80000").Clear

'Formats
Range("AN22").Value = "EliminatingRepeatsAgain"
Range("AN23").Value = "Frame"
Range("AN23").Offset(0, 1).Value = "t"
Range("AN23").Offset(0, 2).Value = "x"
Range("AN23").Offset(0, 3).Value = "Max/Min?"

'First copy&paste "FindingExtrema" data frame, t, x
'Loop interactions
    noptsrange = Range(Cells(24, 32), Cells(15000, 32))
    nopts = WorksheetFunction.Count(noptsrange)
    'MsgBox nopts  ''Debugging Tool

    Do Until i = nopts
    Range("AN24").Offset(i, 0).Value = Range("AF24").Offset(i, 0).Value 'Frame
    Range("AN24").Offset(i, 1).Value = Range("AG24").Offset(i, 0).Value 't
    Range("AN24").Offset(i, 2).Value = Range("AH24").Offset(i, 0).Value 'x
    Range("AN24").Offset(i, 3).Value = Range("AI24").Offset(i, 0).Value  'Max/Min
    i = i + 1
    Loop
''''''''''''''''''''''''''''''''''''''''''''''''''''''''''''''''''''''''''''''''''''''''
i = 0
Do Until i = nopts

If Range("AP25").Offset(i - 1, 0).Value = Range("AP25").Offset(i, 0).Value _
Then
Range("AN25:AQ25").Offset(i, 0).Clear
```

```
608
609   Else
610   End If
611
612   i = i + 1
613   Loop
614
615   'Now to eliminate those blank cells
616   'Formats
617   Range("AS22").Value = "EliminatingBlanksAgain"
618   Range("AS23").Value = "Frame"
619   Range("AS23").Offset(0, 1).Value = "t"
620   Range("AS23").Offset(0, 2).Value = "x"
621   Range("AS23").Offset(0, 3).Value = "Max/Min?"
622
623   'Pasting Data without blanks
624   i = 0
625   Do Until i = nopts
626
627   test = WorksheetFunction.CountA(Cells(24 + i, 40))
628
629   If test > 0 Then
630       Frame = Range("AN24").Offset(i, 0).Value
631       t = Range("AN24").Offset(i, 1).Value
632       amp = Range("AN24").Offset(i, 2).Value
633       MaxMin = Range("AN24").Offset(i, 3).Value
634       entry = Range("AS24:AS8000")
635       k = WorksheetFunction.Count(entry)
636       Range("AS24").Offset(k, 0).Value = Frame
637       Range("AS24").Offset(k, 1).Value = t
638       Range("AS24").Offset(k, 2).Value = amp
639       Range("AS24").Offset(k, 3).Value = MaxMin
640
641   Else
642
643   End If
644   k = k + 1
645   i = i + 1
646   Loop
647
648   'Now recalculate Freq/Amp
649
650   Range("AX15:AY80000").Clear
651
652   'Formating
653   Range("AX18").Value = "Freq:"
654   Range("AX21").Value = "Avg tdiff"
655   Range("AL21").Value = "Avg amp"
656   Range("AX24").Value = "tdiff"
657   Range("AY23").Value = "AbsAmp"
658
659   'count number of interations loop will go through
660       noptsrange = Range(Cells(24, 45), Cells(15000, 45))
661       nopts = WorksheetFunction.Count(noptsrange)
662       'MsgBox nopts ''Debugging Tool
663   i = 0
664
665   Do Until i = nopts - 1
666
667      h = Range("AT25").Offset(i, 0).Value
668      j = Range("AT25").Offset(i - 1, 0).Value
669      TimeDiff = h - j
670      Range("AX25").Offset(i, 0) = TimeDiff
671       i = i + 1
672   Loop
673
674   i = 0
675   Do Until i = nopts
676      amp = Range("AU24").Offset(i, 0).Value
```

```
    v = Abs(amp)
    Range("AY24").Offset(i, 0) = v

    i = i + 1
Loop

avgtimerange = Range(Cells(25, 50), Cells(25 + nopts - 1, 50))
avgtime = WorksheetFunction.Average(avgtimerange)
multi2 = avgtime * 2
inverse = 1 / multi2
Frequency = inverse

Range("AX22").Value = avgtime
Range("AX19").Value = Frequency

avgamprange = Range(Cells(24, 51), Cells(24 + nopts, 51))
avgamp = WorksheetFunction.Average(avgamprange)
Range("AY22").Value = avgamp

Range("M18").Value = Frequency
Range("M19").Value = avgamp

'Checking Frequency Calculation

g = Range("M18").Value
f = Range("P20").Value

percentdiff = 100 * Abs(g - f) / WorksheetFunction.Average(g, f)

If percentdiff < 3 _
Then Exit Sub

If percentdiff > 3 _
Then Call ExtraElimination2

End Sub

Sub ExtraElimination2()

Range("BA15:BM80000").Clear

'Formats
Range("BA22").Value = "EliminatingRepeatsAgain2"
Range("BA23").Value = "Frame"
Range("BA23").Offset(0, 1).Value = "t"
Range("BA23").Offset(0, 2).Value = "x"
Range("BA23").Offset(0, 3).Value = "Max/Min?"

'First copy&paste "FindingExtrema" data frame, t, x
'Loop interactions
    noptsrange = Range(Cells(24, 45), Cells(15000, 45))
    nopts = WorksheetFunction.Count(noptsrange)
    'MsgBox nopts ''Debugging Tool

    Do Until i = nopts
    Range("BA24").Offset(i, 0).Value = Range("AS24").Offset(i, 0).Value 'Frame
    Range("BA24").Offset(i, 1).Value = Range("AT24").Offset(i, 0).Value 't
    Range("BA24").Offset(i, 2).Value = Range("AU24").Offset(i, 0).Value 'x
    Range("BA24").Offset(i, 3).Value = Range("AV24").Offset(i, 0).Value  'Max/Min
    i = i + 1
    Loop
''''''''''''''''''''''''''''''''''''''''''''''''''''''''''''''''''''''''''''''''''''''
i = 0
Do Until i = nopts

If Range("BC25").Offset(i - 1, 0).Value = Range("BC25").Offset(i, 0).Value _
Then
Range("BA25:BD25").Offset(i, 0).Clear

```

```
Else
End If

i = i + 1
Loop

'Now to eliminate those blank cells
'Formats
Range("BF22").Value = "EliminatingBlanksAgain"
Range("BF23").Value = "Frame"
Range("BF23").Offset(0, 1).Value = "t"
Range("BF23").Offset(0, 2).Value = "x"
Range("BF23").Offset(0, 3).Value = "Max/Min?"

'Pasting Data without blanks
i = 0
Do Until i = nopts

test = WorksheetFunction.CountA(Cells(24 + i, 53))

If test > 0 Then
    Frame = Range("BA24").Offset(i, 0).Value
    t = Range("BA24").Offset(i, 1).Value
    amp = Range("BA24").Offset(i, 2).Value
    MaxMin = Range("BA24").Offset(i, 3).Value
    entry = Range("BF24:BF8000")
    k = WorksheetFunction.Count(entry)
    Range("BF24").Offset(k, 0).Value = Frame
    Range("BF24").Offset(k, 1).Value = t
    Range("BF24").Offset(k, 2).Value = amp
    Range("BF24").Offset(k, 3).Value = MaxMin

Else

End If
k = k + 1
i = i + 1
Loop

'Now recalculate Freq/Amp

Range("BK15:BL80000").Clear

'Formating
Range("BK18").Value = "Freq:"
Range("BK21").Value = "Avg tdiff"
Range("BL21").Value = "Avg amp"
Range("BK24").Value = "tdiff"
Range("BL23").Value = "AbsAmp"

'count number of interations loop will go through
    noptsrange = Range(Cells(24, 58), Cells(15000, 58))
    nopts = WorksheetFunction.Count(noptsrange)

i = 0

Do Until i = nopts - 1

   h = Range("BG25").Offset(i, 0).Value
   j = Range("BG25").Offset(i - 1, 0).Value
   TimeDiff = h - j
   Range("BK25").Offset(i, 0) = TimeDiff
    i = i + 1
Loop

i = 0
Do Until i = nopts
   amp = Range("BH24").Offset(i, 0).Value
   v = Abs(amp)
```

```
815      Range("BL24").Offset(i, 0) = v
816
817      i = i + 1
818   Loop
819
820   avgtimerange = Range(Cells(25, 63), Cells(25 + nopts - 1, 63))
821   avgtime = WorksheetFunction.Average(avgtimerange)
822   multi2 = avgtime * 2
823   inverse = 1 / multi2
824   Frequency = inverse
825
826   Range("BK22").Value = avgtime
827   Range("BK19").Value = Frequency
828
829   avgamprange = Range(Cells(24, 64), Cells(24 + nopts, 64))
830   avgamp = WorksheetFunction.Average(avgamprange)
831   Range("BL22").Value = avgamp
832
833   Range("M18").Value = Frequency
834   Range("M19").Value = avgamp
835
836   'Checking Frequency Calculation
837
838   g = Range("M18").Value
839   f = Range("P20").Value
840
841   percentdiff = 100 * Abs(g - f) / WorksheetFunction.Average(g, f)
842
843   If percentdiff < 3 Then Exit Sub
844   If percentdiff > 3 Then MsgBox "Too Many repeats, Check the video"
845
846   End Sub
847
848
```

REFERENCES

Marla, V. T.; Shambaugh, R. L.; Papavassiliou, D. V. Use of an Infrared Camera for Accurate Determination of the Temperature of Polymer Filaments. *Ind. Eng. Chem. Res.* 2007, *46* (1), 336–334.

Table IV.1**.** The table depicts the selection of the extrema in the x-position over time graphs.

Zero's Range			1st zero to 2nd zero	Max/Min Interval?	Extrema Point	Repeats?
A	to	B	+ to -	Max	A	No
B	to	D	- to +	Min	C	No
D	to	G	+ to -	Max	E , F	Yes, Eliminate F
G	to	H	- to +	Min	G	No
H	to	J	+ to -	Max	I	No
J	to	K	- to +	Min	J	No
K	to	L	+ to -	Max	K	No
L	to	N	- to +	Min	M	No
N	to	P	+ to -	Max	O	No
P	to	R	- to +	Min	Q	No

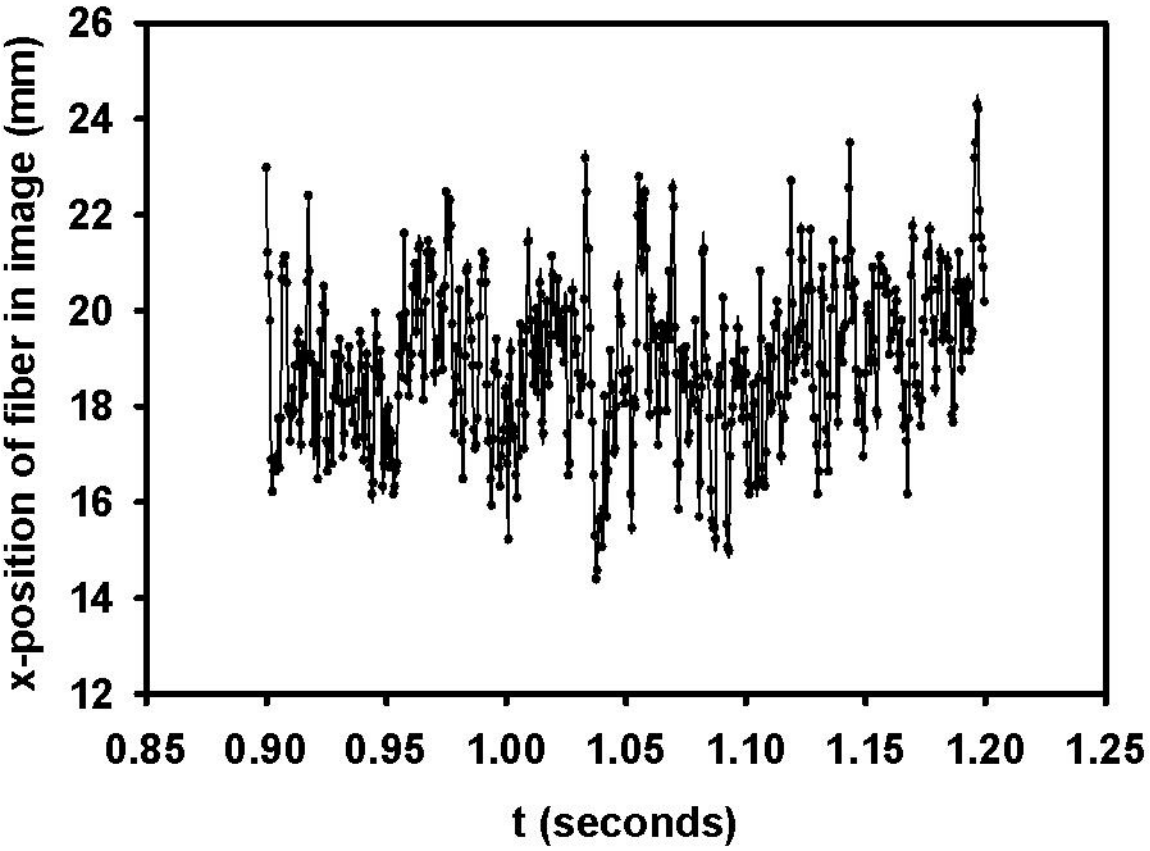

Fig. IV.1 Unnormalized x-position versus time data for a time interval 0.90 to 1.20 seconds for the 20 mm chords, with a leading edge distance z_1 of 5 mm and a louver configuration of f_1,f_2= 8,8. The positional data were taken at z = 9 cm below the die head.

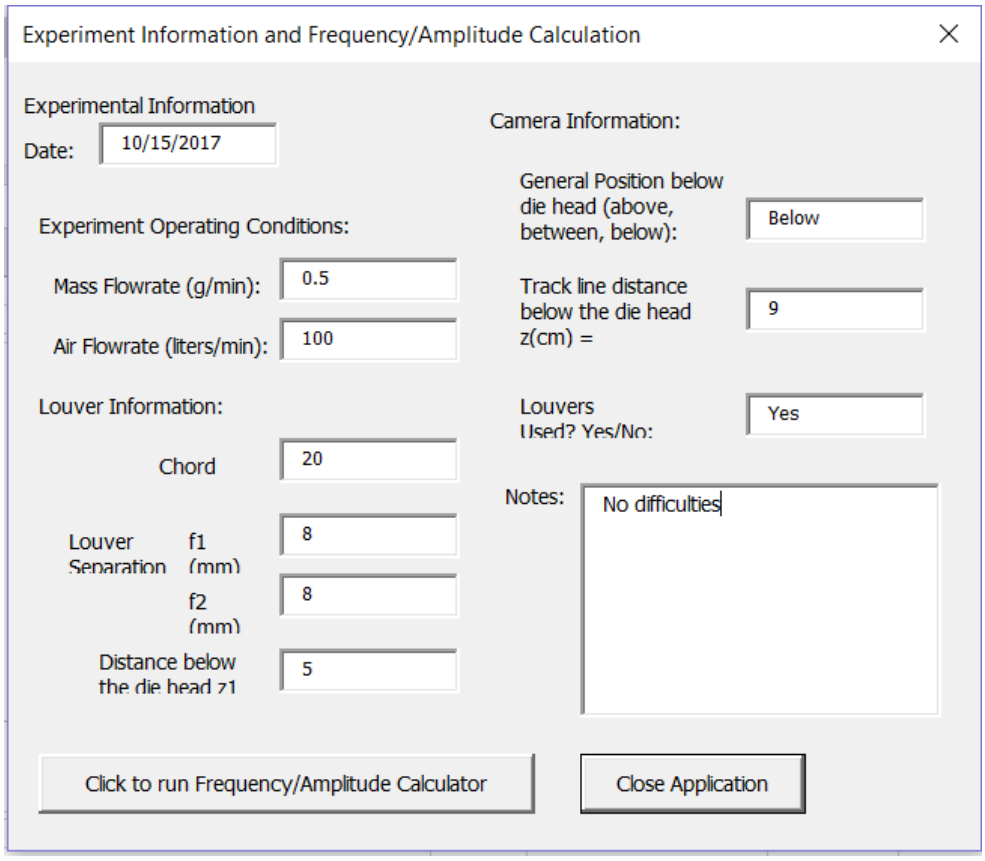

Fig. IV.2. User form application for the VBA code written to calculate the frequency and amplitude of the fiber filament vibrating in the air field.

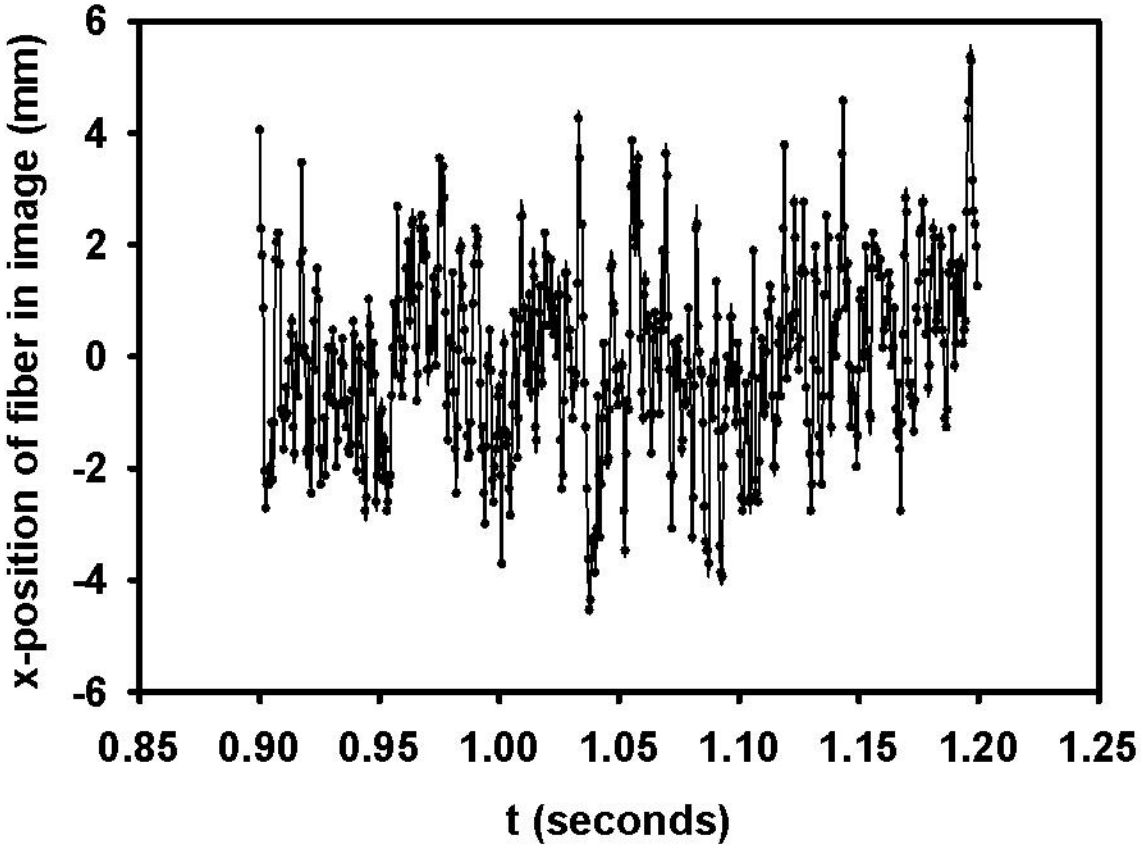

Fig. IV.3. Same as Fig. IV.1 except the data has been normalized to be centered about the x-axis.

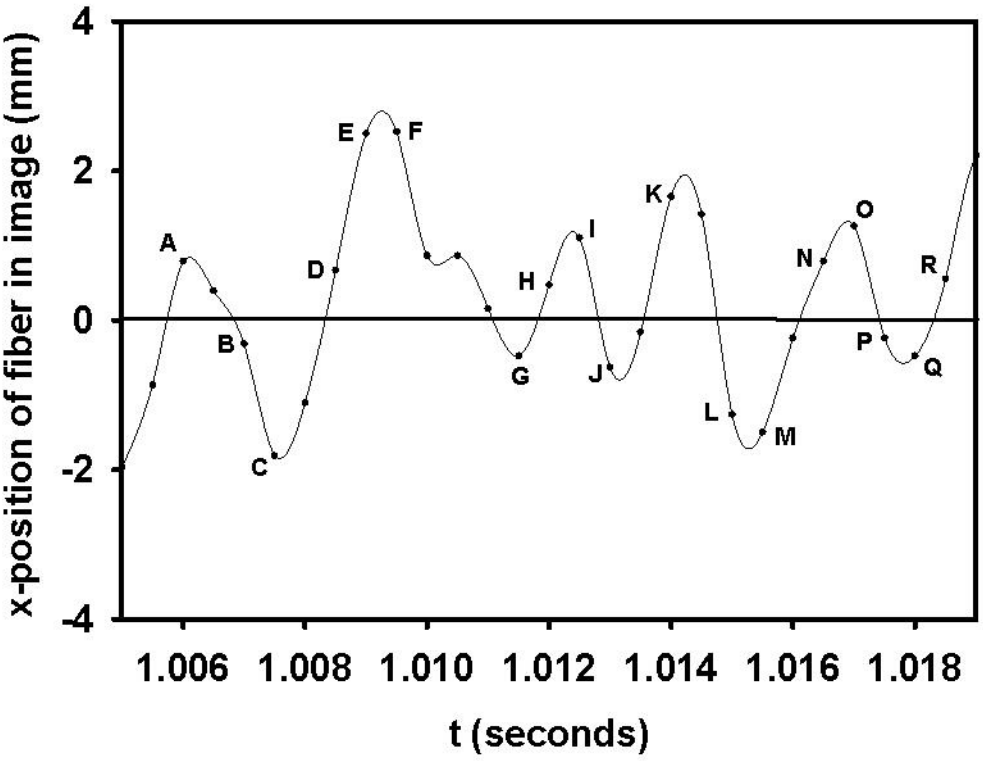

Figure IV.4. Same as the Fig IV.3 except the time interval has been reduced to 1.006 to 1.02 seconds. Letters A through R represent “zero” and extrema points.

APPENDIX V:

NIKON D3200 CAMERA AND ONLINE FIBER IMAGING

The Nikon D3200 Camera with a 105 mm Nikon lens will be used to determine online fiber diameter. This digital camera can be connected to a laptop through a USB connection. It has a variety of shooting settings, including manual, where the user can adjust the camera to desired aperture sizes and shutter speeds. Smaller aperture sizes (corresponding to larger f-stop values) provide better depth of view, or more distance forward and back where the target is still in crisp focus. However, a smaller aperture lets in less light to the camera, making it hard to see the target object. Larger aperture sizes let more light in, making a brighter image, but the depth of view decreases, meaning there is a smaller range an object can move in and still remain in crisp focus. Shutter speeds control how much light is let into a camera at a time. A fast shutter speed will limit the amount of light let into the camera at a time, allowing the user to obtain images of objects moving rapidly without a smearing affect. However, if too little light is let in, then the image is dark, and it is difficult to see the object. Slow shutter speeds will let more light in at a time. This is useful for imaging slow objects or creating smearing effects in fast moving objects. Figs. V.1 and V.2 show a water fountain spout imaged at the same f-stop value of 5.6 (a moderately wide aperture) and different shutter speeds of 1/500 seconds (slow) and 1/1600 seconds (fast). The slower shutter speed produces a bright image of the water spout, but the water is somewhat blurred. The fast shutter speed produces a very crisp image of the water, but its image is darker.

A melt blown fiber is both small and moves very rapidly, a very hard combination to image. In order to obtain a clear image of the fiber without smearing effects, a balance

between shutter speeds, lighting, and aperture size will need to be selected. Some images of the fiber have been produced using wide to moderately wide apertures, high shutter speeds, and additional lighting from two Bayco 8.5inch clamp-on flood lamps. Figs V.3, V.4, and V.5 show the fiber in the melt blowing field at 11 cm below the die. The camera was positioned at 16 cm away from the fiber. The air flowrate was 60 slpm and the mass flowrate was 1 g/min. The shutter speed was 1/4000 seconds, and this was the highest shutter speed that could be used and still have enough light to observe the fiber (even with the additional flood lights). Fig V.3, V.4, and V.5 were done at f-stops of 16, 10, and 6.3 respectively. Fig V.3 yields a fairly crisp image, but the image is dark, and part of the fiber is in shadow. Fig V.4 had a f-stop of 10 (medium aperture). The fiber image is crisp, but still somewhat dark. Fig V.5 had a f-stop of 6.3 (large aperture). The fiber is brighter, but there is significant blurring.

Fig. V.1. Image of a water fountain spout obtained with an aperture size of 5.6 f-stop and a shutter speed of 1/500 seconds.

Fig. V.2. Image of a water fountain spout obtained with an aperture size of 5.6 f-stop and a shutter speed of 1/1600.

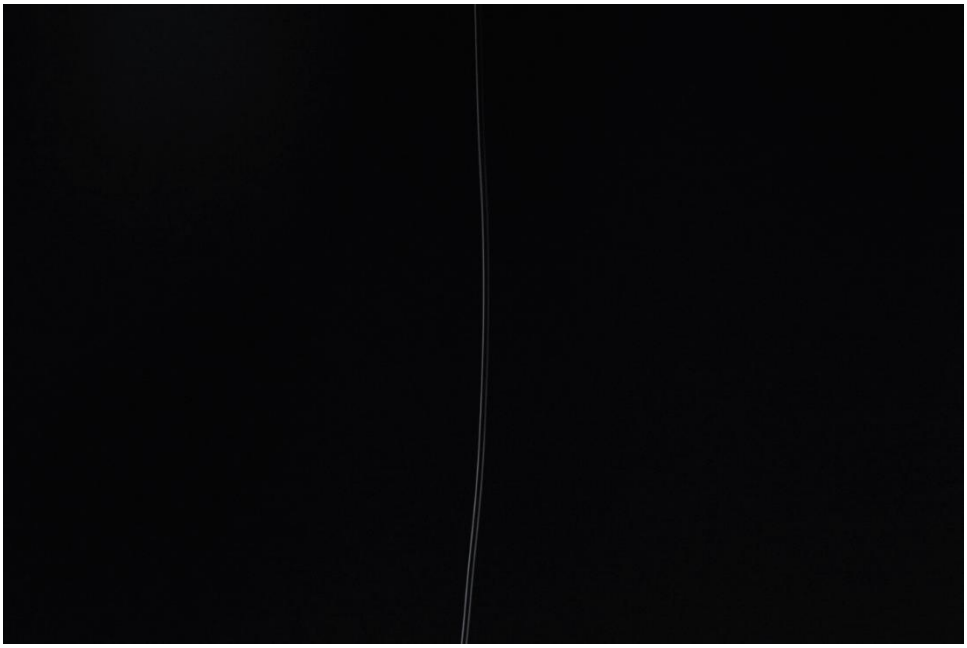

Fig. V.3. Online image of a melt blown fiber taken with a Nikon 3200D camera. The camera had a 1/4000 second shutter speed and a f-stop of 16 (small aperture).

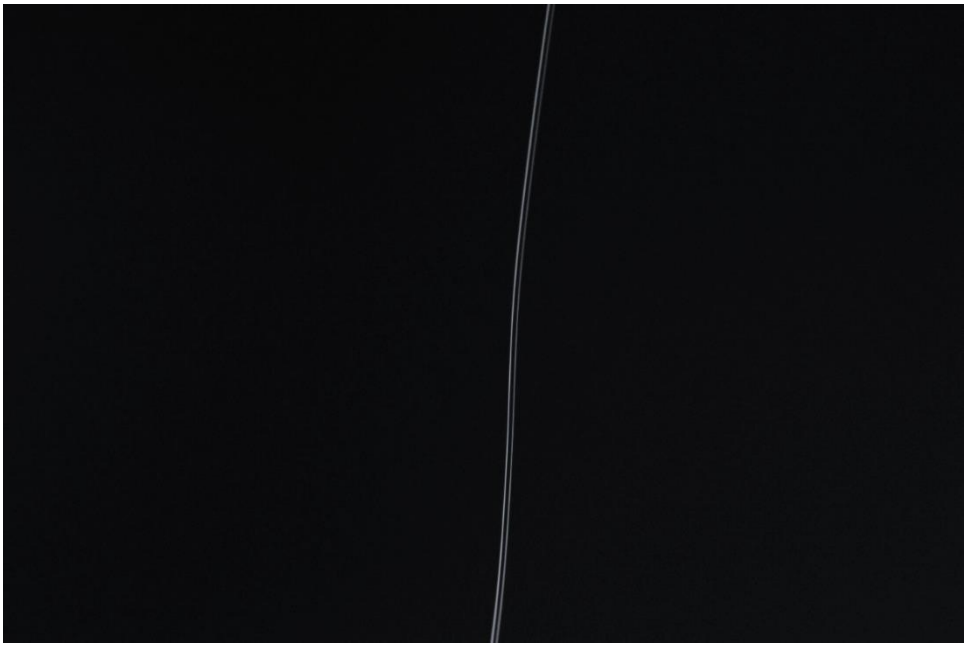

Fig. V.4. Online image of a melt blown fiber taken with a Nikon 3200D camera. The camera had a 1/4000 second shutter speed and a f-stop of 10 (medium aperture).

Fig. V.5. Online image of a melt blown fiber taken with a Nikon 3200D camera. The camera had a 1/4000 second shutter speed and a f-stop of 6.3 (large aperture).

APPENDIX VI:

UNDERSTANDING THE FLOW FIELD BETWEEN PARALLEL LOUVERS

As the air field controls the main attenuation of the melt blowing fiber, an understanding of the air field between the louvers is of interest. As described by Shambaugh et al. (2015), for a pair of parallel louvers, continuity dictates that there is a constant average air velocity between the louver pair. This imposes a higher air velocity on the fiber filament as the louvers block the air jet from entraining ambient air. However, it would also be of interest to determine the characteristics of the velocity profile between the louvers, as the velocity profile can affect the vibrational characteristics of the fiber threadline. A full study through computational fluid dynamics of the air field with louvers below the die is needed, but will not be completed here. However, an approximation of the boundary layer on the louvers and an estimate of the characteristics of the air field between the louvers will be presented here.

A louver can be approximated as a flat plate with an impinging air jet at the leading-edge. With this assumption, the boundary layer on the louver plate can be determined. The centerline air velocity and temperature for an air jet produced from a sharp 60 degree slot die with a flush tip can be determined through correlations developed by Tate and Shambaugh (2004) and Harpham and Shambaugh (1997):

(Eq. 1) $\frac{v_o}{v_{jo}} = 2.88\left(\frac{z}{h}\right)^{-0.532}$

(Eq. 2) $\frac{\theta_o}{\theta_{jo}} = 1.53\left(Z(h)\right)^{-0.511}$

The air velocity and air temperature of the air jet at the die face are v_{jo} and Θ_{jo} respectively. v_o and Θ_o are the centerline air velocity and temperatures. Z(h) is a function that corrects for the changing air density with temperature where ρ_∞ is the ambient air density and ρ_o is the centerline air density:

(Eq. 3) $$Z(h) = \left(\frac{z}{h}\right)\left(\frac{\rho_\infty}{\rho_o}\right)^{\frac{1}{2}}$$

The air kinematic viscosity and density dependence on temperature can be described by:

(Eq. 4) $$\nu\left(\frac{m^2}{s}\right) = (1 * 10^{-9})T(K)^{1.6761}$$

(Eq. 5) $$\rho\left(\frac{kg}{m^3}\right) = 354.79T(K)^{-1.001}$$

These relationships were determined by fitting the air viscosity and density data obtained from Appendix I of Welty et al. (2008).

The air velocity and temperature found at $z = z_1$ will be considered constant between the louvers until $z = z_2$ similar to the method done by B. Shambaugh et al. (2012) (see Figure 1.3). The Reynolds number based on the chord length can be determined:

(Eq. 6) $$Re_c = \frac{v_o c}{\nu}$$

where v_o is the centerline air velocity, c is the chord length of the louver, and ν is the kinematic viscosity of the air at the centerline temperature Θ_o. This is the Reynolds number at the louver trailing-edge. The local Reynolds number down the length of the louver is determined by

(Eq. 7) $$Re_c = \frac{v_o z'}{\nu}$$

where z' is the distance down the louver chord and $0 < z' < c$. The boundary layer thickness can be determined by the Blasius solution (Eq. 8) for flow over a flat plate when the Re_c is less than 10^5 and by the von Karman solution for turbulent flow over a flat plate (Eq. 9) for Re_c greater than 10^5:

(Eq. 8) $\delta = \frac{5c}{\sqrt{Re_c}}$

(Eq. 9) $\delta = \frac{0.376c}{Re_c^{\frac{1}{5}}}$

If twice the boundary layer thickness (for two louvers in the air field) is smaller than the louver separation f, then the flow is not fully developed, and the air velocity is still changing with respect to z as well as x. Also of potential interest, the Reynolds number based on louver separation can also be determined by:

(Eq. 10) $Re_f = \frac{v_o f}{\nu}$

Where f is the separation between parallel louvers in millimeters.

For a 100 liter/min air flowrate the die face air velocity can be determined from

(Eq. 11) $v_{jo} = \frac{Q}{A} = \frac{Q}{2*b*l}$

where A is the cross-sectional area of the two air slots, b is the slot width, l is the slot length, and Q is the air flowrate. For a slot length of 74 mm and a slot width of 0.65 mm, the air velocity at the die face is 17.3 m/s. The air temperature at the die face, Θ_{jo}, is 300 °C. Figures VI.1 and VI.2 show the air velocity and temperature profiles for this air flowrate and Table VI.1 lists the jet air velocities and temperatures at each leading-edge distance of z_1. Also listed are the corresponding kinematic viscosities, densities, and

Reynolds number based on louver separation f. TableVI.2 shows the Reynolds number and the boundary layer thickness based on the Blasius solution for different chord lengths at the same leading-edge distances of z.

At an air flowrate of 100 liters/min the Reynolds numbers based on chord length are at a magnitude of 10^4, which is in the laminar regime for a flat plate. The greatest boundary layer thickness at the trailing-edge of 40 mm chord louvers is 1.35 mm thick, making a total thickness of 2.7 mm between the louvers that has viscous effects. This is nearly half the region between the louvers for a louver separation of 6 mm. As the combined boundary layer thickness between the louvers is less than that of any of the louver separations of 10, 8, or 6 mm, the flow between the louvers is not fully developed.

Tables VI.1 and VI.2 also included calculations for higher air flowrates of 500 and 1000 liters/min. Only for the latter case does the Reynolds number reach a magnitude of 10^5. For this case, the boundary layer thickness is calculated with both the Blasius and von Karman solutions. It is believed the actual boundary layer thickness falls between these solutions. For these higher air flowrates, the boundary layer thickness decreases regardless of which solution is used.

REFERENCES

Harpham, A. S.; Shambaugh, R. L. Velocity and Temperature Fields of Dual Rectangular Jets. *Ind. Eng. Chem. Res.* 1997, *36* (9), 3937-3943.

Tate, B. D.; Shambaugh, R. L. Temperature Fields below Melt Blowing Dies of Various Geometries. *Ind. Eng. Chem. Res.* 2004, 43 (17), 5405-5410.

J. R. Welty; C. E. Wicks; R.E. Wilson; G. L. Rorrer. *Fundamentals of Momentum, Heat, and Mass Transfer,* 5th ed.; John Wiley & Sons, Inc: New Jersey, 2008; pg 679.

Table VI.1. For different air flowrates, the air velocity and temperature at the louver leading edge of z_1 is shown as well as the air kinematic viscosity and density, and the Reynolds numbers based on louver separation f (Eq. 10).

		Air Velocity and Temperature		Air Properties		Re_f (Eq. 10)		
Air Flowrate (liters/min)	z_1 (mm)	vo (m/s)	Θo (°C)	v (m2/s) *10^5	ρ (kg/m3)	Re_f f=10 mm	Re_f f=8 mm	Re_f f=6 mm
100	5	24.37	202.33	3.30E-05	0.71	7.39E+03	5.91E+03	4.43E+03
	10	16.85	147.48	2.57E-05	0.82	6.55E+03	5.24E+03	3.93E+03
	15	13.58	122.03	2.29E-05	0.88	5.93E+03	4.75E+03	3.56E+03
	20	11.66	106.52	2.13E-05	0.92	5.48E+03	4.38E+03	3.29E+03
500	5	121.84	202.33	3.30E-05	0.71	3.69E+04	2.95E+04	2.22E+04
	10	84.27	147.48	2.57E-05	0.82	3.28E+04	2.62E+04	1.97E+04
	15	67.92	122.03	2.29E-05	0.88	2.97E+04	2.37E+04	1.78E+04
	20	58.28	106.52	2.13E-05	0.92	2.74E+04	2.19E+04	1.64E+04
1000	5	243.69	202.33	3.30E-05	0.71	7.39E+04	5.91E+04	4.43E+04
	10	168.53	147.48	2.57E-05	0.82	6.55E+04	5.24E+04	3.93E+04
	15	135.83	122.03	2.29E-05	0.88	5.93E+04	4.75E+04	3.56E+04
	20	116.56	106.52	2.13E-05	0.92	5.48E+04	4.38E+04	3.29E+04

Table VI.2. For different air flowrates, the Reynolds number based on chord length (Eq.7) is shown as well as the boundary layer thickness calculated with the Blasius solution (Eq.8) or the von Karman solution (Eq. 9).

Air Flowrate		c = 20 mm			c = 30 mm			c = 40 mm		
(liters/min)	z_1 (mm)	Re_c (Eq.7)	δ (mm) (Eq.8)	δ (mm) (Eq. 9)	Re_c (Eq.7)	δ (mm) (Eq.8)	δ (mm) (Eq. 9)	Re_c (Eq.7)	δ (mm) (Eq.8)	δ (mm) (Eq. 9)
100	5	1.48E+04	0.82	N/A	2.22E+04	1.01	N/A	2.95E+04	1.16	N/A
	10	1.31E+04	0.87	N/A	1.97E+04	1.07	N/A	2.62E+04	1.24	N/A
	15	1.19E+04	0.92	N/A	1.78E+04	1.12	N/A	2.37E+04	1.30	N/A
	20	1.10E+04	0.96	N/A	1.64E+04	1.17	N/A	2.19E+04	1.35	N/A
500	5	7.39E+04	0.37	N/A	1.11E+05	0.45	0.00	1.48E+05	0.52	1.39
	10	6.55E+04	0.39	N/A	9.83E+04	0.48	N/A	1.31E+05	0.55	1.42
	15	5.93E+04	0.41	N/A	8.90E+04	0.50	N/A	1.19E+05	0.58	1.45
	20	5.48E+04	0.43	N/A	8.21E+04	0.52	N/A	1.10E+05	0.60	1.48
1000	5	1.48E+05	0.26	0.70	2.22E+05	0.32	0.96	2.95E+05	0.37	1.21
	10	1.31E+05	0.28	0.71	1.97E+05	0.34	0.99	2.62E+05	0.39	1.24
	15	1.19E+05	0.29	0.73	1.78E+05	0.36	1.01	2.37E+05	0.41	1.27
	20	1.10E+05	0.30	0.74	1.64E+05	0.37	1.02	2.19E+05	0.43	1.29

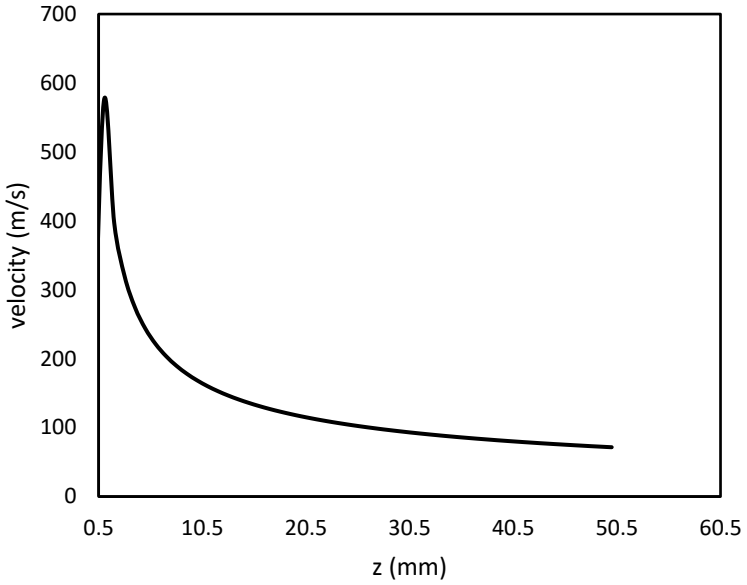

Figure VI. 1. Centerline air jet velocity for z distance below the die head.

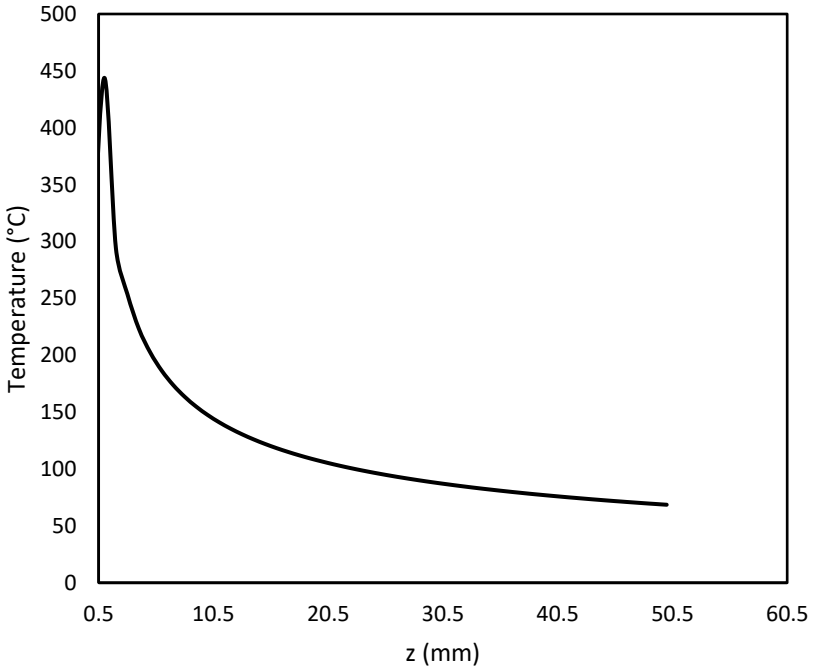

Figure VI. 2. Centerline air jet temperature for z distance below the die head.